NTNU
Norwegian University of
Science and Technology

Simulation of expansion driven flow instabilities in long risers

Tor Brox Kjeldby

Master of Science in Product Design and Manufacturing
Submission date: June 2010
Supervisor: Ole Jørgen Nydal, EPT

Norwegian University of Science and Technology
Department of Energy and Process Engineering

Problem Description

Oljeselskap erfarer at gass-væske strøm i lange brønner og i stigerør kan gi ustabil produksjon, med alternerende gass og væskestrøm. Det er i hovedsak kompressibiliteten til gassen som kan gi opphav til ustabil strøm.

"Stigerørslugging" er et uttrykk for det fenomenet at væske samles i et bend og et stigerør, og blåses ut med en karakteristisk frekvens. Kompresjon og ekspansjon av gassen oppstrøms er bestemmende for graden av ustabil strøm, stigerørslugging krever tilstrekkelig mengde fri gass oppstrøms. Denne form for ustabilitet er velkjent, og var også en hovedmotivasjon for oppstarten av utviklingen av OLGA simulatoren ved IFE på begynnelsen av 80 tallet.

En annen form for ustabil strøm skyldes gassekspansjonen i et stigerør eller en brønn. En strømningsmekanisme er da at gass som kommer inn i stigerøret ekspanderer og gir en aksellerasjon av blandingen som medfører ytterligere økt gasstrøm inn i stigerøret. Slike system kan gi ustabil strøm selv for små gassvolum før stigerøret. Det er tidligere utført noen småskala strømningsforsøk med ekspansjonsdrevet ustabil strøm i flerfaselaboratoriet ved EPT, og det er nå ønskelig å vurdere disse i forhold til numeriske simuleringer.

Assignment given: 19. January 2010
Supervisor: Ole Jørgen Nydal, EPT

Simulation of expansion driven flow instabilities in long risers

by

stud.techn.

Tor Brox Kjeldby

Master thesis

NTNU
Norwegian University of
Science and Technology

Norwegian University of Science and Technology

Faculty of Engineering Science and Technology

Department of Energy and Process Engineering

June 2010

Norges teknisk-
naturvitenskapelige universitet
NTNU

Institutt for energi- og prosessteknikk

NTNU

EPT-M-2010-11

MASTEROPPGAVE

for

Stud.techn. Tor Brox Kjeldby

Våren 2010

Simulering av ekspansjonsdrevet ustabil strøm i lange stigerør

Simulation of expansion driven flow instabilities in long risers

Bakgrunn

Oljeselskap erfarer at gass-væske strøm i lange brønner og i stigerør kan gi ustabil produksjon, med alternerende gass og væskestrøm. Det er i hovedsak kompressibiliteten til gassen som kan gi opphav til ustabil strøm.

"Stigerørslugging" er et uttrykk for det fenomenet at væske samles i et bend og et stigerør, og blåses ut med en karakteristisk frekvens. Kompresjon og ekspansjon av gassen oppstrøms er bestemmende for graden av ustabil strøm, stigerørsslugging krever tilstrekkelig mengde fri gass oppstrøms. Denne form for ustabilitet er velkjent, og var også en hovedmotivasjon for oppstarten av utviklingen av OLGA simulatoren ved IFE på begynnelsen av 80 tallet.

En annen form for ustabil strøm skyldes gass ekspansjonen i et stigerør eller en brønn. En strømningsmekanisme er da at gass som komme inn i et stigerør ekspanderer og gir en akselerasjon av blandingen som medfører ytterligere økt gassstrøm inn i stigerøret. Slike system kan gi ustabil strøm selv for små gassvolum før stigerøret. Det er tidligere utført noen småskala strømningsforsøk med ekspansjonsdrevet ustabil strøm i flerfaselaboratoriet ved EPT, og det er nå ønskelig å vurdere disse i forhold til numeriske simuleringer.

Mål

Det skal utføres numeriske simuleringer av småskala strømningsforsøk som viser ekspansjonsdrevet ustabil strøm. Simuleringene skal utføres med tilgjengelig programvare (f.eks. OLGA) simulatoren samt med en slug følge modell ved EPT.

Oppgaven bearbeides ut fra følgende punkter

1. Litteratur studie av ekspansjonsdrevet ustabil strøm i lange stigerør eller brønner
2. Simulering av strømningsforsøk fra laboratoriet med tilgjengelig programvare
3. Simulering, og eventuell modifisering av slugfølgeprogrammet ved EPT
4. Rapportering i artikkelform

" - "

Senest 14 dager etter utlevering av oppgaven skal kandidaten levere/sende instituttet en detaljert fremdrift- og eventuelt forsøksplan for oppgaven til evaluering og eventuelt diskusjon med faglig ansvarlig/veiledere. Detaljer ved eventuell utførelse av dataprogrammer skal avtales nærmere i samråd med faglig ansvarlig.

Besvarelsen redigeres mest mulig som en forskningsrapport med et sammendrag både på norsk og engelsk, konklusjon, litteraturliste, innholdsfortegnelse etc. Ved utarbeidelsen av teksten skal kandidaten legge vekt på å gjøre teksten oversiktlig og velskrevet. Med henblikk på lesning av besvarelsen er det viktig at de nødvendige henvisninger for korresponderende steder i tekst, tabeller og figurer anføres på begge steder. Ved bedømmelsen legges det stor vekt på at resultatene er grundig bearbeidet, at de oppstilles tabellarisk og/eller grafisk på en oversiktlig måte, og at de er diskutert utførlig.

Alle benyttede kilder, også muntlige opplysninger, skal oppgis på fullstendig måte. For tidsskrifter og bøker oppgis forfatter, tittel, årgang, sidetall og eventuelt figurnummer.

Det forutsettes at kandidaten tar initiativ til og holder nødvendig kontakt med faglærer og veileder(e). Kandidaten skal rette seg etter de reglementer og retningslinjer som gjelder ved alle (andre) fagmiljøer som kandidaten har kontakt med gjennom sin utførelse av oppgaven, samt etter eventuelle pålegg fra Institutt for energi- og prosessteknikk.

I henhold til "Utfyllende regler til studieforskriften for teknologistudiet/sivilingeniørstudiet" ved NTNU § 20, forbeholder instituttet seg retten til å benytte alle resultater og data til undervisnings- og forskningsformål, samt til fremtidige publikasjoner.

Ett -1 komplett eksemplar av originalbesvarelsen av oppgaven skal innleveres til samme adressat som den ble utlevert fra. Det skal medfølge et konsentrert sammendrag på maksimalt én maskinskrevet side med dobbel linjeavstand med forfatternavn og oppgavetittel for evt. refererings i tidsskrifter).

Til Instituttet innleveres to - 2 komplette kopier av besvarelsen. Ytterligere kopier til eventuelle medveiledere/oppgavegivere skal avtales med, og eventuelt leveres direkte til de respektive. Til instituttet innleveres også en komplett kopi (inkl. konsentrerte sammendrag) på CD-ROM i Word-format eller tilsvarende.

NTNU, Institutt for energi- og prosessteknikk, 12. januar 2010

Olav Bolland
Instituttleder

Ole Jørgen Nydal
Faglig ansvarlig/veileder

Preface

This thesis concludes my work with the fifth year master project, at Department of Energy and Process Engineering, NTNU during the spring semester 2010. I would like to thank my supervisor professor Ole Jørgen Nydal for his guidance and advice throughout my work. I would also like to thank Angela De Leebeeck for helping with configuring her simulator version enabling use on my computer.

Trondheim, June 1, 2010

Tor Brox Kjeldby

Sammendrag

Numeriske simuleringer har blitt utført for en serie eksisterende småskalaforsøk med ustabilt gassløft utført i flerfaselaboratoriet ved NTNU. Simuleringene har blitt utført med to forskjellige endimensjonale flerfasesimulatorer. I det eksperimentelle oppsettet akkumuleres gass i et bend på stigerørets innløp for deretter å propagere inn i stigerøret som et resultat av ekspansjonsdrevet aksellerasjon i stigerøret. Dette gir opphav til syklisk strømning, som resulterer i ustabil produksjon med karakteristikker av typen forbundet med tetthetsbølgeustabilitet. Ingen liknende eksperimentelle bidrag har blitt funnet i litteraturen. Simuleringer med og uten slugfølging har blitt utført med den kommersielt tilgjengelige simulatoren OLGA. Simuleringene uten slugfølging har blitt utført på et fint grid med cellelengde i størrelsesorden én rørdiameter, og representerer dermed en framgangsmåte forbundet med slugfanging (slug capturing). Simuleringene med slugfølging utført med OLGA er basert på et grovere grid. SLUGGIT er en ikke-kommersiell slugfølgingssimulator utviklet ved NTNU, basert på et bevegelig grid. Denne simulatoren finnes i flere versjoner som alle er implementert i C++ ved bruk av objektorienterte teknikker. En av disse versjonene har blitt modifisert slik at en gasskilde kan inkluderes på ønsket sted langs røroppsettet. Både OLGA uten slugfølging såvel som SLUGGIT har vist seg egnede for reproduksjon av de ustabile ekspansjonsdrevne strømningene observert i eksperimentene.

Abstract

A series of former small scale experiments on unstable gas lift conducted at the NTNU multiphase laboratory have become subject to numerical simulations with two different multiphase one-dimensional flow simulators. In the experimental setup the injected gas accumulates in a riser inlet bend configuration and then discharges into the riser due to expansion driven flow acceleration in the riser. This gives a cyclic flow, resulting in unstable production with characteristics similar to those associated with density wave instability. No similar experimental contributions have been found in the literature. Simulations with and without slug tracking have been performed with the commercially available simulator OLGA. The simulations without slug tracking have been conducted on a fine grid with a cell length in the order of one pipe diameter, thus representing a slug capturing approach. The OLGA simulations with slug tracking have been conducted on a coarser grid. The SLUGGIT simulator is a non-commercial in-house NTNU slug tracking simulator based on a moving grid formulation. This simulator exists in several versions which are all implemented in C++ by use of object oriented techniques. One of these versions has been modified to handle a gas source at any location along the pipeline. Both OLGA without slug tracking as well as the SLUGGIT have proven capable of reproducing the unstable expansion driven flows shown in the experiments.

Contents

1 Introduction **1**

2 Objectives **3**

3 Instability phenomena and their mechanisms **4**

4 Literature survey **10**

5 The experimental setup **22**

6 The slug tracking simulator SLUGGIT **25**
6.1 SLUGGIT modification - version I 28
6.2 SLUGGIT modification - version II 31

7 Visualization of results **34**

8 Simulations **35**

9 Results **39**
9.1 OLGA - series I 43
9.1.1 Gas injection rate $= 2.000 \cdot 10^{-5}[kg/s]$ 43
9.1.2 Gas injection rate $= 2.621 \cdot 10^{-5}[kg/s]$ 44
9.1.3 Gas injection rate $= 2.642 \cdot 10^{-5}[kg/s]$ 46
9.1.4 Gas injection rate $= 3.500 \cdot 10^{-5}[kg/s]$ 47
9.2 OLGA - series II 50
9.2.1 Gas injection rate $= 2.000 \cdot 10^{-5}[kg/s]$ 51
9.2.2 Gas injection rate $= 2.642 \cdot 10^{-5}[kg/s]$ 52
9.2.3 Gas injection rate $= 3.500 \cdot 10^{-5}[kg/s]$ 53
9.3 SLUGGIT - series I 55
9.3.1 Gas injection rate $= 2.000 \cdot 10^{-5}[kg/s]$ 55
9.3.2 Gas injection rate $= 3.500 \cdot 10^{-5}[kg/s]$ 56
9.3.3 Gas injection rate $= 4.970 \cdot 10^{-5}[kg/s]$ 57
9.3.4 Gas injection rate $= 5.000 \cdot 10^{-5}[kg/s]$ 59
9.3.5 Gas injection rate $= 8.500 \cdot 10^{-5}[kg/s]$ 60
9.4 SLUGGIT - series II 62
9.4.1 Gas injection rate $= 2.000 \cdot 10^{-5}[kg/s]$ 62
9.4.2 Gas injection rate $= 3.350 \cdot 10^{-5}[kg/s]$ 63
9.4.3 Gas injection rate $= 3.650 \cdot 10^{-5}[kg/s]$ 64
9.4.4 Gas injection rate $= 5.000 \cdot 10^{-5}[kg/s]$ 65
9.4.5 Gas injection rate $= 8.500 \cdot 10^{-5}[kg/s]$ 66
9.5 SLUGGIT - series III 68
9.5.1 Gas injection rate $= 2.000 \cdot 10^{-5}[kg/s]$ 68
9.5.2 Gas injection rate $= 3.350 \cdot 10^{-5}[kg/s]$ 70
9.5.3 Gas injection rate $= 3.650 \cdot 10^{-5}[kg/s]$ 71
9.5.4 Gas injection rate $= 5.000 \cdot 10^{-5}[kg/s]$ 72

9.5.5 Gas injection rate $= 8.500 \cdot 10^{-5}[kg/s]$ 73
9.6 SLUGGIT - series IV 75
9.6.1 Gas injection rate $= 2.000 \cdot 10^{-5}[kg/s]$ 75
9.6.2 Gas injection rate $= 3.350 \cdot 10^{-5}[kg/s]$ 76
9.6.3 Gas injection rate $= 3.650 \cdot 10^{-5}[kg/s]$ 78
9.6.4 Gas injection rate $= 5.000 \cdot 10^{-5}[kg/s]$ 79
9.6.5 Gas injection rate $= 8.500 \cdot 10^{-5}[kg/s]$ 80
9.7 An alternative approach 82

10 Comparison and discussion **86**
10.1 Experiments vs simulations 86
10.2 Simulation series comparison 98
10.3 SLUGGIT pressure oscillations 103
10.4 Sources of error 104

11 Conclusion and recommendations **106**

Appendices

A Visualization of OLGA - series I **I**

B Visualization of OLGA - series II **IV**

C Visualization of SLUGGIT - series I **VI**

D Visualization of SLUGGIT - series III **IX**

E Visualization of SLUGGIT - series IV **X**

F OLGA input files **XIII**

G PVT table **XVIII**

H SLUGGIT input file **XIX**

I Matlab filter **XXIII**

J Matlab plotting file **XXV**

1 Introduction

The topic of two-phase flow in vertical pipes shows a wide range of industrial applications, both in thermal and isothermal systems. In order to make a liquid flow in an upward direction inside a vertical pipe, a pressure difference is required to overcome the gravitational and frictional terms. In many situations the available pressure difference in the given system shows insufficient to balance these terms. A common solution to this is to reduce the density of the liquid column by introducing two-phase flow (or increase the void fraction in existing two-phase flow). In thermal systems this may be obtained by introduction of a boiling regime producing bubbles in lower parts of the pipe, a method applied in self circulated industrial water pipe steam generators as well as in household coffee machines. In isothermal (or near isothermal) systems boiling can not be utilized for reduction of the mixture density. A possible solution is then to apply artificial gas lift. This approach is typically based on compression of a suitable lift gas outside the pipe with subsequent injection into the lower parts of the pipe. The gas bubbles injected into the fluid contribute to a reduction of the mixture density with corresponding reduction of the gravitational force contribution.

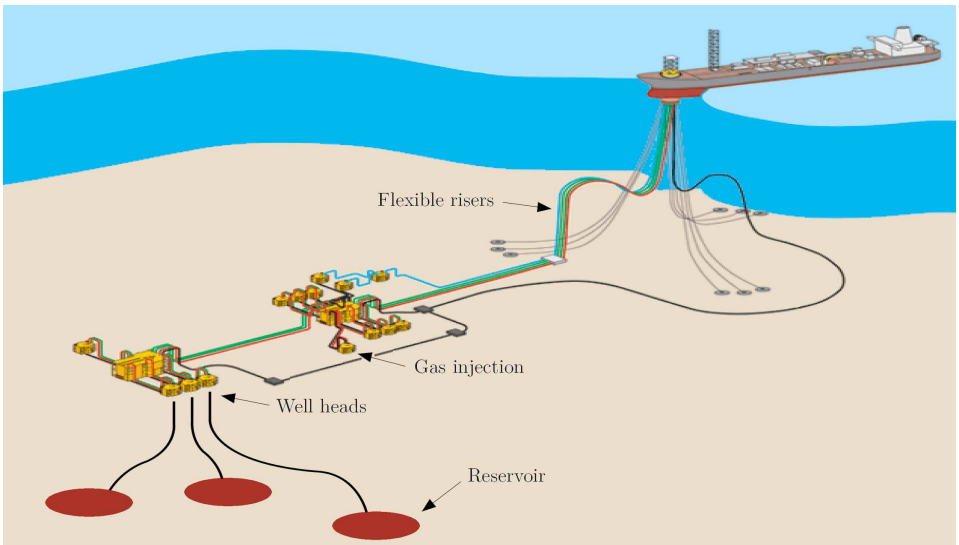

Figure 1: Subsea production system with gas lift, from [1]

A common employer of the gas lift technique is the petroleum industry. Figure 1 shows a typical production system with gas lift. In many cases the available pressure difference between reservoir and well head, or between riser inlet and outlet shows insufficient to make the oil flow naturally from the well. Another situation arises when the available pressure difference is sufficient to make the oil flow, but to low to give the desired production rate. Gas lift may be applied in both these situations, in form of continuous gas lift (CGL) or intermittent gas lift (IGL).

Intermittent gas lift differs from the continuous gas lift technique in that the gas is injected periodically in time by a control strategy. Such a strategy may in some situations represent a more efficient and economical alternative. Depending on the gas lift configuration used and its characteristics, different instability phenomena giving unstable production may be observed. This thesis focuses on the consept of continuous gas lift and its instability mechanisms.

2 Objectives

- Perform a literature survey on expansion driven flow instabilities in long risers and wells
- Write a Matlab program capable of preparing OLGA results for dynamic visualization with the NTNU in-house visualization tool PLOTIT
- Conduct a series of OLGA simulations, with and without slug tracking, spanning the whole gas injection flow rate range used in the former NTNU experimental series chosen for comparison
- Modify the in-house NTNU slug tracking simulator SLUGGIT to enable gas lift simulation. This involves introduction of a gas source, gas accumulation in time at the source location as well as section management operations enabling splitting of slugs
- Conduct a series of SLUGGIT simulations with the modified simulator, spanning the whole gas injection flow rate range used in the NTNU experiments
- Write a Matlab program capable of plotting simulation results from OLGA and SLUGGIT within equal visual frames
- Compare the simulation results with experimental data from NTNU
- Create animations for .zip file inclusion as part of the master thesis hand-in

3 Instability phenomena and their mechanisms

Unstable flows in vertical pipes may be classified into several different phenomena or ”headings”. The term ”heading” originates from the petroleum industry and may be translated into ”unstable production phenomenon” due to gas accumulation in a certain part of the process equipment. Four main heading phenomena are known from the petroleum industry, with the terms in front of ”heading” describing where gas is building up / discharging in a cyclic manner:

- Casing heading
- Tubing heading
- Pipeline heading (Severe slugging)
- Formation heading

The term ”casing heading” thus adresses flow instabilities caused by cyclic accumulation of gas in the riser casing. In connection with early built natural flowing wells without any packer installed (seal between the casing and the tubing in the lower parts of the well), casing heading instability was possible to occur due to the compressibility of large gas volumes enabled to accumulate between the casing and the tubing in the full length of the pipe. This is illustrated by Figure 2. Modern natural flowing wells have got a packer installed and do hence not suffer the problem with gas entering the annulus between the casing and the tubing.

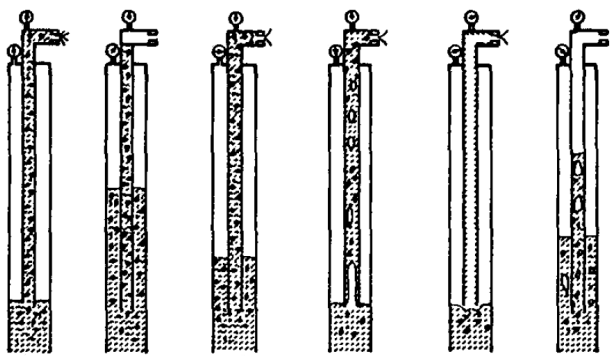

Figure 2: Casing heading cycle in a naturally flowing well completed without packer, from [2]

Gas lifted modern wells with a packer installed may though be subject to casing heading in configurations where the gas flow through the injection valve is subcritical. Subcritical flow conditions in the injection valve allows pressure changes occuring in the tubing to influence the pressure in annulus, thus providing the required access to the compressible volume needed inside annulus for casing heading to occur. If the gas flow conditions in the injection valve are critical,

the pressure in annulus will not be affected by pressure changes occuring in the tubing. Casing heading will hence not occur. In order to obtain critical flow in the gas injection valve, a certain ratio between tubing pressure and casing pressure is needed. Regular valves not tailored for gas lift operation do typically require a ratio of approximately 1/2. A common procedure in oil industry to obtain critical flow through the gas injection valve over a wider production rate spectrum, is to replace the original gas lift valve with a nozzle venturi valve often requiring a pressure ratio of only 1/10 for critical flow to occur. The steps during one casing heading cycle might be summarized as follows:

- At cycle start the annulus pressure down-hole is lower than the bottom-hole tubing pressure. There is no gas flow from annulus through the down-hole gas injection valve into the tubing. The production rate of gas/liquid is low. At the same time, gas is injected into annulus through the gas injection choke at the well head, causing the annulus pressure to build up

- When the annulus pressure has reached the bottom-hole tubing pressure, gas starts to flow into the tubing through the injection valve. The injected gas reduces the mixture density in the tubing and the bottom hole pressure starts to decrease due to reduced hydrostatic pressure. The liquid column with gas bubbles rises inside the tubing. As it approaches the well head, it causes the well head pressure to increase

- Gas flowing from annulus into the tubing causes the annulus pressure to decrease as the new gas injected at the well head through the injection choke is injected at a lower rate

- The reduced annulus pressure gives a subsequent reduction in gas injection rate into the tubing. This causes the velocity of the gas and liquid column in the tubing and hence the production rate, to decrease. The well head tubing pressure is now decreasing, and the bottom hole tubing pressure is again increasing. When bottom hole tubing pressure reaches the annulus pressure, the gas injection stops. The pressure starts to rebuild inside annulus

Exploration of the second, and less investigated instability phenomenon, was first encountered in oil industry in wells producing in an unstable cyclic manner,- in situations when the flow through the gas injection valve was known to be critical. Casing heading instability was hence not possible, and the unstable production was adressed to the "tubing heading" phenomenon. When the gas injection rate is constant, as is the case under critical flow conditions in the injection valve, variations in liquid flow into the tubing will change the mixture density and hence the phase fraction. This change in mixture density close to the pipe inlet will propagate through the pipe as a density wave (sometimes referred to as a void wave). The density wave mechanism can be interpreted as the propagation of mass fraction from the bottom of the pipe as a result of switching boundary conditions. The steps during one density wave cycle might be summarized as follows:

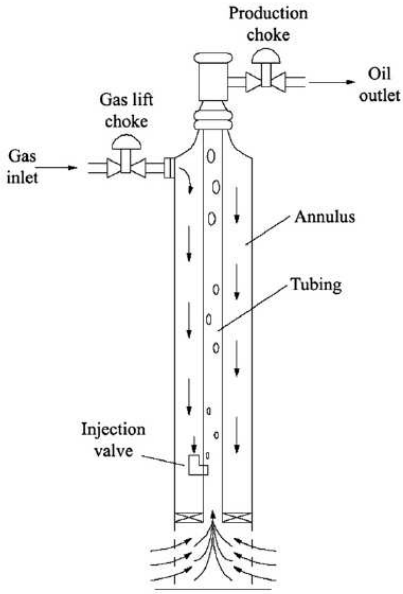

Figure 3: Gas lifted oil well completed with packer, from [3]

- At cycle start the tubing is filled with liquid. As the bottom hole pressure is higher than the reservoir pressure, there is no liquid inflow from the reservoir. Some of the gas injected through the injection valve travels towards the well head as bubbles, giving a small production. The main part of the injected gas is accumulated at the bottom hole

- At some point a gas mass sufficiently high to make the liquid column move upwards has accumulated at the bottom hole. As the liquid column travels upwards, the gas inside the column expands due to reduced hydrostatic pressure, giving rise to further acceleration of the flow. This causes a reduction in bottom hole pressure, which in turn enhances inflow from the reservoir. As a result, the bottom hole gass mass fraction drops close to zero

- As the liquid column approaches the well head, a peak in liquid production is reached. Shortly after observation of the peak in liquid production, the part of the column containing the major amount of the injected gas approaches the well head, giving rise to a peak in gas production

- As low gas fraction fluid flows in from the reservoir, the bottom hole pressure increases. As the major part of the lift gas injected during the cycle has been transported through the well head together with the liquid, the upward movement of the liquid column is reduced and finally brought to a rest. This gives rise to a further increase in bottom-hole pressure. A new cycle starts with injection of lift gas through the injection valve

In addition to the two phenomena casing heading and tubing heading one might encounter a third instability phenomenon. This is associated with configurations of the type shown in Figure 4, where gas and liquid is supplied to the inlet of an upward inclined pipe through a downward inclined pipe, in which the flow regime typically is stratified. The liquid supplied by the downward inclined pipe then blocks the low-point in an intermittent manner thus restricting the gas from passing the low-point continuously. When gas enters the upward inclined pipe a "natural" gas lift results. Steady or quasi-steady production characteristics may be obtained. Flow instabilities associated with this configuration are generally adressed as "terrain slugging". In terrain slugging the compressible volume is represented by the gas in the stratified region in the downward inclined pipe and by any gas volume upstream this pipe. When the downward inclined pipe is ending up with a riser, the terrain slugging phenomenon is sometimes referred to as riser slugging.

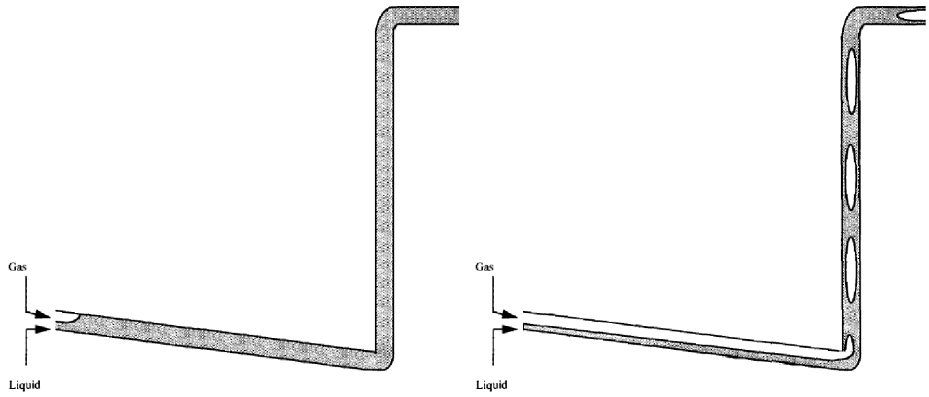

(a) Terrain slugging type I (b) Terrain slugging type II

Figure 4: Terrain slugging, from [4]

Terrain slugging is typically divided into two subcategories, namely terrain slugging type I and terrain slugging type II. The terrain slugging type I cycle is characterized by gas periodically entering the riser as a result of a corresponding periodical liquid blocking of the riser inlet. The type II cycle is characterized by gas continuously entering the riser inlet, thus resulting in a more stable "natural gas lift" behaviour. The terrain slugging type I cycle is typically called severe slugging. The terrain slugging type I cycle might be summarized by the following steps:

- The riser is initially filled with gas. Liquid from the two-phase flow in the pipeline enters the pipeline / riser low-point and starts to accumulate
- The liquid flowing towards the blocking adds to the low-point, causing the liquid level to grow in both the riser and the pipeline. This causes the pressure to increase in the pipeline

- As the liquid reaches the riser top, no further increase in hydrostatic pressure at the riser inlet is possible. As a consequence the gas and liquid supplied through the pipeline start to move towards the low-point
- As the two-phase flow reaches the riser inlet, gas bubbles start to propagate into the riser, reducing the mixture density and hydrostatic pressure. This promotes further gas inflow, finally resulting in the liquid column being blown out of the riser with a "burst-like" behaviour
- This causes the pipeline pressure to drop, after which a new liquid blocking is formed. A new cycle starts

The terrain slugging type II cycle might be summarized as follows:

- The riser is initially filled with liquid, and separated from the pipeline two-phase flow by a small liquid portion blocking the riser inlet. Upstream this liquid blocking the pipeline is subject to stratified two-phase flow conditions
- The stratified zone approaches the liquid blocking at the low-point at the riser inlet, resulting in some gas entering the riser, and a decrease in hydrostatic pressure at the riser inlet. This promotes increased gas inflow
- Gas flowing into the riser causes a decrease in pipeline pressure, which in turn lead to a decrease in riser gas inflow
- The reduced riser gas inflow results in a new pressure buildup in the pipeline, and the start of a new cycle

The severity of the terrain slugging type I cycle is mainly governed by the available upstream gas volume represented by the gas in the two phase flow in the pipeline. A large upstream gas volume requires a long time of pressure buildup and a large perturbation in gas volume for the pressure to decrease as the liquid has started to blow out from the riser. A small upstream gas volume requires a shorter pressure buildup time, implying higher slugging frequency and reduced slugging severity. This might be illustrated by carrying out a perturbation to the gas volume upstream the riser inlet, by means of removing a gas volume ΔV from the pipeline and adding it in the riser, as an analogy to the gas volume required to replace a liquid volume produced at the riser outlet. By the reasoning given in Equation 1, the relation given by Equation 2 can be used to estimate the effect on ΔP caused by a perturbation in gas volume. As can be seen, a large gas volume V in the denominator requires a corresponding large perturbation in volume ΔV for a desired pressure drop ΔP to result. The faster the pressure in the pipeline drops, the faster one slugging cycle ends, as the pipeline / riser inlet pressure represents the driving potential of the terrain slugging.

$$PV = n\bar{R}T \Rightarrow \frac{\partial P}{\partial V} = -\frac{n\bar{R}T}{V^2} \Rightarrow \frac{\partial P}{\partial V} = -\frac{P}{V} \tag{1}$$

$$\Delta P \sim -\frac{P}{V}\Delta V \tag{2}$$

The same reasoning can be used to demonstrate the effect of riser outlet choking on the slugging cycle. As the flow conditions in the riser tubing are known to be subcritical, one may utilize the fact that a pressure change at one location in the tubing will influence the pressure in the whole length of the tubing, and that an increase in outlet pressure due to choking, will make the pressure increase at the riser inlet. As the numerator in Equation 2 is increased, a corresponding reduced perturbation in volume ΔV is required to obtain the desired pressure drop.

The fourth instability phenomenon formation heading results in unstable production showing similar behaviour as when casing heading is present, but differs from the casing heading phenomenon in that gas is accumulating and discharging from the formation.

The unstable production phenomena encountered in oil and gas industry may be divided into two system instability groups:

- Static instability: When a system shows positive feedback to a flow perturbation. The following phenomena belong to this group:
  - Casing heading
  - Pipeline heading (terrain slugging)
  - Formation heading
- Dynamic instability: When a system shows negative feedback to a flow perturbation. The following phenomenon belongs to this group:
  - Tubing heading (density wave)

4 Literature survey

The primary topics found in the literature relevant to this thesis mainly concern previous experimental work, modelling efforts and stability analyses made on two-phase flow in vertical pipes, conducted to investigate the density wave instability, casing heading and terrain slugging. Some contributions found in the literature not directly aimed at investigating instability mechanisms in gas lift systems have been included as background information, if considered relevant to investigation of the gas lift technique.

A contribution to exploration of the density wave phenomenon was given by [5], by which a detailed observation of the density wave mechanism was utilized to derive a distributed delay model for the density wave propagation in the tubing. The physical model of void fraction in the pipe was based on the assumption of negligible friction due to low flow rates and constant temperature. In addition the gas was considered ideal and the pressure was assumed to vary linearily between the well inlet and outlet. A hydrostatic pressure balance based on mixture density in space and time was applied along with a slip relation and a linear definition of mixture density. Mass conservation equations were employed for both the phases, and the gas velocity was assumed to be constant.

Simulation results showed that the model was capable of simulating the density wave phenomenon. Next, a stability analysis of the model was conducted along with the design of a control strategy capable of controlling the model to a predefined steady state. The control strategy was then tested in OLGA 2000 showing similar performance as when applied to the model. The authors pointed out the gas injection rate as the critical parameter governing the magnitude of instability. They also indicated the main restriction of their control routine to be the requirement of downhole measurements.

Based on the results presented in [5], an extended study was presented by [6]. A casing model was derived and connected to the existing distributed delay model. Thereby a model representing a well system with both tubing and casing was obtained. A stability criterion obtained for the tubing model was combined with the dynamics of the casing to obtain a stability criterion representing the interconnected tubing and casing system. The stability of this system was studied through the small gain theorem. As by [5], OLGA simulations were performed for verification of the model.

A modified version of the distributed delay model proposed by [5] was given by [7]. Three major weaknesses in the model by [5] relating to the mixture density definition used, the assumption of no-slip between the gas and the liquid, and also the boundary conditions applied were pointed out. A new and improved distributed delay model was presented.

Instead of requiring no-slip implying that the gas mass fraction would be Riemann invariant, the new model chose the product of gas density and void fraction to be Riemann invariant, thus removing the requirement of making assumptions on the slip. Regarding boundary conditions it was shown that simplifications made by [5] introduced large error to the stability analysis compared to when an accurate boundary condition definition was used.

A contribution to the investigation of how the density wave and the casing heading phenomena interact with each other during simultaneous presence was given by [8]. A modified version of the casing heading model used by [3] was combined with the density wave model given by [7]. The combined model was used to simulate the two interacting instability phenomena and the results were compared with simulation results from OLGA, and with field data.

Another contribution to the investigation of gas-lift instability was given by [9]. The two main gas lift instability mechanisms, casing heading and density wave, were simulated for two hypotetical wells both representing typical North sea gas lift configurations. The simulations were performed in OLGA 2000, and conducted as parametric studies. The influence of different well settings were investigated. Both steady state and dynamic simulations were performed, and measures on the production loss due to gas lift instabilities were obtained. In addition the effect of application of feedback control to the unstable wells was investigated. The effect of four parameters (gas injection rate, gas-lift valve size, productivity index and choke opening) on the casing heading phenomenon was investigated. It was observed that static choking could be used for reduction of gas-lift instabilities, though at the cost of lost production. It was also observed that the same wells were enabled to produce close to the steady state production when feedback control was applied. During density wave simulations it was observed that no production resulted if the gas injection rate was set low enough. The fluid did not reach the tubing outlet. When the injection rate was increased, the liquid started to flow out of the tubing outlet in a periodic manner. Long periodic time was the typical characteristic of the flow. Further increase of the gas injection rate contributed to increase frequency and amplitude of the oscillations. When the injection rates were high enough, the well stabilized. At the lowest gas injection rates the density wave instability was observed to slightly enhance the production, but it was concluded that the range of gas injection rates capable of increasing the production was not of interest in real gas lift wells. The capability of the OLGA simulator of simulating the main characteristics of the casing heading phenomenon was demonstrated. In situations where the casing heading phenomenon was known to be absent, the observability of the density wave was demonstrated. Air and water was used as simulation fluids, and the simulations were conducted isothermal. All the simulations were initiated with the steady state preprocessor result as initial condition.

Another contribution to numerical simulation and experimental investigation of the density wave phenomenon was given by [10]. The experiments were conducted in a two-phase air-water test facility consisting of a 15 [m] long vertical pipe representing the riser with an internal diameter of 45 [mm]. The lift gas was injected at a position 0.5 [m] from the pipe inlet at a constant mass flow rate. The riser outlet was equipped with a choke which could be manouvered by a control algorithm. The flow loop was exposed to atmospheric pressure downstream the choke. The pressure at the riser inlet was equivalent to the hydrostatic pressure from the liquid level in the separator tank which was located approximately 3 [m] below the pipe outlet. In addition another valve was included upstream the riser inlet to enable varying productivity index PI $[kg/Pas]$. Experiments carried out showed that the lift gas injection rate had to be kept low to make the density wave

instability arise. High lift gas rates promoted stable production. In addition the valve at the inlet had to be kept fully open to make the density wave instability appear. The density wave phenomenon was successfully reproduced by OLGA simulations, although the unstable regions in stability maps produced during the experiments, were slightly larger than the unstable regions in the maps resulting from the simulations. In addition simulations where performed for a full scale well producing only water with air as lift gas. The well simulated was 2600 [m] deep with lift gas being introduced 100 [m] above the well inlet at a rate of 0.4 $[kg/s]$. The effect of manual choking at the well outlet was tested during the simulations. The density wave phenomenon was observed to completely dampen out at a valve opening of 20 %. Nevertheless the average liquid production from the well was higher in this situation compared to the average liquid production with 100 % choke opening. A control algorithm for the outlet valve was then implemented in OLGA, using only the pressure right upstream and right downstream the valve as input parameters. Simulation results showed that inclusion of the control algorithm significantly increased the productivity of the well. Liquid production rates close to the steady state solution were observed.

The numerical simulations indicated that the density wave phenomenon can appear when a well is operating at the unstable equilibrium of the Inflow Performance Relationship (IPR) and the Tubing Performance Relationship (TPR). The curve representing (IPR) relates the mean liquid flow rate to a given pressure drop in the reservoir. The curve representing (TPR) predicts the liquid flow rate to the pressure drop in the tubing for a fixed ratio between gas injection rate and average liquid inflow rate. Two intersection configurations between (IPR) and (TPR), plotted for different Gas Liquid Ratios (GLR), are shown in Figure 5. Flowing Bottom Hole Pressure (FBHP) is plotted at the vertical axes and liquid flowrate at the horizontal axes.

The two points of intersection presented in both Figure 5a and 5b represent two possible points of operation. The intersection to the left in each plot (at the lowest liquid flow rates) represent unstable equilibria. This may be illustrated by introducing a perturbation by a small reduction in liquid inflow in both the plots. It can be observed that the (FBHP) must now be larger than the value the reservoir can provide, which is not possible. The well will die. If a small positive perturbation in liquid inflow is applied, a lower (FBHP) than the value provided by the reservoir is needed. The liquid flow rate values will then increase towards the values of the right intersection points. These points of intersection represent the points of stable gas lift operation. The right point of intersection in Figure 5a represents friction dominated flow. This can be concluded from the positive slope of the (TPR) at the intersection. The right point of intersection in Figure 5b represents an operational condition where friction is less important. This can be seen from the negative slope of the (TPR) at the point of intersection. The two points of intersection in Figure 5b are located close together, indicating that a gas injection rate close to the minimum value required for the well to flow is used. The points of intersection in Figure 5a and 5b where density wave instability may occur, are concluded to correspond to the left points of intersection in both figures, i.e. at the unstable equilibria.

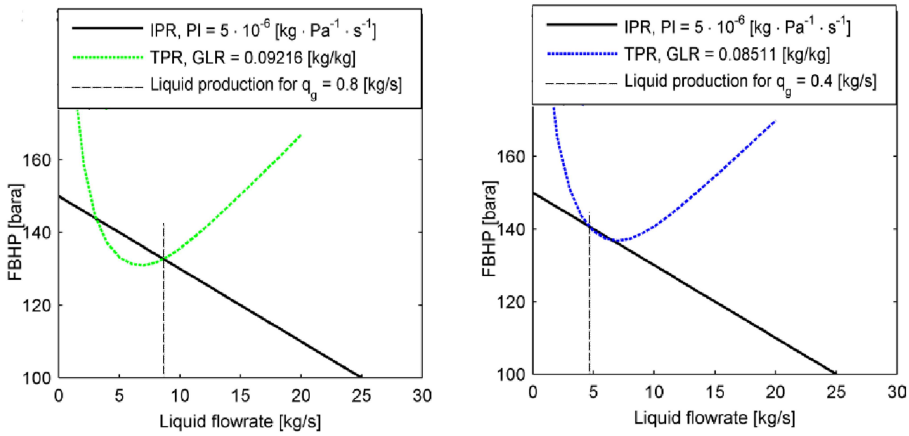

(a) Stable equilibrium

(b) Unstable equilibrium

Figure 5: Typical (IPR) and (TPR) curves, from [10]

An analysis of the stability and performance of an airlift pump was made by [11]. The experimental setup used is shown in Figure 7a. A model based on separate one dimensional mass and momentum equations for air and water was developed. The assumption of irrotational potential flow in the region from the water free surface to the air injection point was applied. The ideal equation of state and an empirical bubble rise velocity correlation was used as closure models. The water was modelled incompressible and the air was injected through a porous nozzle ensuring production of small bubbles. Both friction and variation of variables across the pipe cross section were neglected. Based on the model, analytical solutions describing the pump characteristics were obtained. These solutions were compared with the experimental results on non-dimensional form. Good correspondence was observed. A linear stability analysis was performed based on the model and used for generation of neutral stability curves. During experiments, the flow was observed stable at the lowest air injection rates. As the rate was increased, unstable conditions were encountered. Further increase of the injection rate was observed to stabilise the flow. This might indicate that the unstable phenomenon observed was due to density wave instability. The size of the injected bubbles was observed to have large influence on the gas injection rates at which unstable production was obtained.

Another contribution to the investigation of the density wave mechanism in vertical risers was given by [12]. A model describing two-phase flow in a vertical riser was developed based on mass and momentum balances on mixture properties in space and time along with the assumption of incompressible gas and liquid. The lift gas injection rate was set constant, and an equation describing the inflow performance was included together with a choke equation at the tubing outlet. The model was then linearized by replacement of instantaneous terms by mean terms and fluctuation terms. Second order perturbation terms were left out. After

introduction of a delay term, the model was normalized. The resulting equation described the propagation of a density wave in the tubing by an infinite number of solutions. After insertion of a wave solution, a characteristic equation was obtained, which was used for generation of neutral stability relations. As the generation of a neutral stability curve succeded, it was concluded that the density wave mechanism would probably occur if the gas was assumed incompressible. Further it was concluded that density wave instability is not likely to occur in real well systems when gas is assumed incompressible, as the characteristic parameters required to obtain density wave instability are far away from normal operational conditions. A new modified linear stability analysis similar to the analysis performed by [11] which included gas compressibility was then conducted. The new modified analysis was then used to investigate the effect of productivity index, tubing diameter, system pressure and well depth on the stability of the well. It was observed that density wave instability was impossible to occur in naturally flowing wells, no matter how low gas injection rate was set. Based on this observation, a hydrostatic pressure balance gave the relation in Equation 3 as a necessary criterion for the density wave to occur. P_R is the reservoir pressure and P_{sep} is the separator pressure.

$$\frac{P_R - P_{sep}}{\rho_l g L} < 1 \tag{3}$$

It was also observed that an increase in productivity index, tubing diameter, system pressure and well depth may increase the density wave instability. Dynamic simulations in OLGA were performed and compared to the results from the linear stability analysis. Good correspondence was observed. Static choking was demonstrated to effectively dampen casing heading instability through simulations. The effect of static choking on density wave instability was demonstrated to either dampen or further increase the severity of the instability, depending on what combinations of other characteristic parameters being used.

The effect of the density wave phenomenon on the stability of air lift pumps was investigated by [14]. A linear stability analysis was conducted for a set of transient flow equations and its predictions compared with experimental results. A numerical model and a stability criterion were presented. Both the experimental results and the stability analysis showed that the influencing parameters had complex effects and were strongly interacting. The same variation of a parameter could be observed to have opposite effects depending on the values of the other influencing parameters applied. The effect of the compressibility of the gas between the air injection valve and the air lift pump injection point was observed to strongly influence the magnitude of instability. A definition of unstable air lift pump operation was given, namely oscillations in liquid production at a frequency of 1 [Hz] or lower. The pumping characteristics were at some operating conditions (low air injection rates) reported to show violent expulsion of liquid jets at the pump outlet.

The flow regime behaviour in a riser transporting heavy liquid metal was investigated experimentally by [15],[16]. The experimental work was carried out with water and air, and subatmospheric pressure was utilized to obtain the correct similarity parameters of the real heavy liquid metal system. It was demonstrated that the transition from bubbly flow to slug flow was strongly influenced by the

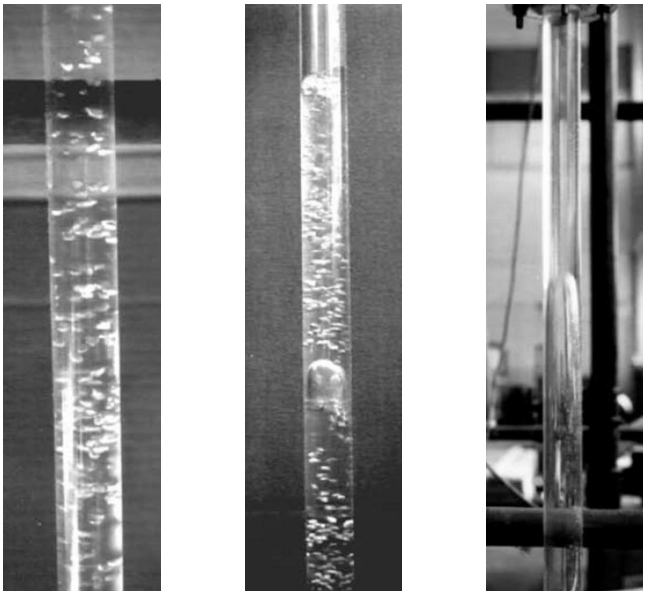

(a) Bubbly (b) Bubbly to slug transition (c) Slug

Figure 6: Flow regimes, from [13]

density wave phenomenon.

Other contributions to the investigation of the density wave phenomenon by use of two-fluid models have been given by [17], [18] and [19]. Stability analyses of the two-fluid models were performed, and the closure relations used in combination with the two-fluid models were observed to have great influence on the density wave characteristics. Small phasic slip was observed to enhance dampening of the unstable behaviour.

A contribution to the experimental investigation of density wave propagation in bubbly flows was given by [20] which conducted a series of experiments on oil lifted by air inside a vertical pipe represented by a concentric annulus with hydraulic diameter $D_h = 17.4$ $[mm]$ and with a length of 1 $[m]$. Several probes capable of detecting void fraction were distributed along the pipe length axis, and spectra made by cross correlation of the signals from consequtive probes were used to determine the celerity of the density waves. Two simultaneous density wave propagation observations were made. The low celerity case was represented by a bubbly flow density wave. The fast celerity observation was related to the propagation of bubble clusters. The size of the clusters was found to increase with increasing void fraction, and the celerity of the clusters was observed to increase with increasing global void fraction. After transition to slug flow the celerity was observed to correspond well with the terminal rise velocity of Taylor bubbles.

[21] gives an overview of several earlier contributions to investigation of bubble size influence on gas lift efficiency. Simulation results and experimental data are

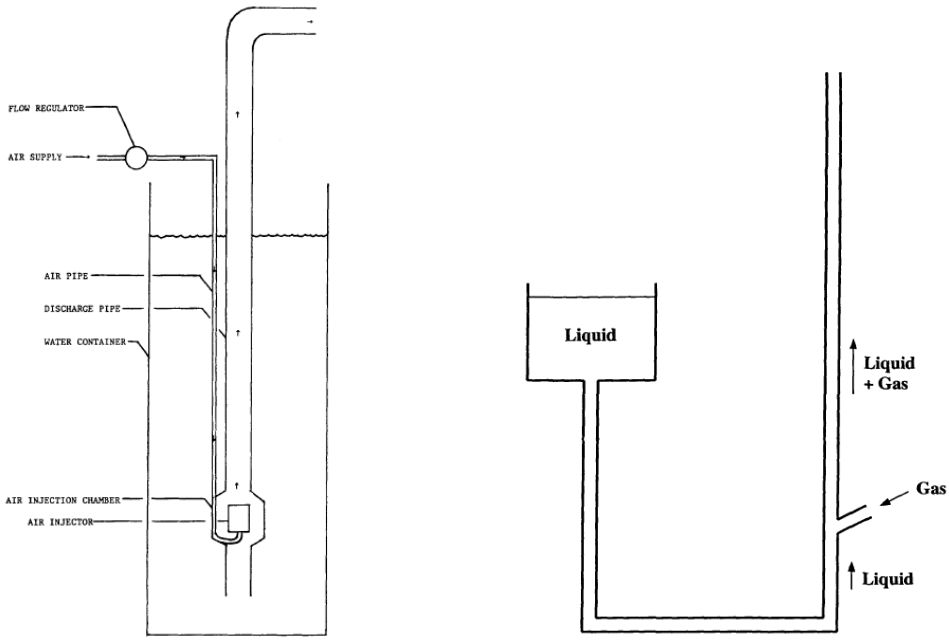

(a) Experimental setup used by [11] (b) Experimental setup used by [14]

Figure 7

presented, and the bubble size is pointed out as a critical parameter for the gas lift efficiency. A decreased bubble size contributes to postpone the transition from bubbly flow to slug flow by allowing a higher void fraction to define the point of transition. This contributes to reduce the bubble relative velocity and increase the bubble recidence time, thus promoting better utilization of the injected lift gas. Several methods for avoiding bubble coalescence, and increasing bubble breakup are presented.

A contribution to the development of general stability criteria for gas lifted wells was given by [22]. Based on first order stability analysis of gas lift systems, the Asheim casing heading stability criterion 1 and 2 were developed. The first criterion quantifies the stabilization as a result of the inflow responses of reservoir fluid and lift gas. The second criterion quantifies stabilization caused by a reduction in gas system pressure. Both the reservoir system and the gas injection system were assumed to respond to a decrease in tubing pressure. The reservoir system response is stabilizing as a decrease in tubing pressure causes heavy fluids from the reservoir to enter the tubing. The gas injection system shows a destabilizing effect as a reduction in tubing pressure enables even more gas to flow into the tubing through the injection valve. This gives a reduction in tubing mixture density and hydrostatic pressure which increases the gas inflow.

Another contribution to the development of stability criteria for flowing oil wells and gas-lifted wells was given by [23]. A mathematical model describing the relevant

well and reservoir variables was developed. The differential equations describing the pressure dependent variables were then subject to Laplace transformation and subsequent combination by Cramer's rule. A characteristic equation containing three constants was then obtained. A well was predicted stable when all three constants showed the same sign. Othervise the well was predicted unstable.

Based on both the stability criteria by [22] and [23], a new unified stability criterion for continuous gas lift wells was proposed by [24]. Field data were presented to illustrate the behaviour of casing heading instability. The unified model took into account different flow regimes in the surface gas injection valve and the bottom hole gas injection valve. Good correspondance between the new model and data on casing heading action from Prudhoe Bay, Alaska, was observed.

Another contributor to the development of stability analysis tools for continuous flow gas lift wells was [25]. Based on the combination of three separate models describing the well, the gas injection system and the reservoir, a gas lift well model was developed. The model was then used in combination with the stability criteria by [22] and [24] for generation of stability maps, which in turn were compared with field data. Based on these maps, the effect of injected gas flow rate, injection valve size and tubing diameter was investigated.

An early contribution to experimental investigation of continuous flow gas lift was given by [26]. The resulting characteristics were presented in terms of maps which became subject to comparison with calculations. Severe heading in a gas lift system was observed when the gas injection rate was reduced below a certain level. It was concluded that in continuous gas lift configurations, the lift gas should be injected as deep as possible allowed by the available lift gas pressure. It was emphasized that the maps obtained were likely to be fairly system dependent, and that they not nessesariliy were comparable to other well configurations. The gas lift configuration used during the test was based on lift gas being transported in a thin pipe inside the annulus, thus reducing the compressible volume possible to cause casing heading. This configuration was reported successful by means of an increased range of gas mass injection rates providing stable gas lift conditions.

The use of general stability maps for continuous gas lift wells was also investigated by [27]. Both theoretical and experimental maps were presented. To investigate the stability in deep offshore wells, a field test was conducted. Different gas-lift stability criteria found in the literature were compared and tested against the stability maps. Based on the study, general recommendations for applicability of the different criteria in both design and operation strategy development were given. The study revealed that most of the stability criteria tested underestimated the unstable region.

[28] gave a description of the casing heading phenomenon and addressed the subject of equilibrium conditions in continuous-flow gas lift wells by the introduction of inflow performance relationship and tubing performance relationship diagrams. A possible stepwise procedure on how to design a stable gas lift system and its corresponding diagram is given. Based on the subjects presented by [28], several procedures for avoiding casing heading was given by [29]. A numerical model, originally developed to investigate formation heading, was modified to enable numerical simulations for verification of the different stabilization remedies

proposed. The effect of a deeper injection point as well as both injection and wellhead gas valve sizes was investigated. Different combinations of annulus pressures and injecion valve sizes were also tested.

[30] explains the difference between two possible instability mechanisms in gas lift systems, namely static and dynamic instability. The concept of (IPR) and (TPR) originally proposed by [31] for a naturally flowing well was utilized to explain the mechanisms. The (IPR) and (TPR) were then redefined for use in gas lift calculations, resulting in Shifted Inflow Performance Relationship (SIPR) modified to include the pressure drop from perforation to injection point. The (TPR) was modified not to include pressure drop from the point of perforation to the injection point. In addition, Gas Discharge Performance Relationship (DPR) was introduced, giving the relation between gas flow rate through the injection valve and pressure drop in annulus. A method was then given for combination of these three performance relationships to obtain the Gas Injection Performance Relationship (GPR) which, at intersection with (DPR), gives possible operational points of the gas lifted well. It was emphasized that these points of intersection do not necessarily represent stable points of operation. A gas lift system was defined as subject to static instability if when a small pertubation in flow conditions is introduced, another steady state condition is not obtainable in the vicinity of the original point of operation. A flow was defined as subject to dynamic instability if inertia and feedback effects were known to govern the process. Manual adjustments made on the surface choke and wellhead choke were adressed as less effective methods of avoiding static instability, as they usually cause significantly higher gas injection rates and lower liquid productions rates. Proper injection valve sizing was proposed as the most effective remedy in designing away static instability. A method for assisting the determination of correct injection pressure and valve size was presented based on (GPR) and (DPR) relationships.

[32] developed a casing heading model for a gas lifted well based on two-phase mass and momentum balance equations. A linear stability analysis was performed. A small scale experimental setup was built and used for finding stability limits, oscillation frequencies and the lags of characteristic quantitites along the tubing. The experimental results were compared to results from the linear stability analysis. Increase in gas injection rate, increase in productivity index and increase in head loss at the gas injection point was observed to enhance the stability of the well.

[33] presented a new transient gas lift model and its implementation in a simulator. Conservation equations of mass, momentum and energy formed the base of the model. Both co-current and counter-current multiphase simulation capability was demonstrated. Simulation examples were presented, including three cases aiming at investigating gas lift instability. The first case included a simulation of unstable gas lift. The instability mechanism was reported to be casing heading. The two other cases were simulations of two different remedies for stabilization of the first case. The first remedy involved an increased injection pressure and an increased injection valve size. An increased gas injection rate was hence obtained. The corresponding simulation showed stable gas lift results. The second remedy was replacement of the original injection valve with a new nozzle-venture valve ensuring critical flow conditions in the injection valve and hence constant gas mass

injection rate. The corresponding simulations showed stable gas lift results. A comparison of the simulator stability predictions and the stability criteria by [22] was given.

An early contribution to modelling of the casing heading phenomenon in naturally flowing oil wells was given by [2]. The casing heading cycle was described as a four-stage process, each stage was described by mass and momentum conservation equations. The equations were integrated numerically by a simultaneous procedure, and the predictions were compared with experimental results from a laboratory setup capable of reproducing casing heading instability under air/water two-phase conditions. The severity of the casing heading cycle was observed to increase with either decreasing gas or liquid superficial velocity. The pressure fluctuation range was observed to increase with increasing available annulus volume.

An early contribution to automatic control of the casing heading phenomenon in naturally flowing oil wells was given by [34]. Based on the model developed by [23], involving algebraic and differential equations which were combined to a characteristic equation by use of Laplace transforms, the root locus technique was applied to investigate the performance of different regulator principles. It was found that shallow natural flowing oil wells could be controlled by a P (Proportional) regulator or a PD (Proportional Derivative) regulator. Deeper wells were observed to require PI (Proportional Integral) and PID (Proportional Integral Derivative) regulators. The concept of active well/riser control is an important field of current multiphase flow research for stabilization of severe slugging as well as gas lift instabilities. Several contributions to stabilization of these phenomena have been given. [35] and [36] may be mentioned among others.

A contribution to active control of the casing heading instability was given by [3]. A simplified mathematical model based on mass of gas in annulus and mass of gas and oil in the tubing was first validated against OLGA simulations showing satisfactory results during simulation of the casing heading phenomenon. Based on the mathematical model and a stability analysis of its governing equations, an observer only relying on topside measurements was proposed for use in active control. The performance of the control scheme was investigated by simulations and its practical applicability demonstrated during laboratory experiments. It was shown that the casing heading instability could be dampened by the control routine only relying on topside measurements. The production rate obtained during experiments conducted with the control routine, was observed to be 5% higher than the corresponding open-loop maximum production rate.

An early contribution to numerical simulation of two-phase flow in vertical pipes was given by [37] by the development of a simulator, based on the consept of lifting potential and empirical correlations representing mist flow, slug flow, bubble flow, single phase flow and correlations for the transition between them. An example case was given and the ability of the simulator to capture transient phenomena relating to the compressible casing volume was stated. The effect of different casing diameters was investigated.

Based on mass, momentum and energy balances a new gas lift model was presented in [38]. The model was developed as a tool for optimization of typical gas lift parameters such as injection mass rate and valve parameters at steady state

conditions and was hence not a tool capable of simulating transient phenomena. The gas lift process was assumed adiabatic during the modelling. Calculation of phase transition along the pipeline was implemented in the model.

[39] investigated the mechanisms of severe slugging in a pipeline riser system, and encountered four different flow instability characteristics with their pipe configuration, defined as Type 1, characterized by damped oscillations leading to steady flow, Type 2 characterized by cyclic flow without fallback and Type 3 characterized by cyclic flow with fallback. Type 4 was defined as regions outside the Bøe criterion, comprising steady flow or unsteady oscillations. It was found that steady flow can exist within the severe slugging region, predicted by the Bøe criterion at high liquid flowrates. A region outside the Bøe criterion was also found, representing an unstable steady state, leading to unstable oscillations. The liquid fallback phenomenon was observed at very low liquid flowrates. The term severe slugging was used for the quasi-steady cyclic prosess when the riser blowout shows a severe behaviour or occurs as a spontaneous unstable expansion.

A simplified transient model for pipeline-riser systems capable of predicting the behaviour of severe slugging was presented by [40]. The model was based on one-dimensional, gravity-dominated flow in both the pipeline and the riser. A drift flux model was used for flow in the riser and the liquid phase was assumed incompressible. No mass transfer between the phases was considered. The model was tested against a selection of experimental data. Good agreement was observed inside the Bøe region above the severe slugging stability line. The model was capable of predicting slugging outside the Bøe region.

Different methods for avoiding severe slugging were investigated by [4]. Both the effects of riser outlet choking and introduction of gas lift were investigated. Both the methods proved capable of avoiding severe slugging. Choking proved to be an effective solution. It was found that a relatively large injection rate of lift gas was needed to stabilize the flow, causing the flow regime to approach annular. Gas injection was observed to decrease the slug length and increase the cycle frequency. Theoretical models for eliminaton of severe slugging by choking and gas lift were developed and tested against the experimental results.

The mathematical expression in Equation 4 giving the necessary conditions for severe slugging to occur was derived by [41]. When the relation is satisfied, severe slugging is assumed to occur. The expression was derived from a force balance between the gas pressure in the pipeline, P_p, and the hydrostatic pressure at the riser inlet applied to the liquid portion blocking the riser inlet.

$$U_{sl} \geq \frac{P_p}{\rho_l g \alpha L} U_{sg} \tag{4}$$

The intermittent presence of liquid blocking the riser inlet typically follows a frequency specific for the given riser system. The lower the frequency, the longer it takes for liquid to build up in the pipeline. One contribution to determination of this frequency was given by [42], where an approach based on a simplified mathematical model for estimation of liquid buildup in the pipeline and slug period was proposed.

Two possible methods for elimination of severe slugging based on by-passing

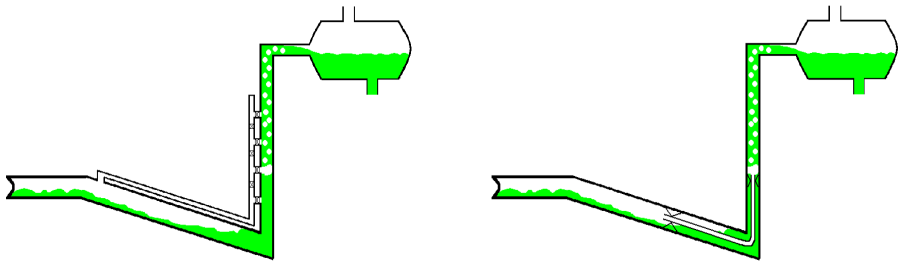

(a) Severe slugging elimination Method I by [43]

(b) Severe slugging elimination Method II by [43]

Figure 8

of the pipeline gas past the riser low point were proposed by [43]. The methods are shown in Figure 8 and have much in common with the gas lift technique. The gas transfer reduces the hydrostatic pressure an reduces the pipeline compressibilty. The severe slugging model by [40] based on a one-dimensional drift-flux formulation was modified to enable gas entry at any point along the riser. All pressure losses associated with the by-pass system and its valves were ignored. The modified model was tested against existing experimental data from riser slugging and then used to predict the potential of the two proposed riser slugging elimination techniques. Both the methods were found to eliminate severe slugging. Method I is pointed out as more feasible as it does not represent an obstacle inside the pipe and hence enables pigging.

5 The experimental setup

The small scale experiments to be simulated originate from a master thesis by [44] and were conducted with water as production fluid and air as lift gas. The experimental setup shown in Figure 9 formed the base for the third out of three experiment series. The first two series were made with a similar setup, but without the riser inlet bend configuration in which gas was allowed to accumulate and then discharge into the riser in a cyclic manner. This experimental configuration was observed to give unstable production with the characteristics of the density wave instability mechanism. This third series has hence been chosen for simulation and comparison in this work. The components used are listed in Table 1.

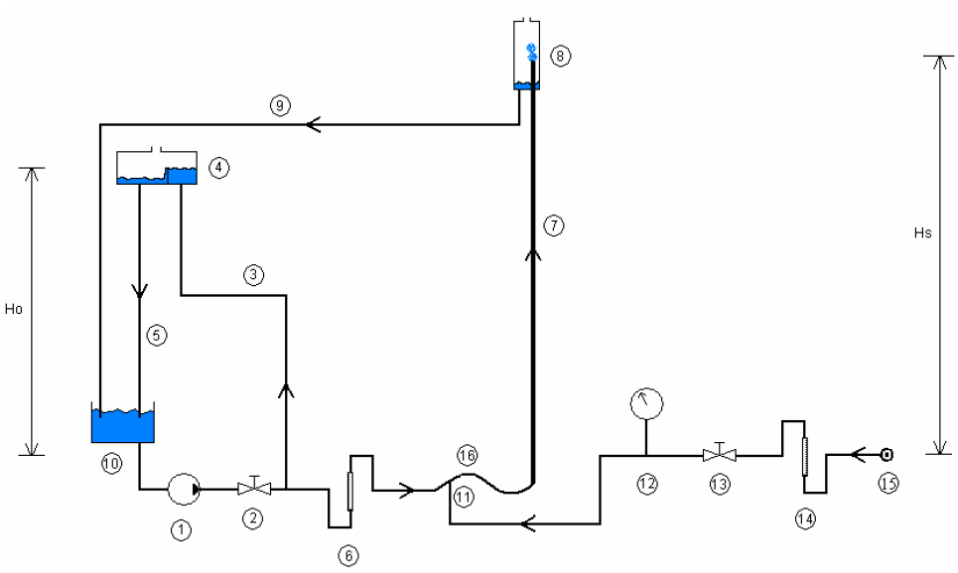

Figure 9: The experimental setup used by [44]

The liquid column between the weir and the riser inlet was utilized to ensure a constant hydrostatic pressure at the riser inlet. The water mass rate produced through the riser varied with the gas injection rate. To ensure water continuously flowing over the weir, the circulation pump had to deliver a variable liquid flow rate. This variable flow rate was obtained by adjustments on the choke at the pump outlet and the pump back pressure. Both the liquid level at the weir and the riser outlet were exposed to atmospheric pressure. The weir and riser outlet heights relative to the injection point are:

- $H_0 = 5.65[m]$
- $H_s = 6.20[m]$

ID in Figure 9	Component
1	Pump
2	Choke
3	Flexible hose 16 [mm] internal diameter
4	Weir
5	Flexible hose 20 [mm] internal diameter
6	Flowmeter water
7	Riser plexiglass 16 [mm] internal diameter
8	Separator
9	Flexible hose 20 [mm] internal diameter
10	Water tank
11	Air injection point
12	Manometer
13	Choke
14	Flowmeter air
15	Compressed air supply 1 [barg]
16	Bend for injected gas to accumulate

Table 1: Experimental setup components table

The lift gas was supplied by the workshop air supply at a constant pressure of 1 [$barg$], and the injected gas mass rate was kept constant by a reduction valve. The injected gas volumetric rate was monitored by a rotameter mounted between the reduction valve and the workshop air supply where the pressure was kept constant at 1 [$barg$]. The injected gas mass rate was obtained by multiplication with air density at 1 [$barg$].

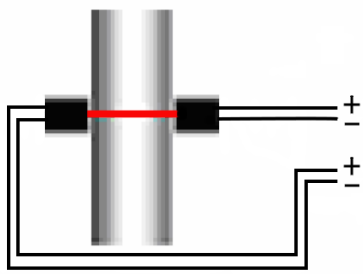

Figure 10: Pair of light emitting diode and detector diode used by [44]

The liquid holdup was monitored at five equally spaced locations with an intermediate distance of 1.5 [m] along the riser by pairs of optic diodes. One diode emitting a light beam and another diode detecting the light as shown in Figure 10. The exact location of the first diode has not been found. A coloring agent was added to the water, enabling the water to break the light beam. When only air was present at a diode location, the beam was not broken. LabWiew was used for data sampling. At the lower gas injection rates the liquid flow rate was reported to periodically exceed the rotameter scale. Liquid flowrate measurements for comparison with simulation results are hence not available. A typical void fraction plot from [44] is shown in Figure 142. The characteristic ranges of gas injection rates reported are:

- $\dot{m}_g = 0.00[kg/s]$ to $\dot{m}_g = 0.39 \cdot 10^{-5}[kg/s]$: There is no liquid production. No information is given on flow regime, but one should expect bubbly flow to be the only possible mechanism for gas trasport out of the system in this low gas injection range

- $\dot{m}_g = 0.39 \cdot 10^{-5}[kg/s]$ to $\dot{m}_g = 6.39 \cdot 10^{-5}[kg/s]$: There is unstable liquid production, with injected gas periodically accumulating in the bend at the riser inlet, and water periodically produced from the riser outlet. The volumetric liquid flowrate is on some occasions too large for detection by the rotameter

- $\dot{m}_g = 6.39 \cdot 10^{-5}[kg/s]$ to $\dot{m}_g = 10.40 \cdot 10^{-5}[kg/s]$: Liquid is continuously produced from the riser outlet. No injected gas accumulates in the bend

(a) Riser pipes interconnected with flexible hose

(b) Assembled riser with auxiliary equipment

Figure 11: The experimental setup used by [44]

μ_l	$1.002 \cdot 10^{-3}$	$[kg/m \cdot s]$
μ_g	$1.825 \cdot 10^{-5}$	$[kg/m \cdot s]$
ρ_l	998	$[kg/m^3]$
M_g	28.97	$[g/mol]$
$\sigma_{g/l}$	$7.29 \cdot 10^{-2}$	$[N/m]$

Table 2: Experimental fluid properties

6 The slug tracking simulator SLUGGIT

The slug tracking simulator SLUGGIT was originally developed by [45]. The original version has later been subject to further modelling contributions aimed at solving spesial flow problems. Three different contributors to the code development are [46], [47] and [48]. Three different program code versions resulted, capable of simulating pigging, detecting hydrodynamic transitions by use of a built in slug capturing scheme and simulating roll waves respectively. The code version developed by [48] is based on the version by [46] and has been used as a base for the modifications implemented in this master thesis.

The main moving building blocks in the SLUGGIT simulator are called sections and borders. The sections are further divided into slug sections representing incompressible slugs with zero void fraction, and bubble sections representing compressible bubbles. Figure 12 illustrates how sections and borders are related to each other. An upwind staggered grid formulation is used, resulting in the definition of scalar quantities in the middle of the sections. Phase velocities are defined at the borders separating the sections. Phase velocitites in sections are calculated as the average of the corresponding left and right section borders.

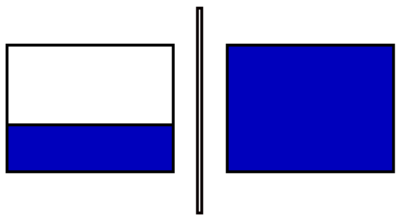

Figure 12: Typical building blocks used in SLUGGIT. From left to right; bubble section, bubble/slug border and slug section

The one-dimensional mass balance equation for each phase is given by Equation 5, which upon integration over the phase volume V_k within a computational section gives Equation 6. This integrated mass balance equation is solved implicitly in stratified sections and explicitly in slug sections, [48].

$$\frac{\partial \rho_k}{\partial t} + \frac{\partial(\rho_k U_k)}{\partial z} = \dot{\rho}_k^s \tag{5}$$

$$\frac{\partial m_k}{\partial t} + \oint_{A_k} \rho_k (U_k - U_b) dA = \dot{m}_k^s \tag{6}$$

Equation 6 is used as a base for derivation of the pressure equation for the two-fluid model given by Equation 10. m_k is replaced with $\rho_k V_k$ and subsequent division by phase density ρ_k is carried out. This gives Equation 7.

$$\frac{V_k}{\rho_k}\frac{\partial \rho_k}{\partial t} + \frac{\partial V_k}{\partial t} + \frac{1}{\rho_k}\oint_{A_k} \rho_k (U_k - U_b) dA = \frac{\dot{m}_k^s}{\rho_k} \tag{7}$$

An equation of state for each of the phases k giving the phase density $\rho_k(P,T)$ becomes subject to partial differentiation with respect to P and T, resulting Equation 8. This expression is then inserted into Equation 7 as a replacement for the $\frac{\partial \rho_k}{\partial t}$ term. This gives Equation 9.

$$\frac{\partial \rho_k}{\partial t} = \left(\frac{\partial \rho_k}{\partial P}\right)_{T_k} \frac{\partial P}{\partial t} + \left(\frac{\partial \rho_k}{\partial T}\right)_P \frac{\partial T_k}{\partial t} \tag{8}$$

$$\begin{aligned} &\frac{V_k}{\rho_k}\left[\left(\frac{\partial \rho_k}{\partial P}\right)_{T_k} \frac{\partial P}{\partial t} + \left(\frac{\partial \rho_k}{\partial T}\right)_P \frac{\partial T_k}{\partial t}\right] + \frac{\partial V_k}{\partial t} \\ &\qquad + \frac{1}{\rho_k}\oint_{A_k} \rho_k (U_k - U_b) dA = \frac{\dot{m}_k^s}{\rho_k} \end{aligned} \tag{9}$$

Equation 9 is then summed for all phases k, giving the pressure Equation 10. This pressure equation is solved in the bubble sections only.

$$\begin{aligned} &\sum_k \frac{V_k}{\rho_k}\left[\left(\frac{\partial \rho_k}{\partial P}\right)_{T_k} \frac{\partial P}{\partial t} + \left(\frac{\partial \rho_k}{\partial T}\right)_P \frac{\partial T_k}{\partial t}\right] + \frac{\partial V}{\partial t} \\ &\qquad + \sum_k \frac{1}{\rho_k}\oint_{A_k} \rho_k (U_k - U_b) dA = \sum_k \frac{\dot{m}_k^s}{\rho_k} \end{aligned} \tag{10}$$

The one-dimensional momentum balance equation for phase k is given by Equation 11. Intergration of Equation 11 over phase volume V_k gives the momentum balance for phase k represented by Equation 12. In stratified sections the pressure P_k is related to the pressure P at the interface between gas and liquid by inclusion of a hydrostatic contribution in the liquid layer by the relation given in Equation 13.

$$\frac{\partial(\rho_k U_k)}{\partial t} + \frac{\partial(\rho_k U_k^2)}{\partial z} = -\frac{\partial P_k}{\partial z} + \frac{\partial \tau_k}{\partial z} - \rho_k g \sin\theta \tag{11}$$

$$\frac{\partial(m_k U_k)}{\partial t} + \oint_{A_k} \rho_k U_k (U_k - U_b) dA = -V_k \frac{\partial P_k}{\partial z} + \oint_{A_k} \tau_k dA - m_k g \sin\theta \tag{12}$$

$$\frac{\partial P_k}{\partial z} = \frac{\partial P}{\partial z} + \rho_k g \cos\theta \frac{\partial h_l}{\partial z} \tag{13}$$

The velocity of the slug tails (the slug rear border) corresponds to the bubble nose velocity of the consequtive bubble nose. This bubble nose velocity is determined from the correlation in Equation 14 which in combination with C_0

and U_0 correlations by [49] decribes the nose velocity of Taylor bubbles. The slug front velocity is determined from a mass balance across the slug front which in its rearranged version is given by Equation 17. U_l is the liquid velocity in the slug which corresponds to the local mixture velocity U_m when the slug is assumed incompressible and the slug void fraction is zero. H_{bubble} and $U_{l,bubble}$ correspond to the holdup and the liquid phase velocity in the neighbouring bubble section.

$$U_{tail} = U_b = C_0 U_m + U_0 \tag{14}$$

$$C_0 = \begin{cases} 1.05 + 0.15\sin^2\theta & |U_m| < 3.6\sqrt{gD}/\cos\theta \\ 1.2 & |U_m| > 3.6\sqrt{gD}/\cos\theta \end{cases} \tag{15}$$

$$U_0 = \begin{cases} (0.35\sin\theta \pm 0.54\cos\theta)\sqrt{gD} & |U_m| < 3.6\sqrt{gD}/\cos\theta \\ 0.35\sqrt{gD}\sin\theta & |U_m| > 3.6\sqrt{gD}/\cos\theta \end{cases} \tag{16}$$

$$U_{front} = \frac{U_l - H_{bubble}U_{l,bubble}}{1 - H_{bubble}} \tag{17}$$

The time integration is implicit, thus allowing larger time steps. The phase fractions of liquid and gas should always sum to one to ensure mass conservation. This criterion is hence checked every time step. Any deviation from unity is compensated by the addition of a mass correction term in the discretized version of the pressure Equation 10 at the next time step. This prevents any mass error from growing in time. The computational sequence during one time step in SLUGGIT is, [46]:

1. Calculate border velocity coefficients
2. Solve pressure and momentum equations simultaneously
3. Update phase velocities and pressures
4. Solve mass equations
5. Update gas and liquid masses
6. Solve energy equations
7. Update enthalpies, densities and volume error
8. Section management operations with splitting and merging of computational sections

The frictional shear stress is included in terms of the Darcy friction factor definition given in Equation 18, where f_k is the phase friction factor between the fluids and the wall. These friction factors are determined from the Haaland correlation given in Equation 19, where Re_k is the phase Reynolds number, ε is the pipe roughness and $D_{h,k}$ is the hydraulic diameter of phase k.

$$\tau_k = \frac{1}{8} f_k \rho_k |U_k| U_k \tag{18}$$

$$\frac{1}{\sqrt{f_k}} = -1.8 \log \left[\frac{6.9}{\mathrm{Re}_k} + \left(\frac{\varepsilon}{3.7 D_{h,k}} \right)^{1.11} \right] \tag{19}$$

The hydraulic diameters $D_{h,g}$ and $D_{h,l}$ for the gas and liquid phases are given by Equation 20 and 21 respectively, where S_g and S_l are the gas and liquid wall perimeters and S_i is the width of the interphase. The interphase shear stress definition used is given by Equation 22, which implies that the interphase friction factor f_i is defined in multiples of the gas friction factor f_g. The value of IFM (Interphase Friction Multiplier) used in this thesis is 1. The value of IFM is probable to have little influence on the results in this thesis, as the velocities are low and the friction contributions are small.

$$D_{h,g} = \frac{\pi D^2}{S_g + S_i} \tag{20}$$

$$D_{h,l} = \frac{\pi D^2}{S_l} \tag{21}$$

$$\tau_i = \frac{1}{8} \cdot IFM \cdot f_g \rho_g \left| U_g - U_l \right| \left(U_g - U_l \right) \tag{22}$$

In addition to slug sections and bubble sections, the current SLUGGIT version supports simulations involving pigs and waves. A pig section possesses many of the same properties as a slug section in that it is treated as an incompressible volume. In addition, a pig occupies a volume of constant magnitude. This is not the case for a slug section, which is allowed to interchange liquid with its neighbouring bubble sections. Both sections and borders are organized in terms of classes, which enable a compressed organization of the different building blocks, and comprehensive code re-use during development of new specialized classes. This can be illustrated by the pig class, which is a class derived from the slug class. Most of the slug class characteristics are re-used, reducing the amount of additional code needed to give the pig its characteristic properties. Neither pigs nor waves are included in the simulations presented in this thesis.

6.1 SLUGGIT modification - version I

The modelling of slugs and bubbles show some major differences as described above. A bubble is modelled as a section containing a stratified incompressible liquid layer with a gas volume above the liquid layer, giving the bubble compressible properties. A slug is modelled incompressible with only liquid present within the section. During gas lift simulations, a gas source delivering a constant mass flow rate of gas is placed in the lower parts of the system. A bubble section covering this lift gas source introduces no problems, as the gas from the source is allowed to add to the existing gas mass in the bubble. On the other hand, when a slug unit covers the gas source, the gas in not allowed to enter the slug, as the slug is only allowed to contain liquid. To handle this situation some modifications have been implemented in the SLUGGIT code. It has been decided to let the gas accumulate

outside the pipe at the source location if a slug covers the source. The accumulation follows the relation given in Equation 23.

$$m_{acc}^{n+1} = m_{acc}^{n} + \dot{m}_g \cdot \Delta t \tag{23}$$

The accumulation continues as long as the gas source is covered by the slug, and the accumulated mass is continuously converted into an equivalent bubble length at the source location by the relation given in Equation 24.

$$L = \frac{m_{acc}4}{\rho_g \pi D^2} \tag{24}$$

When the accumulated mass has reached a value high enough to create a bubble with the desired length L_{final} specified by the user, a splitting sequence is carried out at the slug section, enabling insertion of the bubble. Two different versions of this slug splitting sequence have been implemented and used for gas lift simulations. The first procedure given in this section has been employed for the simulations presented in Section 9.3 to 9.5. The second splitting procedure given in Section 6.2 has been used during the simulations presented in Section 9.6.

By this first splitting procedure, the slug is split at the source coordinate resulting in two shorter slugs devided by a slug/slug border. Next, this border is deleted and two new borders are inserted, namely a slug/bubble and a bubble/slug border. A gas bubble with length $L_{initial}$ and zero holdup is then inserted in between the two slugs. The bubble with length $L_{initial}$ is much shorter than L_{final}, and is inserted in between the two slugs, originating from the splitting as an initial bubble length. A direct insertion of a bubble with length L_{final} would require small time steps and consequent slow simulations to handle the corresponding kick in pressure. After insertion, the bubble with length $L_{initial}$ is allowed to grow to L_{final} at a user defined gas injection rate $\dot{m}_{inject}$. During this injection procedure, the accumulated mass is reduced according to Equation 25, till all accumulated gas mass has been injected. The splitting and insertion procedure is illustrated in Figure 13.

$$m_{acc}^{n+1} = m_{acc}^{n} - \dot{m}_{inject} \cdot \Delta t \tag{25}$$

At insertion of a new bubble, a new issue is encountered relating to the liquid mass conservation. This can be observed inside Figure 13. As can be seen, the bubble needs for its existence a volume of length $L_{initial}$. As the location of bubble insertion is originally covered with liquid, some liquid must hence be removed to give space for the new bubble. This is handled by translation of both the left and the right border of the right slug in Figure 13 by a distance $L_{initial}$ at the moment of bubble insertion. This results in the compression of the rightmost bubble section, which is illustrated by an increase in its liquid holdup. It should be emphazised that the manual border translation of distance $L_{initial}$ to the right promotes an increased pressure in the rightmost bubble, which will influence the pressure in all bubble sections to the right of this bubble at the next time steps. A small value of $L_{initial}$ should hence be used to minimize such pressure effects. At the time step after insertion and border translation, all borders and sections stand free to interact

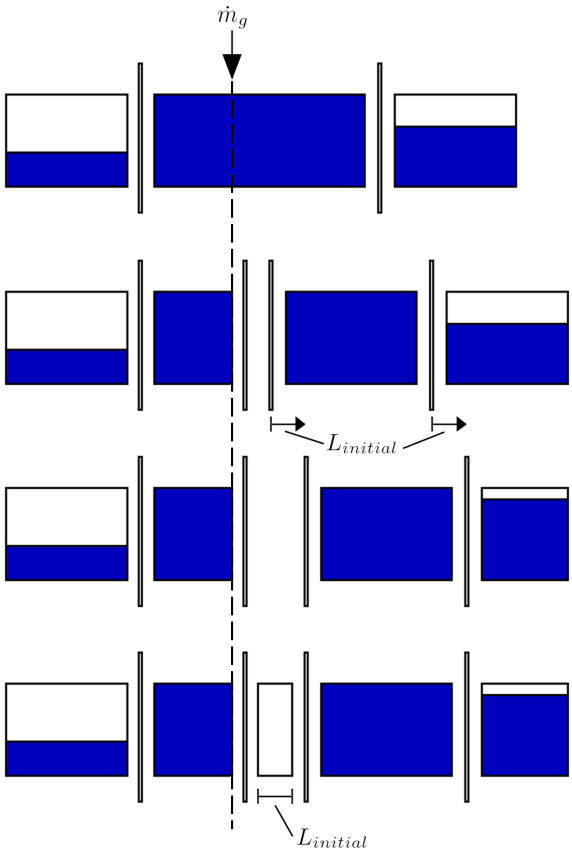

Figure 13: Slug splitting and bubble insertion sequence used in SLUGGIT modification - version I

with each other in accordance with their respective conservation equations during insertion of the remaining accumulated mass into the new bubble. One might also encounter situations where the slug leaves the source location before enough gas mass has accumulated to form a bubble of the desired length L_{final}, and where a neighbouring bubble moves to the former slug location. The accumulated mass is then injected directly into the bubble covering the source at a rate $\dot{m}_{inject}$, and the accumulated mass is reset to zero.

Another special case to consider arises when a newly created bubble which is still under injection of accumulated mass merges with another bubble. The remaining mass to inject is then transferred to the single bubble resulting from the merging. This has been implemented to avoid any undesired loss of gas mass.

The new input parameters through which the user is allowed to influence the bubble creation process resulting from the scenario of a slug covering a source are:

- BUBBLE_INIT_LENGTH - this input parameter corresponds to $L_{initial}$ and defines the initial bubble length in numbers of pipe diameters. Some trial and error testing has been performed to tune this parameter during the different simulations
- BUBBLE_FINAL_LENGTH - this input parameter corresponds to L_{final} and defines the final bubble length in numbers of pipe diameters
- ACC_INJECTION_RATE - this input parameter corresponds to $\dot{m}_{inject}$ and gives the rate $[kg/s]$ at which accumulated mass should be injected into either an existing or a new bubble. Care should be taken not to set this value to low, especially during gas lift simulations. If a too low value is used, the bubbles may reach the riser outlet before the accumulated mass is fully injected. Gas mass will hence be lost without giving any contribution to the reduction of riser mixture density

Some modifications regarding the source location have also been included in the code. The version chosen for modification by [46] enabled inclusion of sources only in static borders. Static borders are located at fixed positions between pipes in the pipeline and are not allowed to move as is the case for non static borders found between bubble and slug sections. As a consequence, it was only possible to place sources in between pipes. To enable larger flexibility and the possibility of including sources at any positions along the pipeline, the source definition was first redefined to be a member of the pipe class instead of being a member of the static border class. All sections have got pointers to the pipe in which they are present. Situations may though arise when a section spans several pipes. This was observed to introduce problems with regard to finding the correct pipe pointer. As a remedy, the source definition was further redefined to instead being a member of the pipeline class.

6.2 SLUGGIT modification - version II

This second bubble insertion procedure was created as an alternative to the procedure given in Section 6.1. During the simulations given in Section 9.3 to 9.5 the time step was observed to be greatly reduced by the automatic time step control every time a slug was split and a new bubble was inserted. As the borders are translated a distance $L_{initial}$ during one time step, their belonging slug section is artificially given a velocity different from the velocity of the neighbouring section velocities. This may be illustrated by the relation given in Equation 26. A large value of $L_{initial}$ applied in combination with a small time step Δt results in a high section velocity U, which again initiates a further time step reduction at the next time step in accordance with Equation 27.

$$\frac{L_{initial}[m]}{\Delta t[s]} = U[m/s] \tag{26}$$

The automatic time step control routine available in SLUGGIT is based on the CFL criterion given by Equation 27. The subscript j indicates that the ratio

between section length and section velocity is checked for all sections within the pipeline. The smallest ratio found is used as maximum value of the next time step.

$$\Delta t < \min(\Delta z/U)_j \tag{27}$$

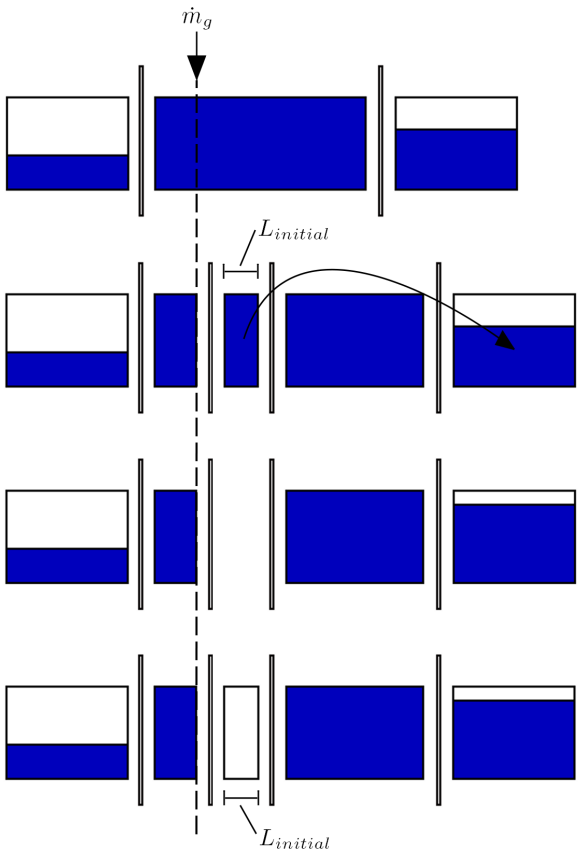

Figure 14: Slug splitting and bubble insertion sequence used in SLUGGIT modification - version II

The new bubble insertion procedure presented in this section avoids this manual border translation. The slug is instead split two times, and the resulting slug in the middle is replaced by the injected bubble. This is illustrated in Figure 14. The liquid mass from the short slug in the middle is transferred to the rightmost bubble section, thus representing a kick in pressure equal to the kick resulting from the procedure in Section 6.1.

An alternative procedure for introduction of a gas source in the SLUGGIT code could have been to implement void fraction in slug sections. This would have given the slug sections compressible properties, and would hence allowed gas to enter

the slug directly, leaving the slug splitting procedures presented in Section 6.1 and 6.2 superfluous. This would have imposed a need for the application of changes to some of the current main assumptions used in SLUGGIT regarding the slugs incompressible properties.

7 Visualization of results

There are some vital flow characteristics that have to be correctly reproduced during the simulations of the experiment series presented in Section 5. The principle of gas lift relies on the injected gas to show a net flow direction equal to the direction of the production fluid, towards the riser outlet. During simulations one might possibly encounter gas injection rates resulting in oscillations violent enough to make the gas flow into the vertical pipe leading to the small basin where the weir is installed. One possible way to avoid this is to constantly check all holdup values in this pipe to make sure they are equal to one. This can be done directly by making trend plots inside OLGA.

As an alternative to this approach, a MATLAB program has been written capable of importing profile plot text files with the file extension .ppl produced by OLGA, and converting these simulation results to a format supported by the NTNU inhouse visualization tool PLOTIT. This enables simultaneous plotting of holdup values from all computational sections at consequtive time steps, thus resulting in an animation of the type shown in Figure 151. This alternative provides an opportunity to get a visual impression of the flow dynamics in the whole pipe, as well as the possibility of quickly verifying holdup values in certain parts of the pipe.

The diameter to length ratio used in the photographic presentation of the animations enclosed in the appendices has been set high. This has been done to enable examination of the holdup profiles and their details. The source code is included in Section I.

For generation of plots representing OLGA and SLUGGIT results of the type shown in Figure 20 some other MATLAB scripts have been written, enabling better control with axes properties as well as quicker storage into .eps format. The source code for one of these scripts is included in Section J.

8 Simulations

The experiments presented in Section 5 have become subject to numerical simulation with two different multiphase flow simulators. The OLGA simulator is commercially available and supports simulations with and without slug tracking. This simulator was developed by IFE in the mid 1980s, and was based on an Eulerian formulation of the two fluid model with fixed computational grid. The model has later been developed to handle three phase simulations. The OLGA version 5.3.2.3 has been used.

The multiphase flow simulator SLUGGIT was originally developed by [45], and is based on the one-dimensional two-fluid model solved on a moving grid following a Lagrangian formulation. The simulator is implemented in C++ by use of object oriented procedures. Several versions of this program are available. The version developed by [48] has been chosen for implementation of the modifications presented in Section 6.

As described, the flow path from the liquid level at $H_0 = 5.65[m]$ to the inlet of the vertical riser shown in Figure 9 was made from flexible pipe. The geometry may therefore have been subject to some variation during the experiments. Some assumptions have been made in order to create a pipe geometry only consisting of straight pipes for use in the simulations. The sharp bends introduced with these simplifications represent additional losses not present during the experiments. These losses might be compensated by an additional loss coefficient in the simulations. As there exists additional uncertainty relating to the exact experimental geometry and the loss coefficients associated with its smooth bends, this has been left out. The geometry chosen for simulation is shown in Figure 16a. The generic setup is shown in Figure 15 where both inlet and outlet nodes have been assigned constant atmospheric pressure, and where the liquid holdup at the pipe inlet has been assigned a value of 1.0. The lift gas is injected at a constant mass flow rate through the source denoted by the blue arrow.

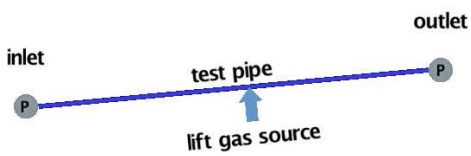

Figure 15: The OLGA flow path, node and source configuration

OLGA contains a steady state pre-processor routine which computes liquid holdup, pressure, flowregime and mass flow along the pipeline. It is based on a three-phase point model in which the steady state conservation equations are solved. It can be run with or without the energy equation option enabled. The pre-processor computed values are stored at the first time step printed to the output file when used as initial conditions for transient simulations.

The OLGA simulations both with- and without slug tracking have been started

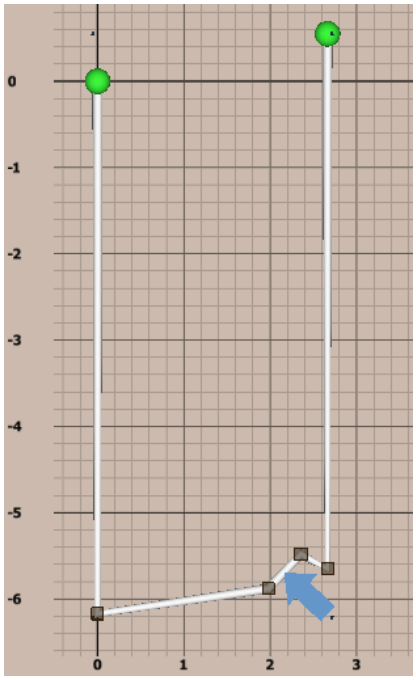

(a) The geometry used during OLGA and SLUGGIT simulations with axis values in meters

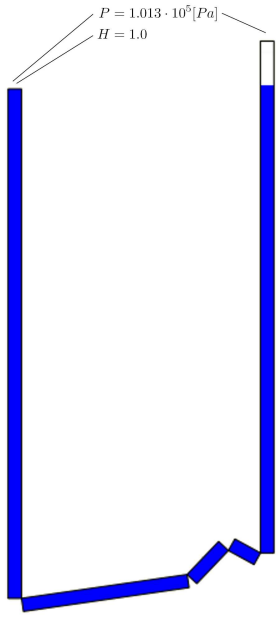

(b) Visualization of the situation from which the SLUGGIT initial conditions are obtained. The pressure and holdup boundary conditions used during both OLGA and SLUGGIT simulations are annotated at the inlet and outlet.

Figure 16

with the initial conditions offered by this pre-prosessor. The energy equation option has been turned off, and the simulations performed at a constant temperature of 20 [°C]. The software PVTsim has been used to generate a PVT file on a format accepted by OLGA. This PVT file was used for initial testing of the simulation setup and was based on pure water representing the liquid phase and a gas phase composed of 21% oksygen and 79% nitrogen. After initial testing of the simulation setup, the PVT file became subject to some manual modifications. The water was given incompressible properties, and its physical properties were set constant. The air was modelled as a gas mixture with molar mass of 28.97 [g/mol], and then modified according to the ideal gas equation of state, which was used to compute two points of pressure. A linear equation of state was hence chosen.

As described in [50], the value denoted R_s in the PVT table represents the gas mass fraction at equilibrium conditions as defined in Equation 31. Inspection of the interfacial mass transfer rate ψ_g given by Equation 32 reveals that the interfacial mass transfer rate depends on the the derivative of R_s with respect to pressure

and temperature. Thus, by setting the value of R_s in the PVT table equal in all table points implies a zero derivative of R_s during interpolation in the table. Zero interfacial mass transfer is then obtained. This procedure was used to avoid any mass transfer during simulation.

$$P = \frac{\rho_g \bar{R} T}{M_g} \tag{28}$$

$$\frac{\partial \rho_g}{\partial T} = -\frac{M_g P}{\bar{R} T^2} \tag{29}$$

$$\frac{\partial \rho_g}{\partial P} = \frac{M_g}{\bar{R} T} \tag{30}$$

$$R_s = \frac{m_g}{m_g + m_l + m_d} \tag{31}$$

$$\begin{aligned} \psi_g &= \left[\left(\frac{\partial R_s}{\partial P} \right)_T \frac{\partial P}{\partial t} + \left(\frac{\partial R_s}{\partial P} \right)_T \frac{\partial P}{\partial z} \frac{\partial z}{\partial t} \right. \\ &+ \left. \left(\frac{\partial R_s}{\partial T} \right)_P \frac{\partial T}{\partial t} + \left(\frac{\partial R_s}{\partial T} \right)_P \frac{\partial T}{\partial z} \frac{\partial z}{\partial t} \right] (m_g + m_l + m_d) \end{aligned} \tag{32}$$

The SLUGGIT simulator is capable of reading PVT files on the format supported by OLGA. Alternatively the molar mass of gas might be supplied in the input file for direct use with the built in ideal equation of state. This is the alternative used for the simulations presented in this thesis. SLUGGIT does not offer the steady state pre-processor option offered by OLGA. The initial conditions used for the gas lift simulations have been obtained by the following procedure: The lift gas source has been left out, and the holdup has been set equal to 1.0, together with atmospheric pressure and phase velocities equal to zero throughout the whole pipeline. The simulator has then been started and run until the liquid level has stabilized at the same level in both the vertical pipes, leaving the situation shown in Figure 16b. All computed values are automatically stored in a restart file. The SLUGGIT gas lift simulations have been started with computational values provided by this restart file as initial conditions, together with the inclusion of the lift gas source. All boundary conditions have been kept unchanged. The energy equation is implemented in the current SLUGGIT version, but this option has been swithed off as for the OLGA simulations. Simulations in this report have been conducted for the same range of flowrates as in the experiments. The geometry shown in Figure 16a has been used in OLGA simulations with and without slug tracking as well as in the SLUGGIT simulations.

All simulations have been run for 600 [s]. They do all show transient development from the steady state pre-processor solution (OLGA) and from the initial conditions represented by Figure 16b (SLUGGIT) before stabilizing at their steady

or quasi steady states. The time needed for the simulations to stabilize varies from 50 to 200 [s] depending on the gas mass injection rate. The interval 300 to 450 [s] has been chosen for plotting of all simulations presented in Section 9.

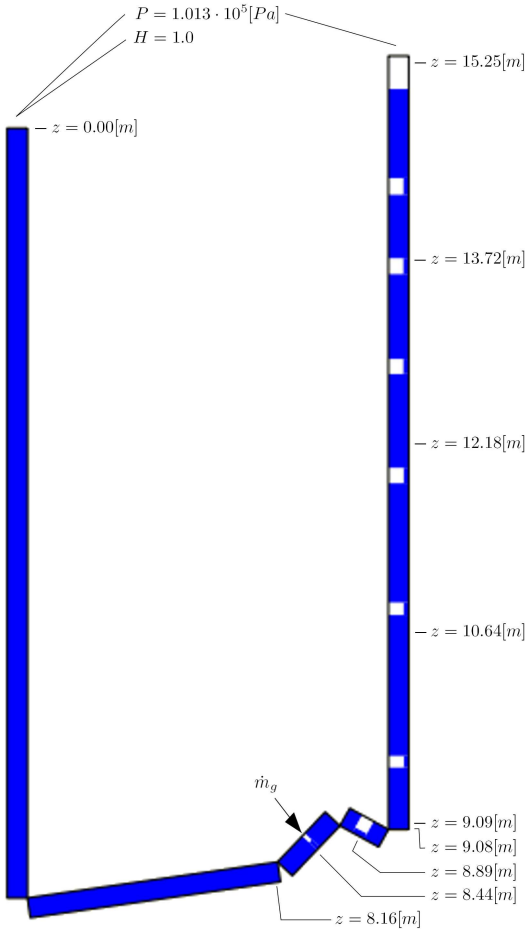

Figure 17: Coordinates relative to pipeline inlet used for plotting of OLGA and SLUGGIT simulation results

9 Results

This section has been organized in terms of simulation series. Two OLGA series and four SLUGGIT series are presented. The six simulation series presented in Section 9.1 to 9.6 are all based on a simulation setup involving five straight pipes. In addition, an alternative simulation configuration based on three pipes has been tested and included in Section 9.7.

In the sections representing SLUGGIT simulations instantaneous time series are plotted. In addition, time series representing moving averages of the instantaneous time series are included if these are observed to clarify or reveal additional trends within the instantaneous time series. Time series representing computed moving average values are denoted with the subscript "avg" on the plotted property. This can be observed in Figure 55. The following variables have been chosen for presentation in this section:

- Holdup at three equally spaced locations along the riser
- Flow regime indicator from the middle of the riser and the middle of the short downward inclined pipe connected to the riser
- Pressure at three equally spaced locations along the riser
- Liquid flow rate at the riser outlet

The OLGA time series have been exported from OLGA and then plotted by use of MATLAB. Data were printed to file from OLGA every 0.1 [s]. This printing time resolution was also used during the SLUGGIT simulations.

As described in Section 6 SLUGGIT solves the pressure in bubble sections only. The output files from the current version of SLUGGIT contain the computed bubble pressures and also slug pressures obtained by interpolation between neighbouring bubble sections. It should be emphazised that this interpolated slug section pressure does not influence the pressure calculation in the bubble section.

As a moving grid formulation is used, it is not possible to extract flow characteristics from fixed computational cells like in OLGA. An existing MATLAB program for plotting of SLUGGIT results has therefore been modified to enable extraction of computed values and subsequent plotting of the SLUGGIT simulation results. The extraction of computed values may follow two different strategies as shown in Figure 18. The strategy shown in Figure 18a was the method contained in the Matlab program before any modifications were applied. The user specifies a desired pipeline axial coordinate z for extraction of data. The program then loads the SLUGGIT result file and searches for sections with left and right border coordinates $z_{sec,L}$ and $z_{sec,R}$ spanning the user specified pipeline coordinate. For extraction of bubble characteristics only, an additional search criterion is included, enabling discrimination between slugs and bubbles by their identifiers.

During the simulations presented in this report the holdup has been defined equal to 1.0 at the pipe inlet together with atmospheric pressure at both inlet and outlet. The first pipe is observed always to contain liquid in its full length. The riser does on some occasions contain slugs with a length close to riser length.

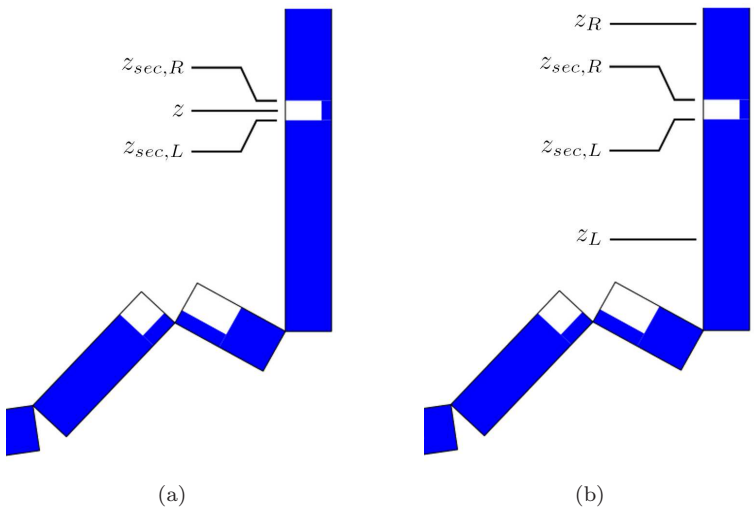

Figure 18: The two procedures used for extraction of computed values stored in SLUGGIT result files

If a section is in contact with either an inlet or an outlet, the section pressure value printed to the output file is set equal to atmospheric. This may introduce atmospheric pressure values in the lower parts of the system upon plotting.

If the section is long but not in contact with an inlet or an outlet, the pressure interpolation procedure may introduce erroneously low values in the lower parts of the systems upon plotting. This can be illustrated by examination of Figure 18a. If one considers a z value from the lower parts of the system spanned by a long slug stretching towards the riser outlet, the slug pressure printed to the output file corresponds to the interpolated pressure in the middle of the slug. This pressure will be approximately 1.3 [bara], as the pressures at the outlet and at the inlet are approximately 1.0 [bara] and 1.6 [bara] respectively. Inclusion of this pressure during plotting of pressure values then introduces values of 1.3 [bara] in the lower parts of the system where one should expect pressure values close to 1.6 [bara].

These two cases involving plotting of slug pressures result in plotting of misleading pressure values. It has therefore been decided only to plot bubble pressure values from the SLUGGIT simulations. The plotting of only bubble pressure values implies that bubbles have to be present at the desired z coordinate on a regular basis if pressure plots showing relatively continuous curves are to be produced. This is difficult to obtain if the original data extraction procedure shown in Figure 18a is applied. The modified procedure shown in Figure 18b has therefore been applied for extraction of bubble pressure values. Instead of requiring the section's left and right border coordinates to span a given z coordinate, the new procedure requires the section's left and right border coordinates $z_{sec,L}$ and $z_{sec,R}$ to be present within a wider region defined by z_L and z_R. This method implies that some of the pressure values extracted may be slightly too high or to low due

to the change in hydrostatic pressure within the region defined by z_L and z_R. On the other hand, this discrepancy is removed when moving average is applied to the extracted pressure values. Pressure values from the riser have been extracted from regions spanning 0.4 [m] to the left and to the rigth of the z coordinates presented in the pressure plot legends of the type included in Figure 47. This gives the following data extraction regions:

- 9.09 [m] riser coordinate - Pressure values are extracted from the region spanned by $z_L = 8.69[m]$ and $z_R = 9.49[m]$
- 12.18 [m] riser coordinate - Pressure values are extracted from the region spanned by $z_L = 11.78[m]$ and $z_R = 12.58[m]$
- 15.25 [m] riser coordinate - Pressure values are extracted from the region spanned by $z_L = 14.85[m]$ and $z_R = 15.27[m]$

This implies that some pressure values from the bend configuration are included in the pressure printed as 9.09 [m]. At the outlet, almost only pressure values extracted from the region 0.4 [m] upstream the print coordinate 15.25 [m] are extracted. This implies that pressure values computed at 15.25 [m] may be slightly too high, and that pressure values computed at 9.09 [m] may bee slightly to low. The pressure values plotted at 12.18 [m] are probable to be correct, as the region for data extraction upstream and downstream the coordinate are equally long and the pipe is vertical.

The original data extraction procedure shown in Figure 18a has been kept for plotting of all variables other than pressure.

Three different production modes based on the liquid production characteristics observed are defined in Figure 19 and used in the following to classify the different simulations presented. The modes are defined as follows:

- Mode 1 - Unstable liquid production with liquid front retraction to a location upstream the gas injection point prior to startup of a new cycle. This mode dominates the lowest gas injection rates and does typically show complete removal of all gas bubbles from the riser prior to startup of a new cycle
- Mode 2 - Unstable liquid production with liquid front retraction to the gas injection point or right downstream the gas injection point prior to startup of a new cycle. This mode involves continuous presence of bubbles in the riser and generation of slugs at a varying rate at the riser inlet during each cycle
- Mode 3 - Stable liquid production with liquid slugs being generated at a constant rate at the riser inlet

The gas injection rates chosen for presentation have been selected to show the typical characteristics observed within each simulation series. This implies that at least one gas injection rate from the region in which transition from unstable to stable production has been included. To enable comparison, the gas injection rate $\dot{m}_g = 2.000 \cdot 10^{-5}[kg/s]$ has been plotted for all the simulation series. It has been

decided not to plot gas injection rates higher than $\dot{m}_g = 3.500 \cdot 10^{-5}[kg/s]$ from the OLGA series as they have both reached their steady state solutions at this gas injection rate.

Screen shots from the animations made with PLOTIT have been included in the appendix for selected gas injection rates. Some selected animations in .avi format have been included electronically in a .zip file as part of the master thesis hand in.

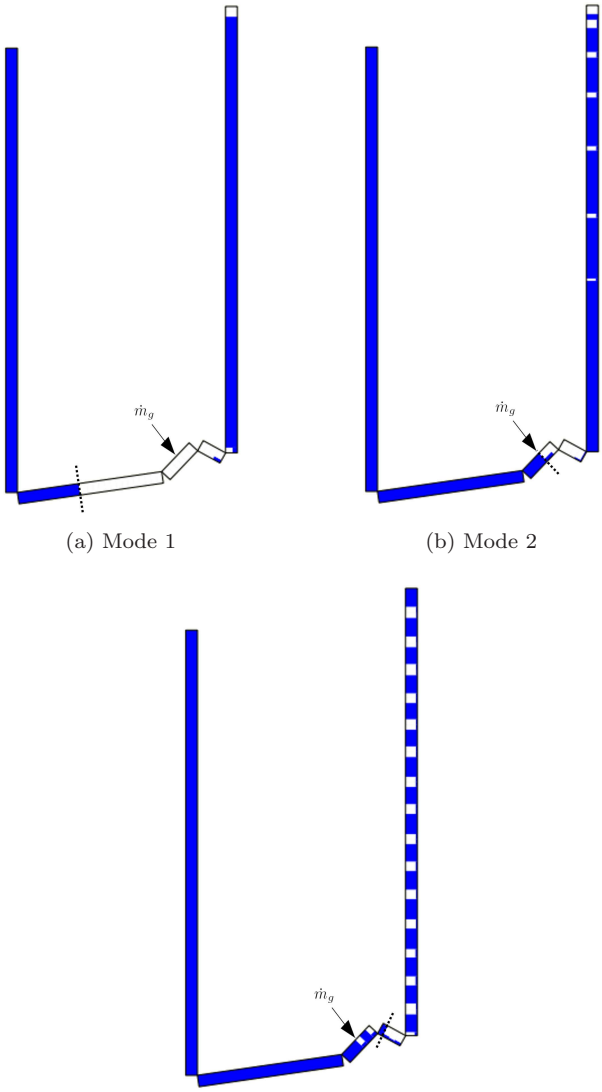

(a) Mode 1

(b) Mode 2

(c) Mode 3

Figure 19: Maximum liquid front retraction in the different production modes

9.1 OLGA - series I

Simulations conducted with a cell length of 10 [mm] have been tested and the results compared against results from simulations conducted with a cell length of 20 [mm]. No significant difference was observed. The results from simulations with 20 [mm] cell length have also been compared to larger cell length simulations. These larger cell length simulations were observed to possess a lack of capability of sustaining the sought oscillatory behaviour in holdup resulting from the density wave mechanism over time at injection rates higher than or equal to $\dot{m}_g = 2.642 \cdot 10^{-5}[kg/s]$. A computational cell length of 20 [mm] has hence been used during the simulations presented in this thesis. Simulation results from four gas mass injection rates have been chosen for presentation. The OLGA flow regime indicators are given in Table 3. Information about the simulation geometry is given in Table 4.

Indicator	Regime
1	Stratified flow
2	Annular flow
3	Slug flow
4	Bubbly flow

Table 3: OLGA flow regime indicators

Pipe	Length [m]	Cells	Cell length [m]	Diameter [m]	Roughness [m]	Inclination θ [°]
1	6.17	300	0.0206	0.016	2E-6	-90.0
2	2.00	100	0.0200	0.016	2E-6	+8.3
3	0.55	27	0.0204	0.016	2E-6	+46.7
4	0.35	17	0.0206	0.016	2E-6	-29.0
5	6.20	300	0.0207	0.016	2E-6	+90.0

Table 4: OLGA - series I simulation setup

9.1.1 Gas injection rate $= 2.000 \cdot 10^{-5}[kg/s]$

The holdup profiles in Figure 20 show a period of approximately 50 [s]. The holdup at the riser outlet drops to zero once every cycle. This can also be observed in Figure 152d to 152i. The corresponding pressure time series in Figure 21 show distinct pressure drops in the riser every time the holdup drops. This indicates a reduction in hydrostatic pressure caused by a reduction in mixture density every time the lift gas passes the riser inlet bend to initiate a cycle of liquid production. The corresponding maxima in liquid mass flow rate at the riser outlet coincide with the minima in pressure and holdup. During one cycle, several flow regimes are present. These are shown in Figure 23. The flow regime being annular in the riser may indicate that the annular liquid zone present within Taylor bubbles have been captured by the fine grid. This simulation represents Mode 1 production.

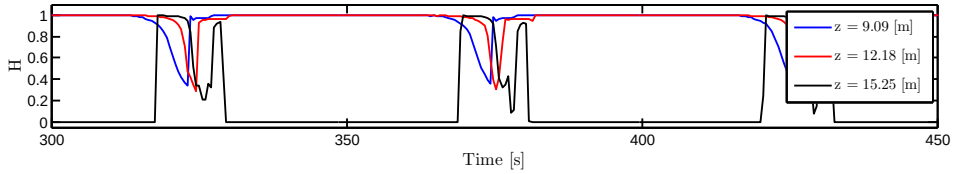

Figure 20: OLGA - series I, $\dot{m}_g = 2.000 \cdot 10^{-5} [kg/s]$

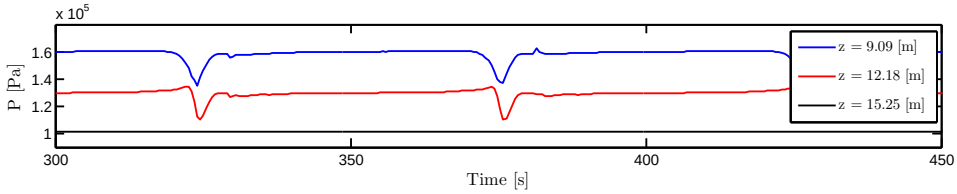

Figure 21: OLGA - series I, $\dot{m}_g = 2.000 \cdot 10^{-5} [kg/s]$

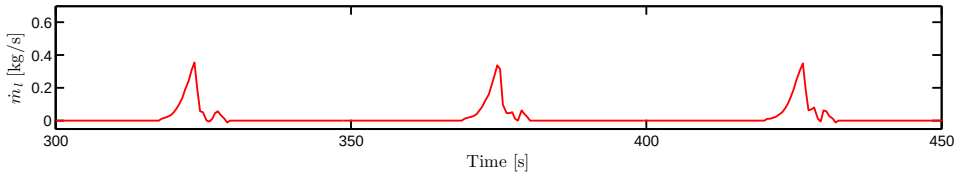

Figure 22: OLGA - series I, $\dot{m}_g = 2.000 \cdot 10^{-5} [kg/s]$

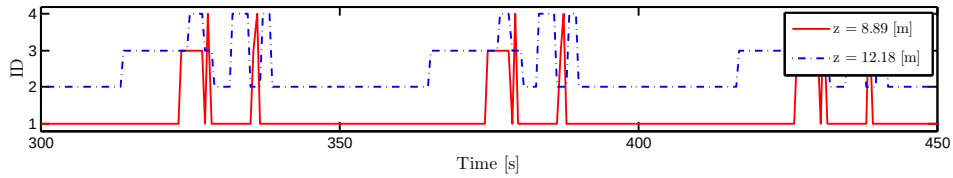

Figure 23: OLGA - series I, $\dot{m}_g = 2.000 \cdot 10^{-5} [kg/s]$

9.1.2 Gas injection rate $= 2.621 \cdot 10^{-5} [kg/s]$

The holdup profile shows similar characteristics as the profile in Figure 20, and Mode 1 production is still governing. The period of the cyclic behaviour has been decreased. This is due to the increase in gas injection rate and the reduced time needed to fill the regions close to the bend with gas before gas enters the riser inlet. Inspection of the pressure series reveals pressure drops coinciding with the liquid

producing part of each cycle, but with minima higher than the ones observed in Figure 21. This is probably caused by a reduction in gas mass accumulation during each cycle and hence corresponding less gas in the riser at the end of each cycle. This gives a general increase in hydrostatic pressure. This is a general trend observed during all the simulations included in this thesis. As the gas mass injection rate is increased, the gas mass allowed to accumulate close to the inlet bend is reduced. This is probably caused by liquid inertia effects. As the gass mass injection rate is low, the waiting time between each cycle is long. This enables the liquid to come to rest and stabilize at the same height in both vertical pipes after each cycle, before enough gas mass has accumulated for the gas front to reach the riser inlet. In situations where the gas mass injection rate is higher, the waiting time between the liquid producing part of each cycle is shorter. This unables the liquid column to come to rest at the end of each cycle. Instead it follows a periodical up and down movement, which at some point brings the front of the accumulated gas in contact with the riser inlet. This initiates an earlier gas propagation into the riser compared to what would be the case if the liquid column was at rest during gas accumulation.

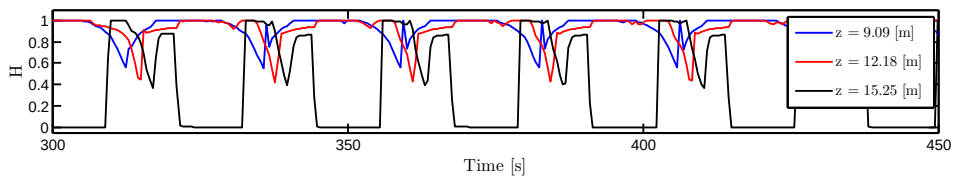

Figure 24: OLGA - series I, $\dot{m}_g = 2.621 \cdot 10^{-5} [kg/s]$

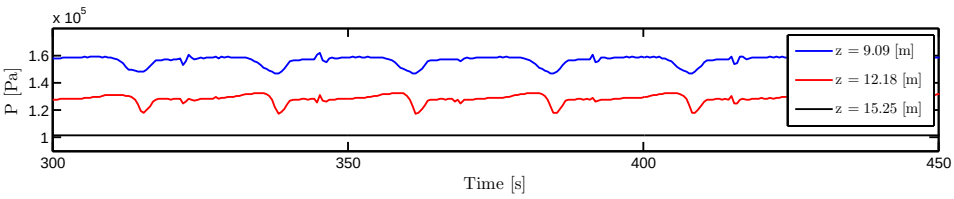

Figure 25: OLGA - series I, $\dot{m}_g = 2.621 \cdot 10^{-5} [kg/s]$

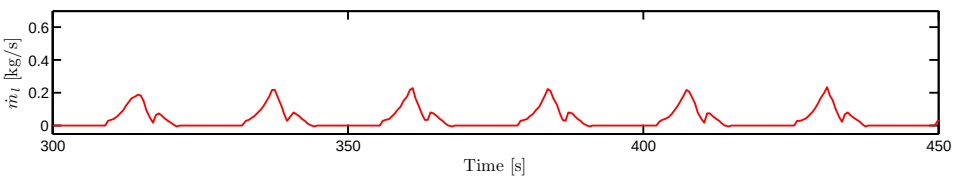

Figure 26: OLGA - series I, $\dot{m}_g = 2.621 \cdot 10^{-5} [kg/s]$

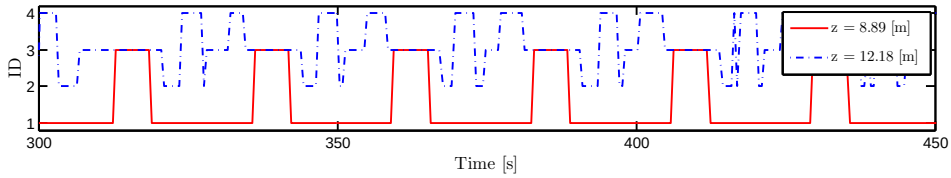

Figure 27: OLGA - series I, $\dot{m}_g = 2.621 \cdot 10^{-5}[kg/s]$

9.1.3 Gas injection rate $= 2.642 \cdot 10^{-5}[kg/s]$

The increase in gas injection rate is observed to remove the tendency of periodical absence of liquid at the riser outlet as observed in Section 9.1.1 and 9.1.2. Instead the holdup from the three locations along the riser oscillate around values in the order of magnitude 0.6 to 0.9. This change is probably caused by slugs and bubbles continuously, but at varying rate entering the riser inlet, indicating that this simulation represents Mode 2 production. This might be explained by inspection of the corresponding flow regimes shown in Figure 31, where the flow regime in the middle of Pipe 5 is observed to be slug flow during the whole simulation. The flow regime in the downward inclined Pipe 4 is observed to change between stratified and slug. The pressure fluctuations have been further reduced. The oscillations in holdup shown in Figure 28 were not possible to obtain during simulation trials where the cell length was longer. The oscillations then quickly died out, leaving a steady state solution without oscillations in holdup.

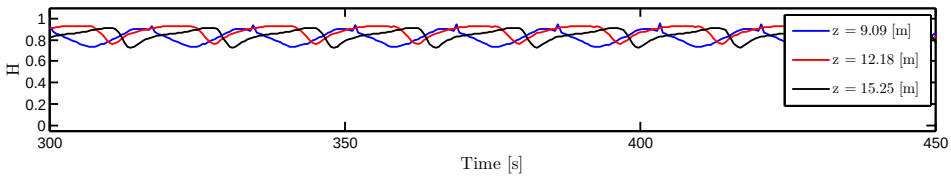

Figure 28: OLGA - series I, $\dot{m}_g = 2.642 \cdot 10^{-5}[kg/s]$

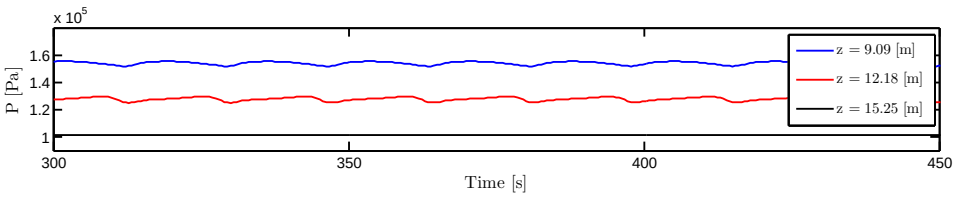

Figure 29: OLGA - series I, $\dot{m}_g = 2.642 \cdot 10^{-5}[kg/s]$

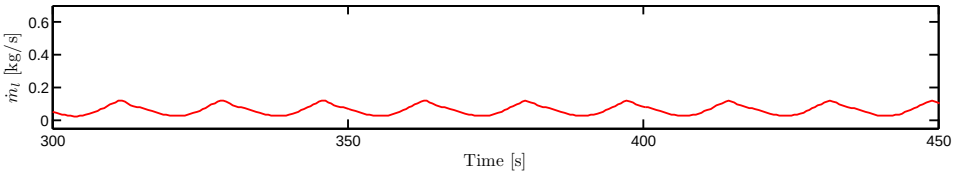

Figure 30: OLGA - series I, $\dot{m}_g = 2.642 \cdot 10^{-5} [kg/s]$

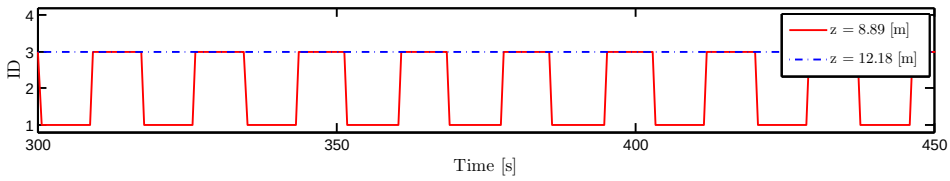

Figure 31: OLGA - series I, $\dot{m}_g = 2.642 \cdot 10^{-5} [kg/s]$

9.1.4 Gas injection rate $= 3.500 \cdot 10^{-5} [kg/s]$

At this injection rate the oscillations in holdup have died and the steady state solution has been reached. The pressure time series show constant values, and the liquid outflow rate at the outlet coincides with the OLGA steady state solution. The flow regimes in both Pipe 4 and Pipe 5 are with no exception slug flow, implying that the production Mode 3 has been reached.

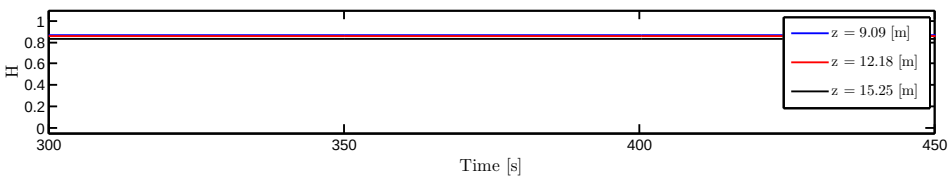

Figure 32: OLGA - series I, $\dot{m}_g = 3.500 \cdot 10^{-5} [kg/s]$

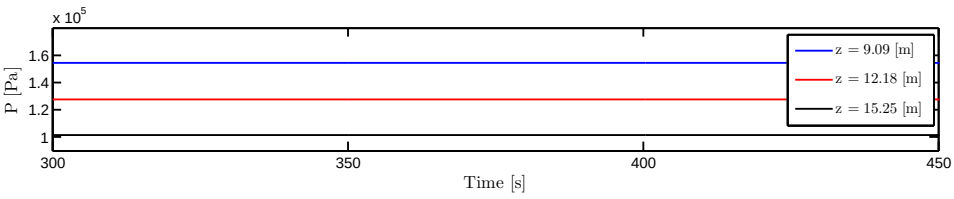

Figure 33: OLGA - series I, $\dot{m}_g = 3.500 \cdot 10^{-5} [kg/s]$

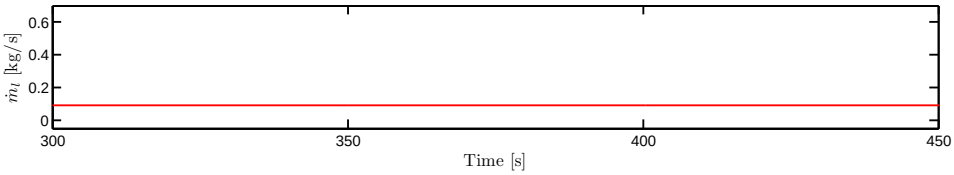

Figure 34: OLGA - series I, $\dot{m}_g = 3.500 \cdot 10^{-5}[kg/s]$

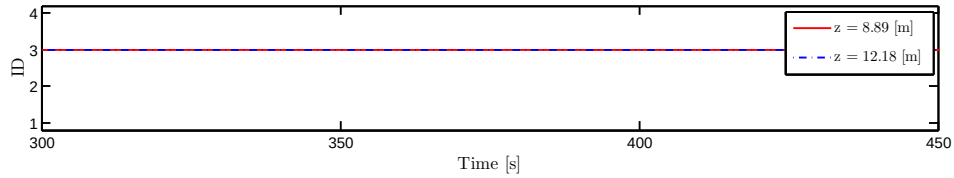

Figure 35: OLGA - series I, $\dot{m}_g = 3.500 \cdot 10^{-5}[kg/s]$

The tendency of the quasi steady behaviour associated with Mode 2 production to die out and stabilize at steady states is observed to increase with gas injection rate and is experienced at gas injection rates higher than $\dot{m}_g = 2.642 \cdot 10^{-5}[kg/s]$. To give a visual impression of this tendency, a series of simulations in the gas mass injection range $\dot{m}_g = 2.642 \cdot 10^{-5}[kg/s]$ to $\dot{m}_g = 3.500 \cdot 10^{-5}[kg/s]$ have been presented in Figure 36, with holdup values plotted for time 0 - 150 [s]. As can be seen, the gas injection rate $\dot{m}_g = 3.500 \cdot 10^{-5}[kg/s]$ which has reached a steady state in Figure 32, is still under development in Figure 36.

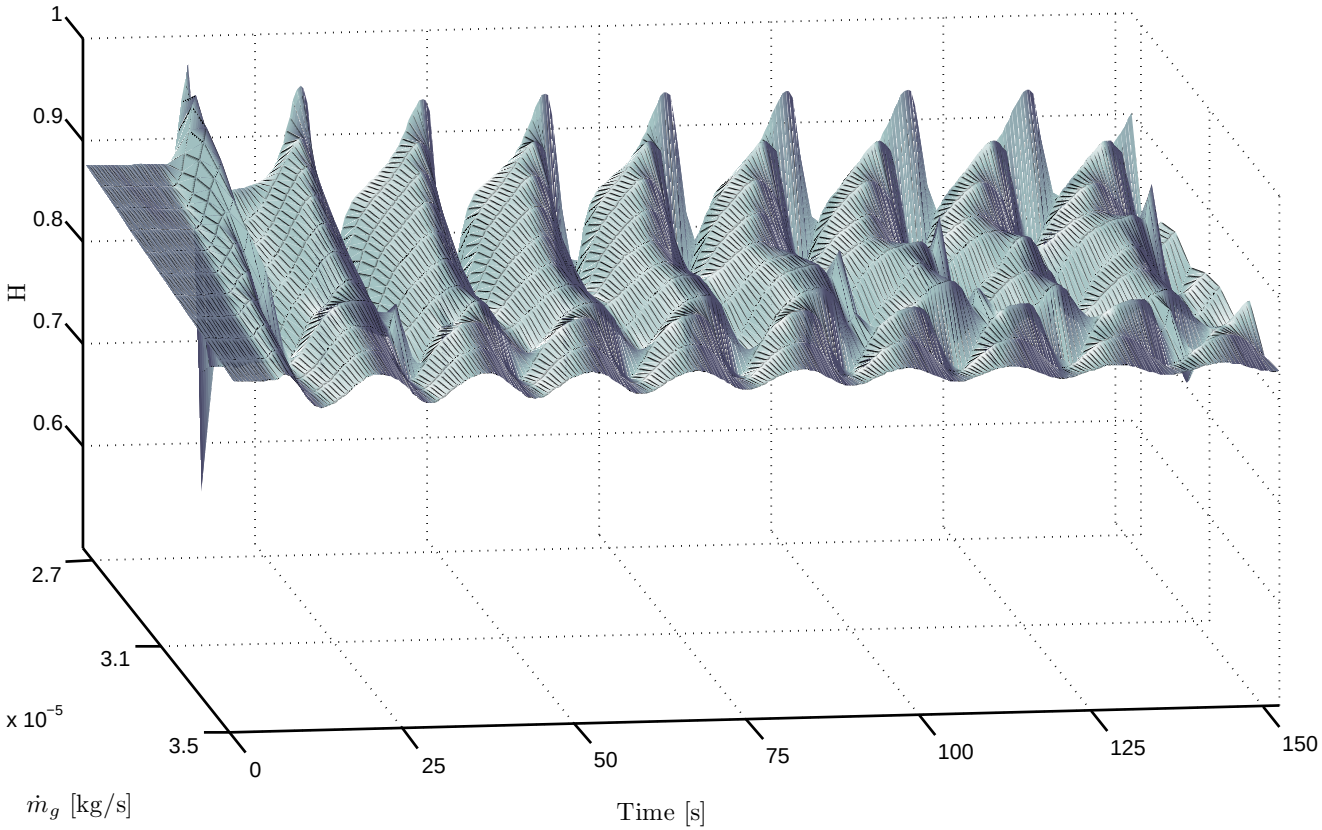

Figure 36: OLGA - series I, simulations developing from the steady state pre-processor initial conditions

9.2 OLGA - series II

Based on the simulations presented in Section 9.1, the same simulation setup is used to simulate the same range of flowrates, but this time with the slug tracking module activated. During simulation trials several cell length configurations were tested. It was found difficult to make the simulation run when short cell lengths were used. This was according to [51] probable to be caused by large pressure gradients arising from a to short cell length. An attempt was made on enabling simulations with these sharp pressure gradients present, simply by expanding the pressure range in the PVT table. This attempt was not found to solve the problem. Based on this testing, a cell length to diameter ratio in the range 20 to 25 was found to make the simulations run for a longer time without breaking down. Simulation results from three gas mass injection rates have been chosen for presentation. The slug tracking module contains a time step control routine. The time step control is based on the number of timesteps a slug front or slug tail needs to pass through a section. The current limit is 10 time steps. If a slug front or tail moves faster, the time step is reduced. In addition, the time step is reduced so that only one front or tail can cross any section boundary during one time step. Table 5 shows the geometrical configuration used.

Pipe	Length [m]	Cells	Cell length [m]	Diameter [m]	Roughness [m]	Inclination θ [°]
1	6.17	15	0.4113	0.016	2E-6	-90.0
2	2.00	5	0.4000	0.016	2E-6	+8.3
3	0.55	2	0.2750	0.016	2E-6	+46.7
4	0.35	1	0.3500	0.016	2E-6	-29.0
5	6.20	15	0.4133	0.016	2E-6	+90.0

Table 5: OLGA - series II simulation setup

OLGA offers two different options for slug initiation during slug tracking simulations. The HYDRODYNAMIC option enables slug initiation when OLGA predicts transition to slug flow from either stratified or annular flow. The LEVEL option enables initiation of slugs when changes in liquid holdup from one cell to another are detected. Terrain slugging is detected in ordinary simulations without the slug tracking module activated. These two options are governed by the following user defined input variables:

- DELAYCONST - this parameter is used to tune the slug initiation frequency when the HYDRODYNAMIC option is used, and specifies the minimum waiting time between generation of slugs in numbers of pipe diameters
- BUBBLEVOID - this parameter defines the minimum void fraction in a bubble at initiation and is used together with the LEVEL option
- SLUGVOID - this parameter defines the maximum void fraction in a slug at initiation and is used together with the LEVEL option

The HYDRODYNAMIC and LEVEL options are conseptually different and show different areas of application. They might be included in simulations

simultaneously or separately. The HYDRODYNAMIC slug initiation method is likely to show largest relevance used in connection with horizontal or near horizontal flows where the hydrodynamic transition mechanism is known to be important. An attempt was done to make the slug tracking simulations run with the HYDRODYNAMIC option enabled as the only slug initiation mechanism. Extensive tuning of the DELAYCONST parameter was performed in an attempt to make the simulation run till the predefined stop time. The general experience was however that a quasi steady state was difficult to obtain and that the simulation in general broke down before the specified stop time. In the case of gas continuously entering the riser inlet at a varying rate, as observed in Figure 28, one might expect the slug initiation frequency at the bend to vary over a large range during one cycle. One might suspect the HYDRODYNAMIC slug initiation procedure not to be capable of generating slugs at the large range of generation frequencies observed during one experimental cycle.

Based on the failure of the HYDRODYNAMIC slug initiation attempt together with the expected high influence of level effects on slug initiation at the riser inlet, it has been decided to run the slug tracking simulations with the LEVEL option enabled. As the pressure in the system is close to atmospheric, one might expect low void fraction in slugs. The parameter SLUGVOID has therefore been assigned a value of 0.05. The parameter BUBBLEVOID has been tuned to give simulation results as close to the results presented in Section 9.1 as possible. After considerable tuning, a value of 0.4046 was found to give the best match. The BUBBLEVOID parameter tuning process was governed by two issues. The first was aimed at obtaining a cycle period as close as possible to the period of approximately 50 [s] shown in Figure 20 at a lift gas injection rate of $\dot{m}_g = 2.000 \cdot 10^{-5} [kg/s]$. The other issue was related to the desired riser flow regime at a gas injection rate of $\dot{m}_g = 2.642 \cdot 10^{-5} [kg/s]$. As observed in Figure 31, this regime is slug flow. To obtain this situation with slugs continuously entering the riser inlet together with the requirement of cycle period as close to 50 [s] as possible, the value 0.4046 was chosen. A value lower than 0.4046 prevents slugs from entering the riser continuously at $\dot{m}_g = 2.642 \cdot 10^{-5} [kg/s]$. A value higher than 0.4046 further decreases the period of the cyclic behaviour at $\dot{m}_g = 2.000 \cdot 10^{-5} [kg/s]$.

9.2.1 Gas injection rate $= 2.000 \cdot 10^{-5} [kg/s]$

Using the input parameters found by the tuning process explained above, gives the holdup time series in Figure 37. The period of the cyclic behaviour is shorter and quite irregular, compared to the value of 50 [s] seen in Figure 20, varying between 25 [s] and 45 [s]. The liquid outflow shows the same trend as in Figure 22 and 26 with narrow peaks, but with an increased irregularity in peak values. This tendency may probably be explained by the observed irregular cycle period, which probably gives varying gas accumulation during each cycle, with corresponding varying liquid transportation. The pressure time series show the same trend as observed in the simulations without slug tracking, but with some scatter introduced. Comparison between Figure 37 and Figure 20 reveals that the holdup values at the outlet do not drop to zero for longer periods in the slug tracking case. The behaviour of the

holdup time series in the middle of the riser with its oscillating behaviour is not possible to observe in the corresponding simulation without slug tracking. This simulation represents Mode 1 production.

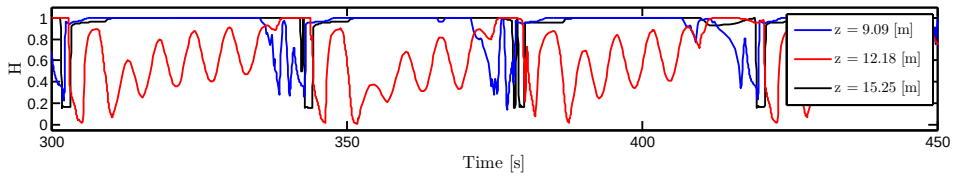

Figure 37: OLGA - series II, $\dot{m}_g = 2.000 \cdot 10^{-5} [kg/s]$

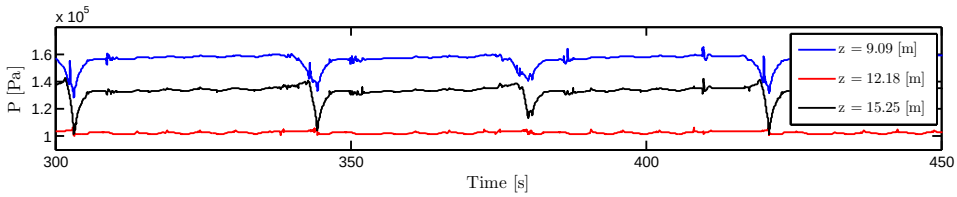

Figure 38: OLGA - series II, $\dot{m}_g = 2.000 \cdot 10^{-5} [kg/s]$

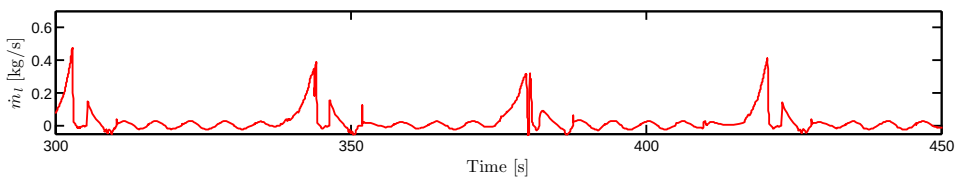

Figure 39: OLGA - series II, $\dot{m}_g = 2.000 \cdot 10^{-5} [kg/s]$

9.2.2 Gas injection rate $= 2.642 \cdot 10^{-5} [kg/s]$

Inspection of the holdup profiles shown in Figure 40 reveals values quickly varying between relatively fixed maximum and minimum values in time, with a constant frequency, implying that slugs are generated at a constant rate at the riser inlet. This corresponds to Mode 3 production. The pressure series show constant values except for the small fluctuations caused by the slugs entering the riser. The liquid flowrate at the outlet is observed to approach the steady state solution.

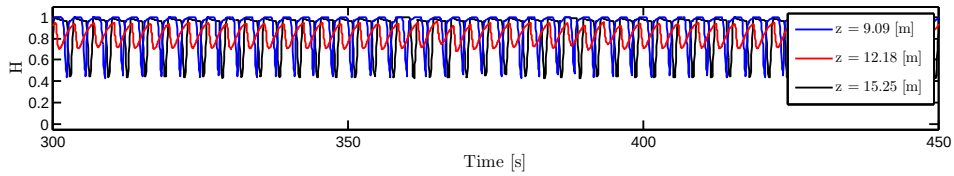

Figure 40: OLGA - series II, $\dot{m}_g = 2.642 \cdot 10^{-5} [kg/s]$

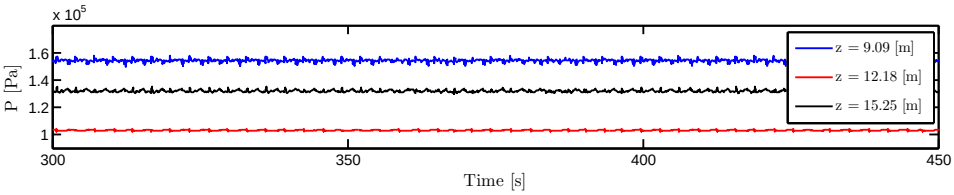

Figure 41: OLGA - series II, $\dot{m}_g = 2.642 \cdot 10^{-5} [kg/s]$

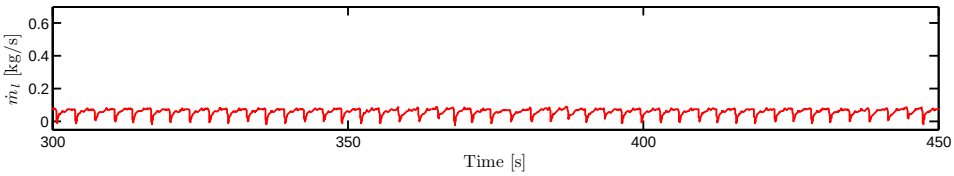

Figure 42: OLGA - series II, $\dot{m}_g = 2.642 \cdot 10^{-5} [kg/s]$

9.2.3 Gas injection rate $= 3.500 \cdot 10^{-5} [kg/s]$

The holdup series in Figure 43 show similar characteristics as the series shown in Figure 40. The rapid shifts in holdup values caused by slugs passing the cell from which data are collected, are even more frequent. This is due to the increased gas injection rate which increases the need of gas and liquid transportation out of the pipe. An increased slug initiation rate hence follows. Similarly to in Section 9.2.2, Mode 3 production is observed.

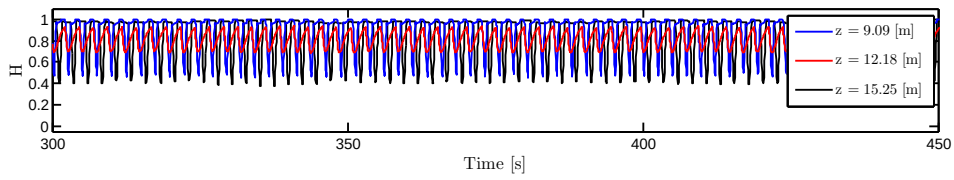

Figure 43: OLGA - series II, $\dot{m}_g = 3.500 \cdot 10^{-5} [kg/s]$

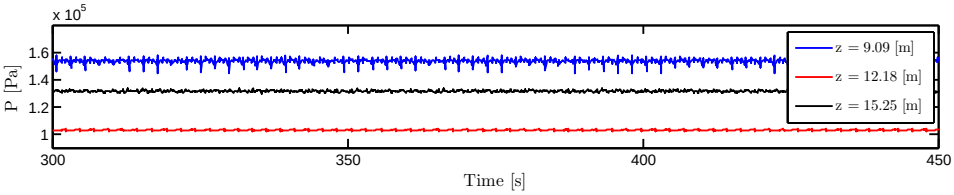

Figure 44: OLGA - series II, $\dot{m}_g = 3.500 \cdot 10^{-5} [kg/s]$

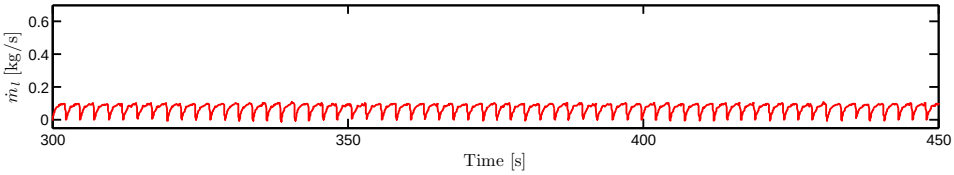

Figure 45: OLGA - series II, $\dot{m}_g = 3.500 \cdot 10^{-5} [kg/s]$

9.3 SLUGGIT - series I

The SLUGGIT simulator modified by the procedure presented in Section 6.1 is in this section used to simulate a series of gas lift experiments. Simulation results from five gas mass injection rates have been chosen for presentation. The geometrical details of the simulation setup are equal to the values given in Table 4 and 5, except for the absence of fixed computational cells. The input parameters used for the simulations in this section are:

- ACC_INJECTION_RATE $= 1 \cdot \dot{m}_g$
- BUBBLE_INIT_LENGTH $= 0.06$
- BUBBLE_FINAL_LENGTH $= 10$
- MIN_BUB_COEFF $= 8$
- MAX_BUB_COEFF $= 50$

9.3.1 Gas injection rate $= 2.000 \cdot 10^{-5}[kg/s]$

Comparison between Figure 46 and Figure 20 shows close correspondence. The time series show similar characteristics, and a cycle period of approximately 50 [s] is observed in both the plots. The pressure plot in Figure 47 is based on pressure values from bubbles, as computed pressure values are only present in bubble sections. Solid lines have been drawn between each available bubble pressure point. The low injection rate implies a relatively low number of bubbles to be present within each cycle. This results in linear curves in some zones inside the plot. Regions showing oscillations in pressure are observed. These oscillations are observed to coincide with the instants of injection of new bubbles. Figure 48 shows a version of the pressure time series to which moving average has been applied. Similar characteristics as seen in Figure 21 is observed. The liquid flow rate shows peaks similar to the ones observed during OLGA simulations. This simulation represents Mode 1 production.

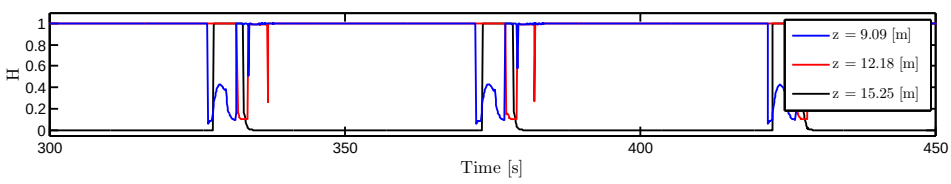

Figure 46: SLUGGIT - series I, $\dot{m}_g = 2.000 \cdot 10^{-5}[kg/s]$

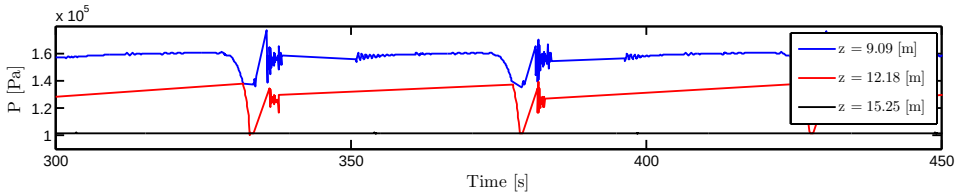

Figure 47: SLUGGIT - series I, $\dot{m}_g = 2.000 \cdot 10^{-5}[kg/s]$

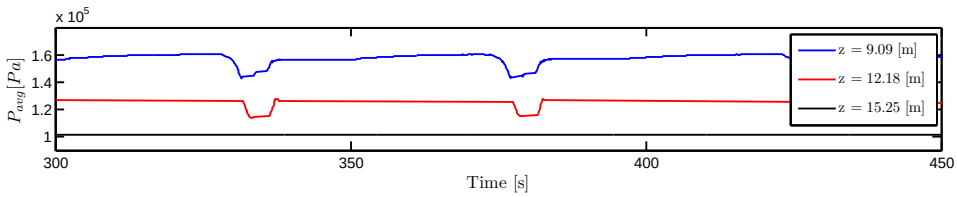

Figure 48: SLUGGIT - series I, $\dot{m}_g = 2.000 \cdot 10^{-5}[kg/s]$

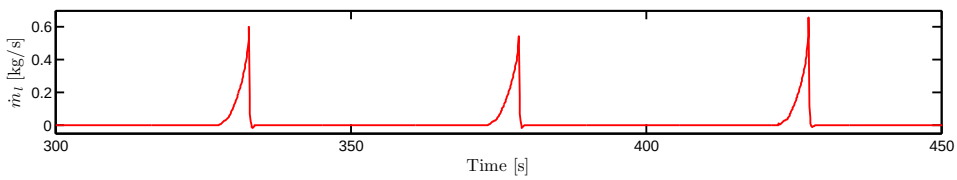

Figure 49: SLUGGIT - series I, $\dot{m}_g = 2.000 \cdot 10^{-5}[kg/s]$

9.3.2 Gas injection rate $= 3.500 \cdot 10^{-5}[kg/s]$

Inspection of the holdup series reveals a reduced cycle period. This is the same tendency as observed during the OLGA simulations as the lift gas injection rate is increased. More frequent fluctuations in holdup are observed along the riser indicating generation of several shorter slugs at the inlet at the beginning of each cycle. It should be noticed that the fluctuations in holdup are more frequent at the outlet compared to what is seen in other parts of the riser. This is caused by the automatic slug removal procedure in SLUGGIT which removes slugs at the pipeline outlet, and does not represent bubbles generated at the riser inlet and then transported to the riser outlet. The portion of the pressure plot showing linear curves is reduced as a result of the increased number of bubbles and the reduced cycle period. Production Mode 1 is still governing.

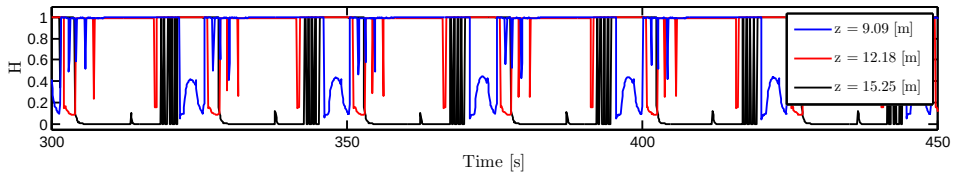

Figure 50: SLUGGIT - series I, $\dot{m}_g = 3.500 \cdot 10^{-5} [kg/s]$

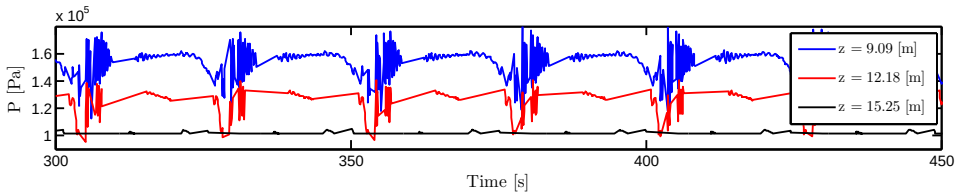

Figure 51: SLUGGIT - series I, $\dot{m}_g = 3.500 \cdot 10^{-5} [kg/s]$

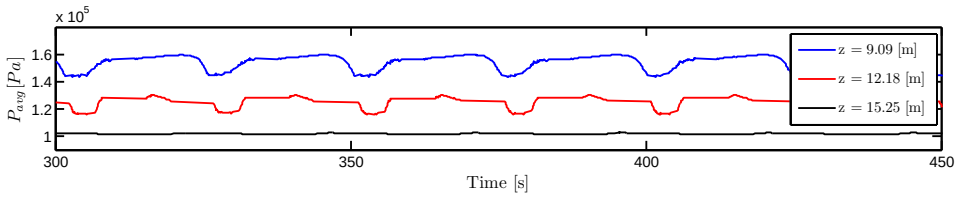

Figure 52: SLUGGIT - series I, $\dot{m}_g = 3.500 \cdot 10^{-5} [kg/s]$

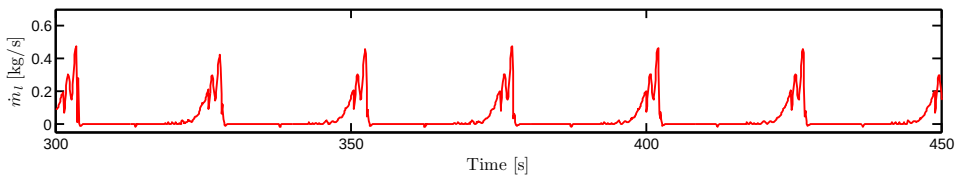

Figure 53: SLUGGIT - series I, $\dot{m}_g = 3.500 \cdot 10^{-5} [kg/s]$

9.3.3 Gas injection rate $= 4.970 \cdot 10^{-5} [kg/s]$

The cycle period is observed further reduced compared to the previous lower gas injection rates. In addition, rapid shifts in holdup are observed in larger parts of the time series, thus indicating a higher slug generation frequency. The high number of slugs allows application of moving average calculation to the holdup time series, the resulting plot is given in Figure 55. The characteristics are similar to those

observed in Figure 28. It can be seen that the time series from the middle of the riser and from the riser outlet are delayed versions of the riser inlet holdup profile. The smoothened holdup profile at the outlet does in general show low values compared to the profiles from the two other sampling points. This is probably caused by the built in slug removal procedure in SLUGGIT, and should not be adressed as an effect of gas expansion alone. This simulation represents Mode 2 production.

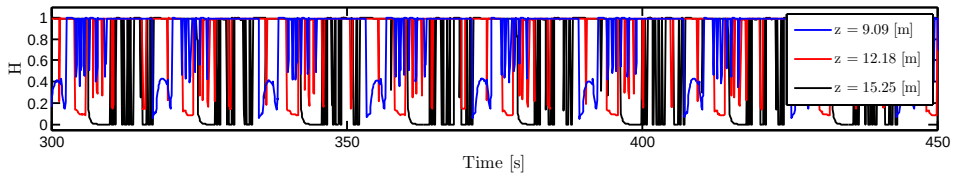

Figure 54: SLUGGIT - series I, $\dot{m}_g = 4.970 \cdot 10^{-5} [kg/s]$

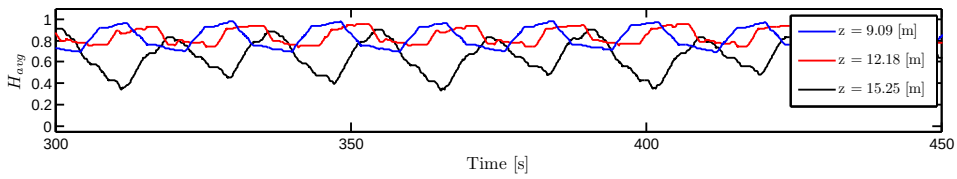

Figure 55: SLUGGIT - series I, $\dot{m}_g = 4.970 \cdot 10^{-5} [kg/s]$

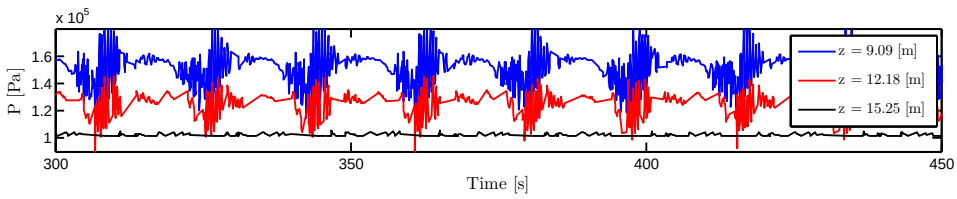

Figure 56: SLUGGIT - series I, $\dot{m}_g = 4.970 \cdot 10^{-5} [kg/s]$

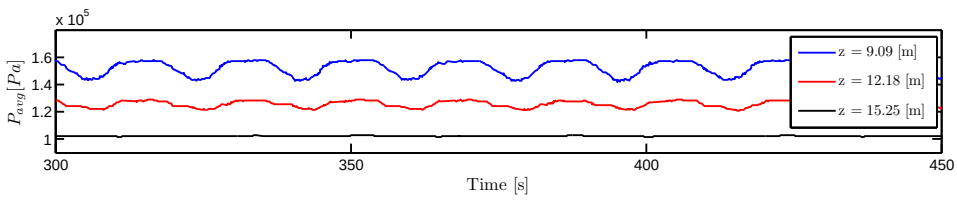

Figure 57: SLUGGIT - series I, $\dot{m}_g = 4.970 \cdot 10^{-5} [kg/s]$

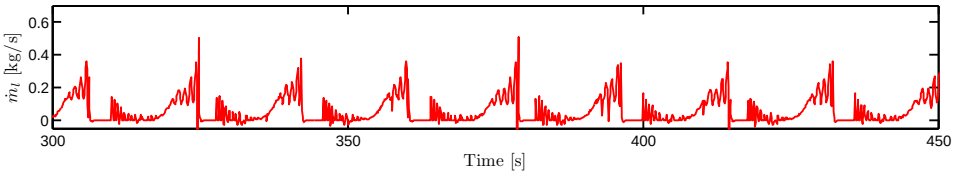

Figure 58: SLUGGIT - series I, $\dot{m}_g = 4.970 \cdot 10^{-5} [kg/s]$

9.3.4 Gas injection rate $= 5.000 \cdot 10^{-5} [kg/s]$

This gas injection rate represents Mode 3 production. Comparison with Figure 54 reveals that the cyclic behaviour can not be observed in Figure 59. Instead, stable generation of larger slugs at the riser inlet dominates. The pressure minimum values are also observed to be higher than at the preceeding lower injection rates, thus indicating a relatively stable presence of liquid mass in the riser. The peaks in liquid production observed at lower gas injection rates resulting from the cyclic behaviour are not present at this injection rate.

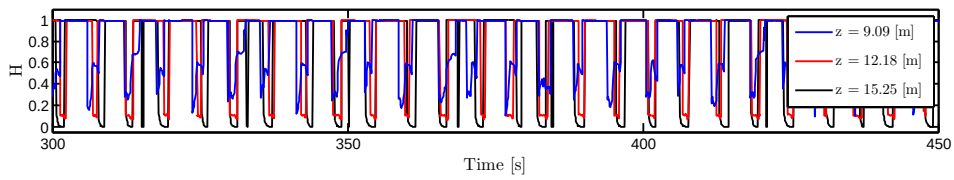

Figure 59: SLUGGIT - series I, $\dot{m}_g = 5.000 \cdot 10^{-5} [kg/s]$

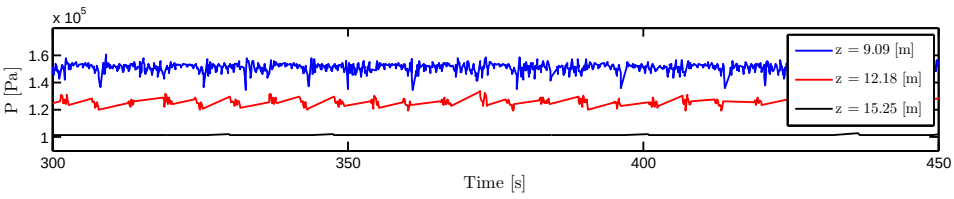

Figure 60: SLUGGIT - series I, $\dot{m}_g = 5.000 \cdot 10^{-5} [kg/s]$

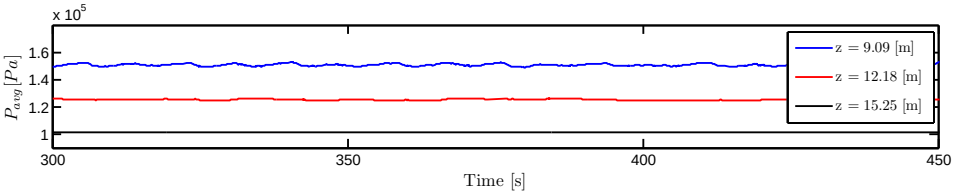

Figure 61: SLUGGIT - series I, $\dot{m}_g = 5.000 \cdot 10^{-5} [kg/s]$

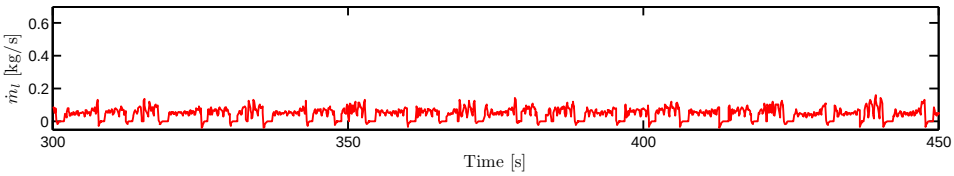

Figure 62: SLUGGIT - series I, $\dot{m}_g = 5.000 \cdot 10^{-5} [kg/s]$

9.3.5 Gas injection rate $= 8.500 \cdot 10^{-5} [kg/s]$

The increased flow rate is observed to further increase the slug generation frequency. The oscillations in pressure are further reduced, and the liquid production is further stabilized. The smooth version of the pressure plot shows almost constant values.

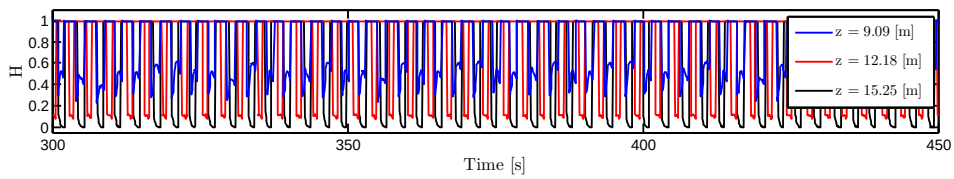

Figure 63: SLUGGIT - series I, $\dot{m}_g = 8.500 \cdot 10^{-5} [kg/s]$

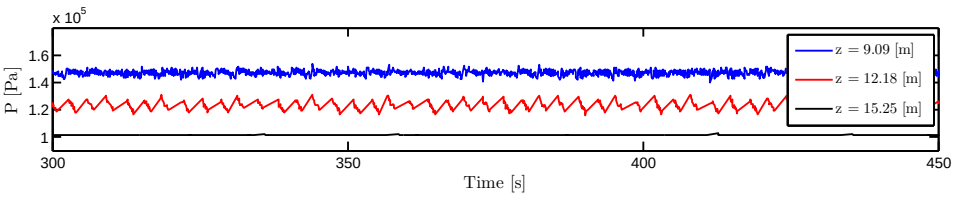

Figure 64: SLUGGIT - series I, $\dot{m}_g = 8.500 \cdot 10^{-5} [kg/s]$

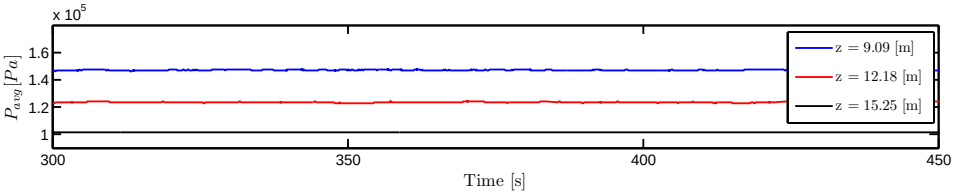

Figure 65: SLUGGIT - series I, $\dot{m}_g = 8.500 \cdot 10^{-5}[kg/s]$

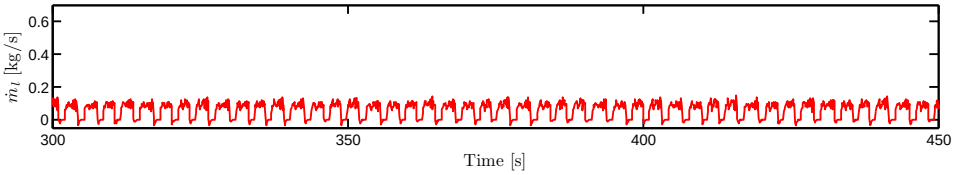

Figure 66: SLUGGIT - series I, $\dot{m}_g = 8.500 \cdot 10^{-5}[kg/s]$

9.4 SLUGGIT - series II

The simulation series presented in Section 9.3 was conducted with $\dot{m}_{inject}$ equal to $\dot{m}_g$. This simulation series presented in this section has been performed to investigate the effect of the $\dot{m}_{inject}$ parameter. A value of $\dot{m}_{inject}$ equal to three times the value of $\dot{m}_g$ has been applied, thus providing a faster injection of the accumulated mass into newly created bubbles. The geometrical details of the simulation setup are equal to the values given in Table 4 and 5, except for the absence of fixed computational cells. The input parameters used for the simulations in this section are:

- ACC_INJECTION_RATE $= 3 \cdot \dot{m}_g$
- BUBBLE_INIT_LENGTH $= 0.06$
- BUBBLE_FINAL_LENGTH $= 10$
- MIN_BUB_COEFF $= 8$
- MAX_BUB_COEFF $= 50$

9.4.1 Gas injection rate $= 2.000 \cdot 10^{-5}[kg/s]$

Comparison of the holdup time series with the series presented in Figure 20 and 46 reveals similar characteristics. A cycle period of approximately 50 [s] is observed. The plots are in general similar to the ones presented at the same gas injection rate in Section 9.3. This is a Mode 1 simulation.

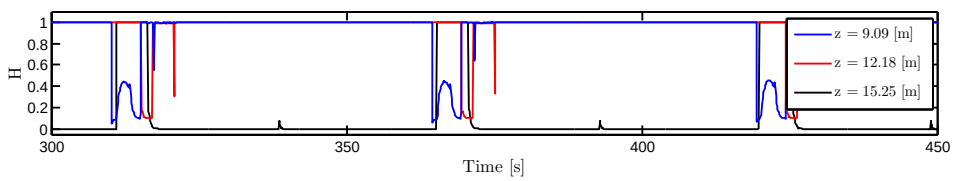

Figure 67: SLUGGIT - series II, $\dot{m}_g = 2.000 \cdot 10^{-5}[kg/s]$

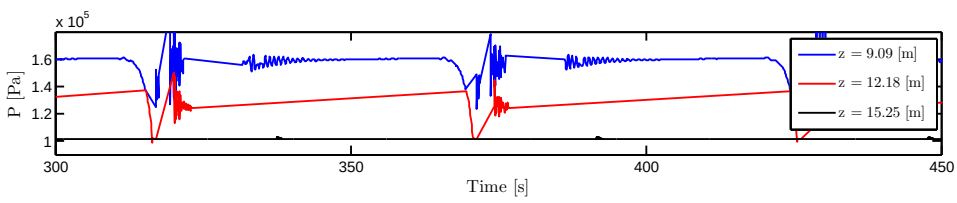

Figure 68: SLUGGIT - series II, $\dot{m}_g = 2.000 \cdot 10^{-5}[kg/s]$

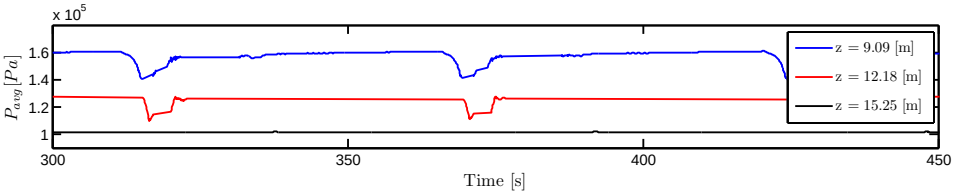

Figure 69: SLUGGIT - series II, $\dot{m}_g = 2.000 \cdot 10^{-5} [kg/s]$

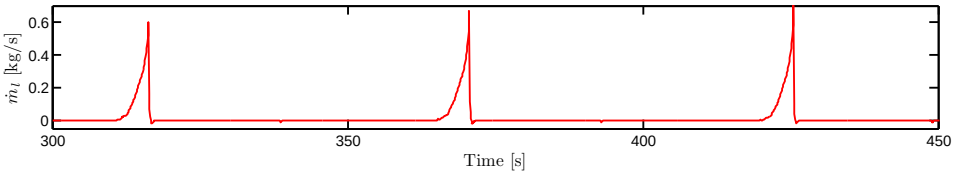

Figure 70: SLUGGIT - series II, $\dot{m}_g = 2.000 \cdot 10^{-5} [kg/s]$

9.4.2 Gas injection rate $= 3.350 \cdot 10^{-5} [kg/s]$

The increased gas injection rate is observed to reduce the period of the cyclic behaviour. The liquid front movement is still violent enough to give this simulation Mode 1 characteristics.

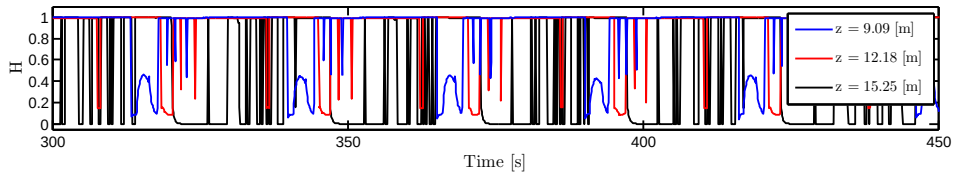

Figure 71: SLUGGIT - series II, $\dot{m}_g = 3.350 \cdot 10^{-5} [kg/s]$

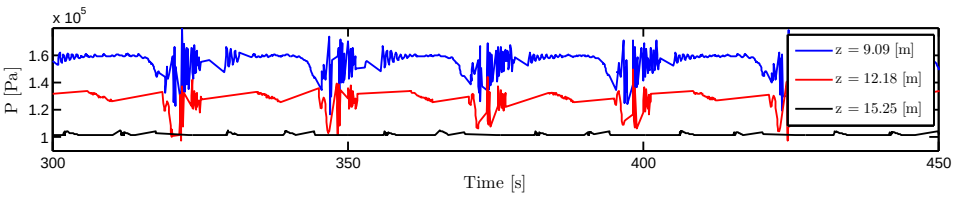

Figure 72: SLUGGIT - series II, $\dot{m}_g = 3.350 \cdot 10^{-5} [kg/s]$

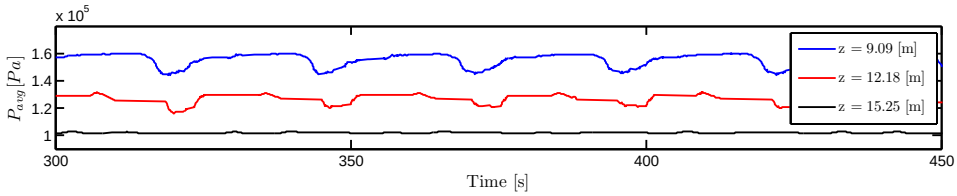

Figure 73: SLUGGIT - series II, $\dot{m}_g = 3.350 \cdot 10^{-5}[kg/s]$

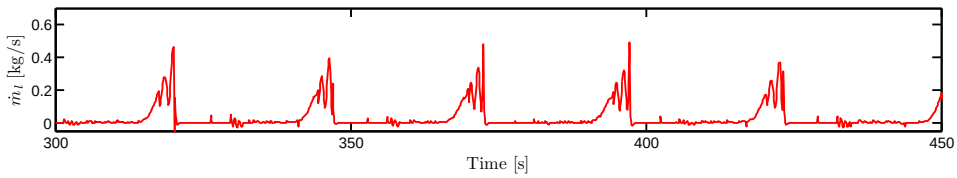

Figure 74: SLUGGIT - series II, $\dot{m}_g = 3.350 \cdot 10^{-5}[kg/s]$

9.4.3 Gas injection rate $= 3.650 \cdot 10^{-5}[kg/s]$

Similarly to what was observed in Section 9.4.2, the number of shorter slugs generated during each cycle is still limited. Moving average has therefore not been applied to the holdup time series in any of these two sections. Contrary to what was observed in Section 9.3.3, it is not possible to obtain generation of a higher number of slugs as a results of the increased gas injection rate. This may possibly be due to inertia effects from the increased injection rate with the inserted gas bubbles being injected three times faster. During this process liquid is displaced in both an upstream and a downstream direction from the injection point. Some of the dynamic animations indicate that the increased injection rate contributes to bring the liquid front in contact with the riser inlet. This gas injection rate represents the limit at which unstable production is observed in SLUGGIT - series II. Any increase in gas injection rate from this value causes the flow to develop into a steady state. This limit is observed to exist at the higher gas injection rate $\dot{m}_g = 4.970 \cdot 10^{-5}[kg/s]$ in Section 9.3. The time series representing pressure and liquid flow rate show similar behaviour to what was observed in Section 9.3. Contrary to what was observed in Section 9.3, it has not been possible to obtain unstable production with Mode 2 characteristics in Section 9.4. This implies that production within Section 9.4 develops directly from Mode 1 production into Mode 3 production.

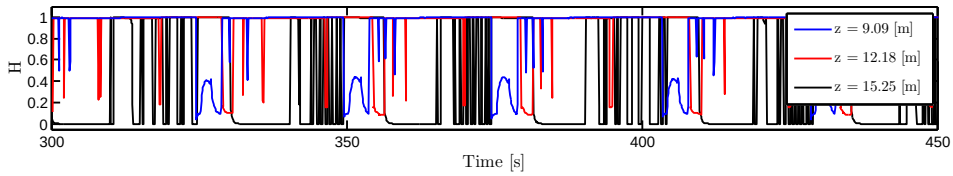

Figure 75: SLUGGIT - series II, $\dot{m}_g = 3.650 \cdot 10^{-5} [kg/s]$

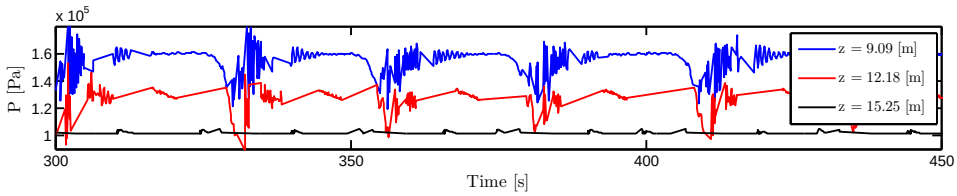

Figure 76: SLUGGIT - series II, $\dot{m}_g = 3.650 \cdot 10^{-5} [kg/s]$

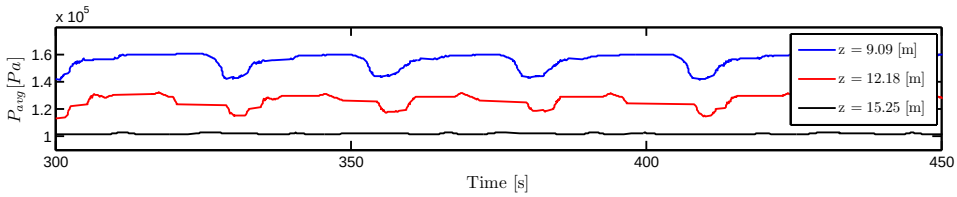

Figure 77: SLUGGIT - series II, $\dot{m}_g = 3.650 \cdot 10^{-5} [kg/s]$

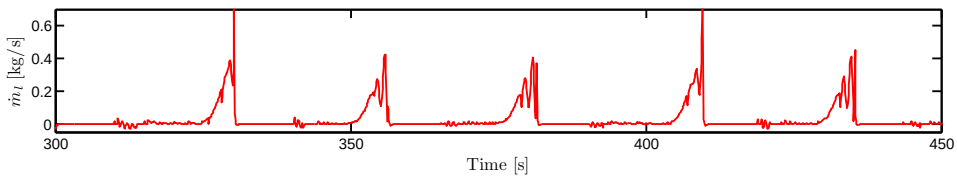

Figure 78: SLUGGIT - series II, $\dot{m}_g = 3.650 \cdot 10^{-5} [kg/s]$

9.4.4 Gas injection rate $= 5.000 \cdot 10^{-5} [kg/s]$

Comparison between the time series presented in this section and the series presented in Section 9.3.4 reveals almost identical characteristics with a slightly increased frequency. An exception is though observed with regard to the riser outlet holdup profile with the observation of an increased slug generation frequency, which is probably caused by the SLUGGIT automatic slug removal procedure, resulting

in rapid shifts in holdup at the riser outlet. Some differences in time series shape are also observed upon comparison of the liquid flow rate plots.

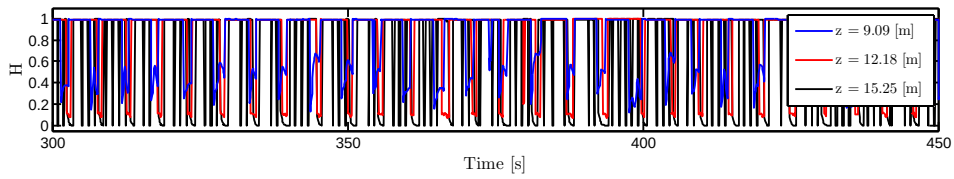

Figure 79: SLUGGIT - series II, $\dot{m}_g = 5.000 \cdot 10^{-5} [kg/s]$

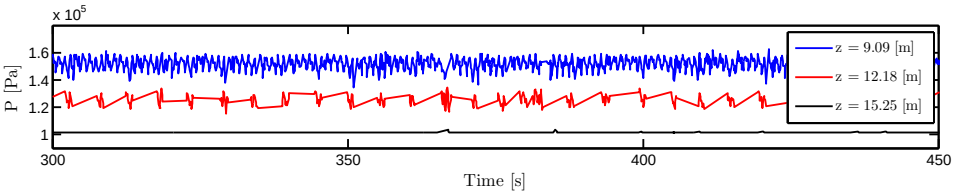

Figure 80: SLUGGIT - series II, $\dot{m}_g = 5.000 \cdot 10^{-5} [kg/s]$

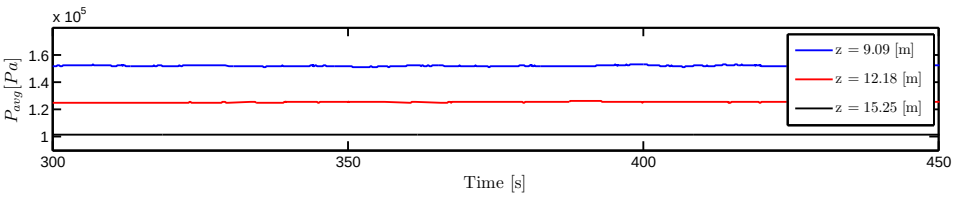

Figure 81: SLUGGIT - series II, $\dot{m}_g = 5.000 \cdot 10^{-5} [kg/s]$

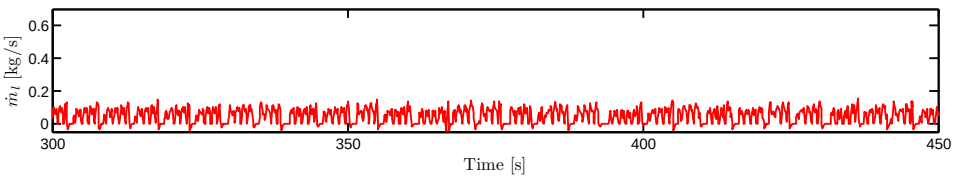

Figure 82: SLUGGIT - series II, $\dot{m}_g = 5.000 \cdot 10^{-5} [kg/s]$

9.4.5 Gas injection rate $= 8.500 \cdot 10^{-5} [kg/s]$

Comparison with the figures in Section 9.3.5 indicates a significantly higher slug generation frequency in the present case, a tendency observed in all the plots by

more frequent shifts in characteristic values. This indicates that the combination of input parameters used in this simulation series contributes to increase the slug generation frequency at the higher flow rates. This trend may also be observed upon comparison of Figure 59 and 79.

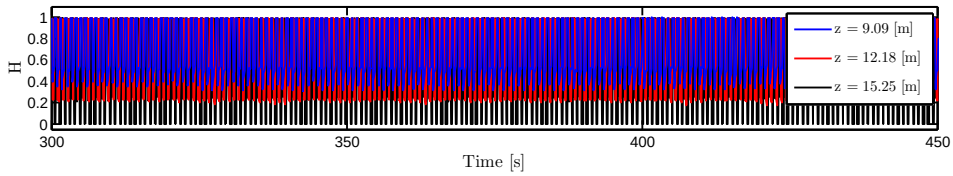

Figure 83: SLUGGIT - series II, $\dot{m}_g = 8.500 \cdot 10^{-5} [kg/s]$

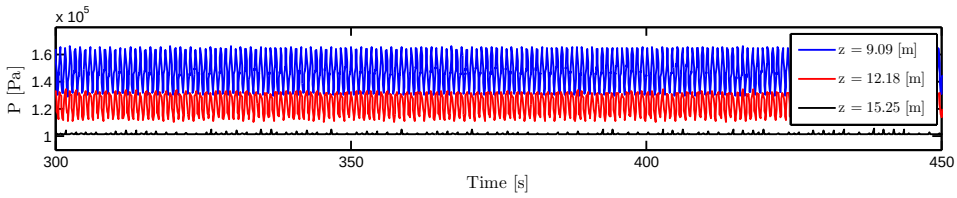

Figure 84: SLUGGIT - series II, $\dot{m}_g = 8.500 \cdot 10^{-5} [kg/s]$

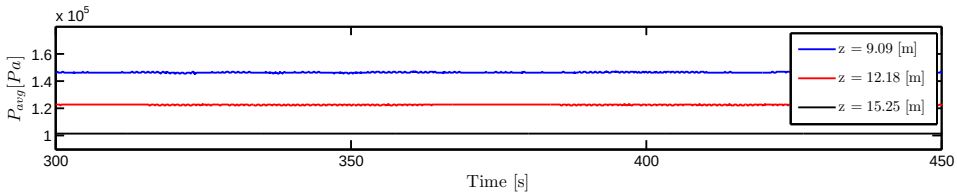

Figure 85: SLUGGIT - series II, $\dot{m}_g = 8.500 \cdot 10^{-5} [kg/s]$

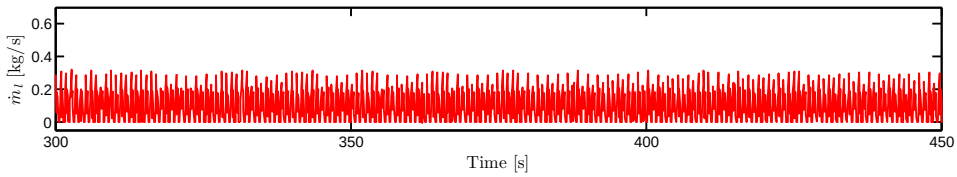

Figure 86: SLUGGIT - series II, $\dot{m}_g = 8.500 \cdot 10^{-5} [kg/s]$

9.5 SLUGGIT - series III

Investigation of the simulation results from Section 9.3 and 9.4 revealed some unexpected flow characteristics with respect to bubble lengths in the vertical riser at the lower gas injection rates. This can be observed by inspection of Figure 156b to 156f in the appendix. As the riser is vertical and the system is gravity dominated, one should expect some liquid to flow back downwards inside these long bubbles, and then form new slugs in the lower parts of the riser. The input parameters enabling bubble section length control in the SLUGGIT simulator are:

- MIN_BUB_COEFF
- MAX_BUB_COEFF

These parameters define the minimum and maximum bubble section lengths in multiples of pipe diameters. The MAX_BUB_COEFF has in the preceding simulations possessed a value of 50. The simulation series presented in this section have been conducted to investigate the effect of this parameter on the bubble lengths in the riser and the generation of slugs at the riser inlet. During simulation the SLUGGIT simulator continuously compares neighbouring bubble sections and their characteristic variables. When two neighbouring bubbles show properties similar enough to meet a bubble section merging criterion, they are merged. Using a value of MAX_BUB_COEFF equal to 50 is equivalent to allowing merging of bubble sections to form bubbles with a maximum length of 50 pipe diameters. A reduction of this value is equivalent to requiring shorter bubble sections with holdup values free to grow on a local base and then form slugs in the lower parts of the riser. A value of 20 has been used in the simulations presented in this section. Attempts have been made to run simulations with values lower than 20. These simulations were observed to run unacceptably slow after reduction of the time step by the automatic time step control every time new bubbles were inserted. The geometrical details of the simulation setup are equal to the values given in Table 4 and 5, except for the absence of fixed computational cells. The input parameters used for the simulations in this section are:

- ACC_INJECTION_RATE $= 3 \cdot \dot{m}_g$
- BUBBLE_INIT_LENGTH = 0.2
- BUBBLE_FINAL_LENGTH = 10
- MIN_BUB_COEFF = 8
- MAX_BUB_COEFF = 20

9.5.1 Gas injection rate $= 2.000 \cdot 10^{-5} [kg/s]$

Comparison with previous OLGA and SLUGGIT simulations at the same gas injection rate reveals a similar cyclic behaviour with a period of approximately 50 [s]. The number of slugs generated at the riser inlet is observed to be higher.

This can also be observed in Figure 159b to 159f where shorter slugs are observed to travel up the riser. These slugs are not present in the previous SLUGGIT simulations and result from the forced shorter bubble lengths obtained through the changed value of MAX_BUB_COEFF. These slugs can also be observed in Figure 90 where the first major peak in liquid production is followed by two smaller peaks representing the two slugs resulting from liquid falling back inside the riser, with consequent blocking of the riser inlet and slug generation. This gas injection rate represents unstable production with Mode 1 characteristics.

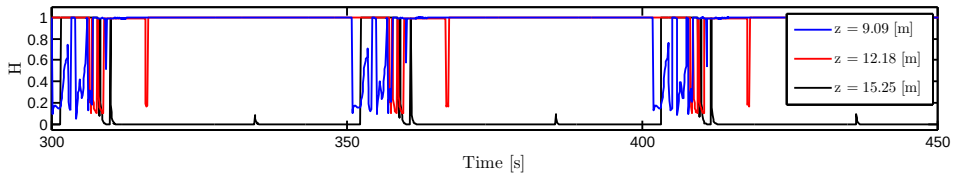

Figure 87: SLUGGIT - series III, $\dot{m}_g = 2.000 \cdot 10^{-5} [kg/s]$

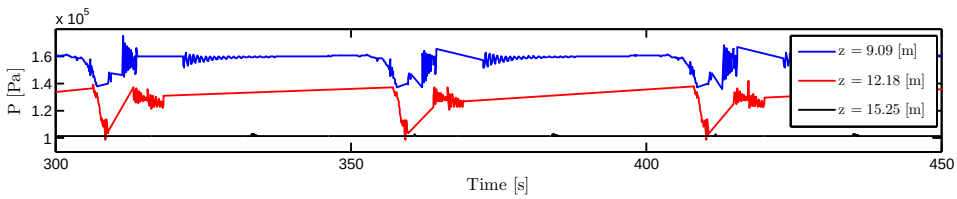

Figure 88: SLUGGIT - series III, $\dot{m}_g = 2.000 \cdot 10^{-5} [kg/s]$

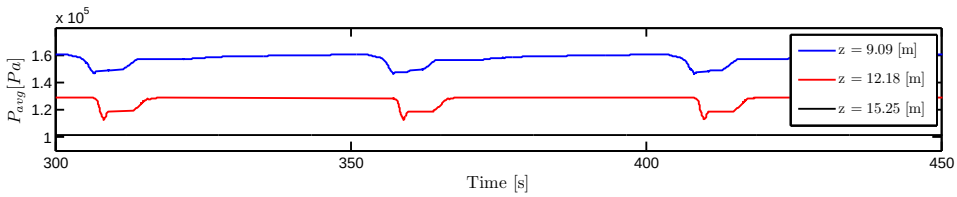

Figure 89: SLUGGIT - series III, $\dot{m}_g = 2.000 \cdot 10^{-5} [kg/s]$

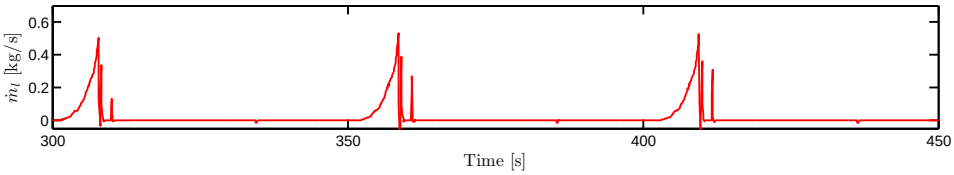

Figure 90: SLUGGIT - series III, $\dot{m}_g = 2.000 \cdot 10^{-5} [kg/s]$

9.5.2 Gas injection rate $= 3.350 \cdot 10^{-5} [kg/s]$

This flow rate represents the operational point where the cyclic behaviour seen in Section 9.1.3 and 9.3.3 with a period of approximately 20 [s] is obtained. An increased number of rapid shifts in holdup values is observed, indicating a higher number of slugs. The smoothened holdup profile from the riser outlet does in general show lower values than the two other profiles. This is likely to result from the automatic slug removal at the riser outlet. The unstable production observed shows Mode 2 characteristics.

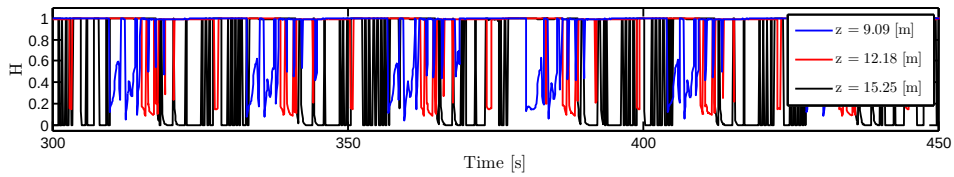

Figure 91: SLUGGIT - series III, $\dot{m}_g = 3.350 \cdot 10^{-5} [kg/s]$

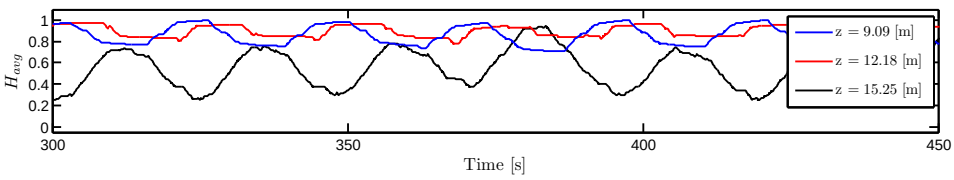

Figure 92: SLUGGIT - series III, $\dot{m}_g = 3.350 \cdot 10^{-5} [kg/s]$

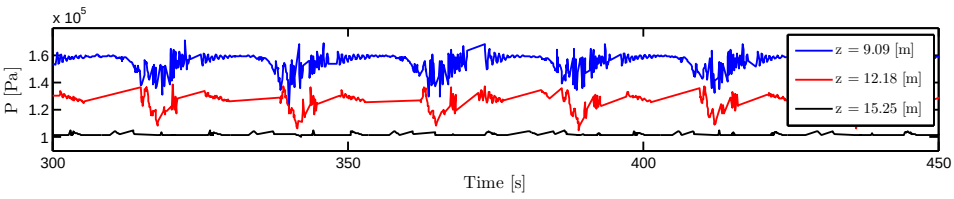

Figure 93: SLUGGIT - series III, $\dot{m}_g = 3.350 \cdot 10^{-5} [kg/s]$

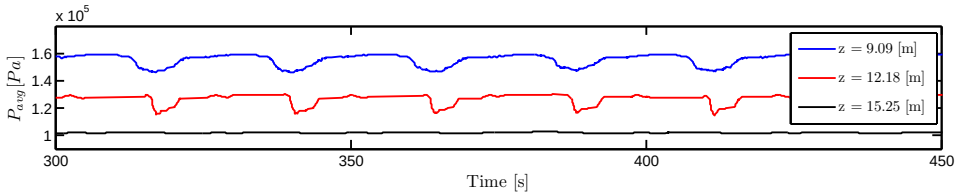

Figure 94: SLUGGIT - series III, $\dot{m}_g = 3.350 \cdot 10^{-5} [kg/s]$

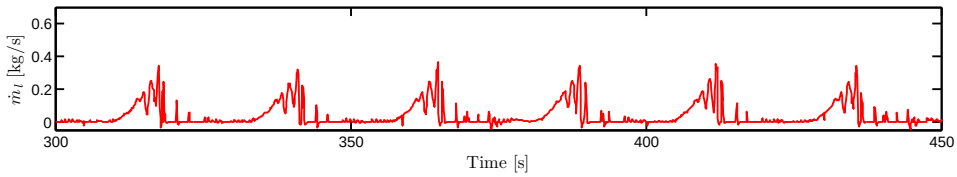

Figure 95: SLUGGIT - series III, $\dot{m}_g = 3.350 \cdot 10^{-5} [kg/s]$

9.5.3 Gas injection rate $= 3.650 \cdot 10^{-5} [kg/s]$

The unstable production obtained at this gas injection rate shows Mode 2 characteristics, similar to the unstable production obtained in Section 9.5.2. This indicates that Mode 2 unstable production in SLUGGIT - series III is present over a wider gas injection rate range than what is the case in SLUGGIT - series I.

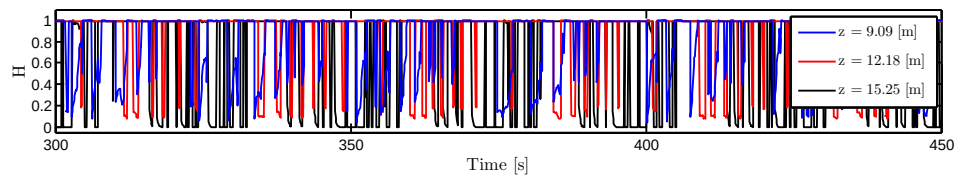

Figure 96: SLUGGIT - series III, $\dot{m}_g = 3.650 \cdot 10^{-5} [kg/s]$

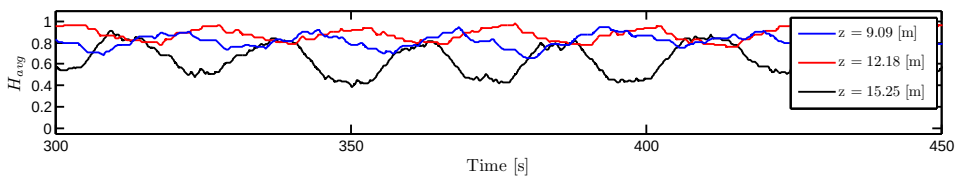

Figure 97: SLUGGIT - series III, $\dot{m}_g = 3.650 \cdot 10^{-5} [kg/s]$

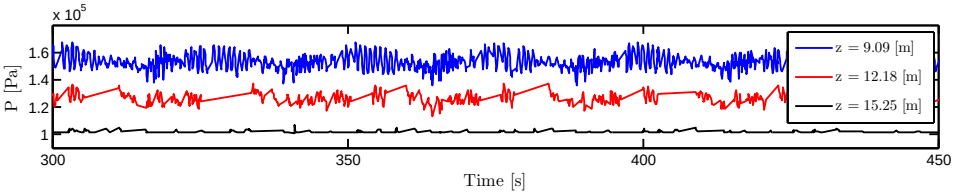

Figure 98: SLUGGIT - series III, $\dot{m}_g = 3.650 \cdot 10^{-5}[kg/s]$

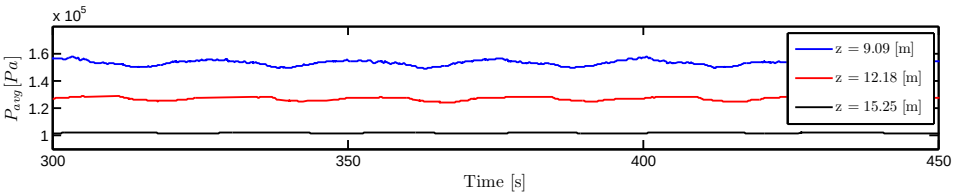

Figure 99: SLUGGIT - series III, $\dot{m}_g = 3.650 \cdot 10^{-5}[kg/s]$

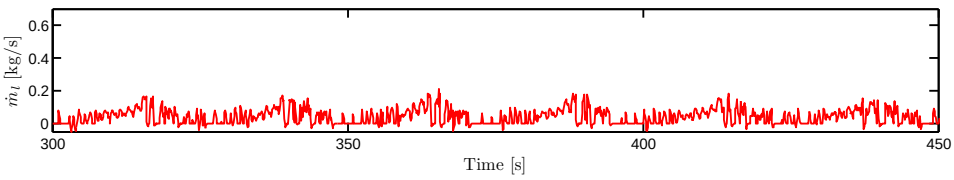

Figure 100: SLUGGIT - series III, $\dot{m}_g = 3.650 \cdot 10^{-5}[kg/s]$

9.5.4 Gas injection rate $= 5.000 \cdot 10^{-5}[kg/s]$

At this flow rate the unstable production has disappeared, and Mode 3 production is obtained. Comparison with Figure 79 illustrates the increased slug generation frequency, resulting from the reduction in allowed maximum bubble length, with liquid flowing back towards the riser inlet and then accumulating at the bend forming small liquid blockings which in turn grow into slugs.

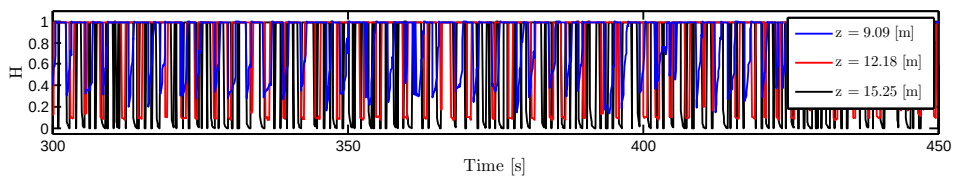

Figure 101: SLUGGIT - series III, $\dot{m}_g = 5.000 \cdot 10^{-5}[kg/s]$

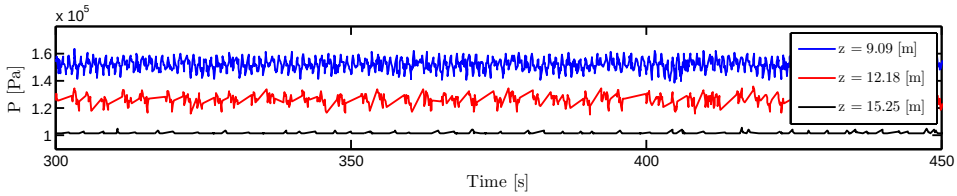

Figure 102: SLUGGIT - series III, $\dot{m}_g = 5.000 \cdot 10^{-5} [kg/s]$

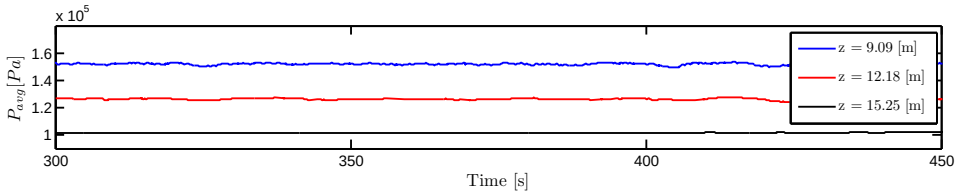

Figure 103: SLUGGIT - series III, $\dot{m}_g = 5.000 \cdot 10^{-5} [kg/s]$

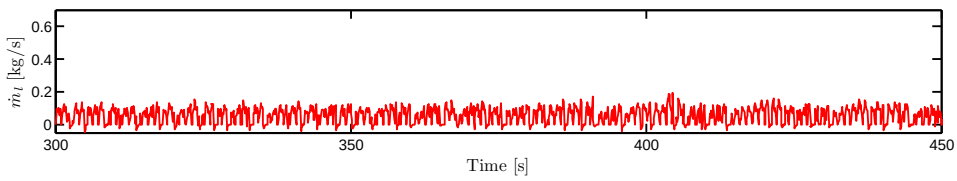

Figure 104: SLUGGIT - series III, $\dot{m}_g = 5.000 \cdot 10^{-5} [kg/s]$

9.5.5 Gas injection rate $= 8.500 \cdot 10^{-5} [kg/s]$

This gas injection rate represents stable Mode 3 production with characteristics similar to those seen in Section 9.4.5. Contrary to what is observed in Section 9.4.5 the holdup values at the outlet do not drop to zero. The oscillations in instantaneous pressure values may originate from gas / liquid column oscillations in the riser. The pressure value extraction method described in Figure 18b may possibly have contributed to amplify the magnitude of the extrema in the plot as pressure values from different vertical locations with corresponding different hydrostatic pressures are included.

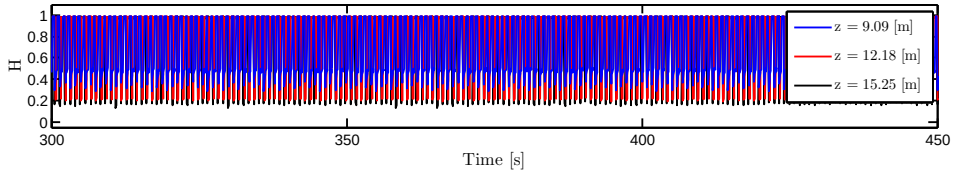

Figure 105: SLUGGIT - series III, $\dot{m}_g = 8.500 \cdot 10^{-5} [kg/s]$

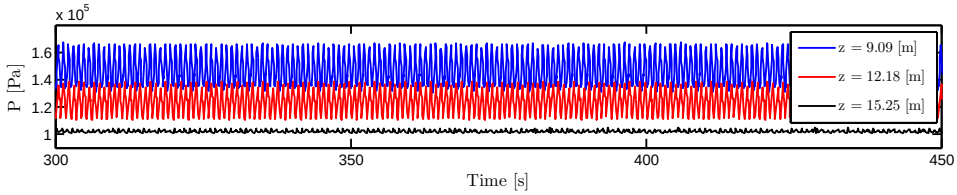

Figure 106: SLUGGIT - series III, $\dot{m}_g = 8.500 \cdot 10^{-5} [kg/s]$

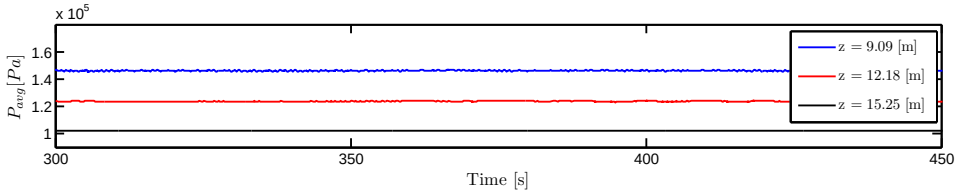

Figure 107: SLUGGIT - series III, $\dot{m}_g = 8.500 \cdot 10^{-5} [kg/s]$

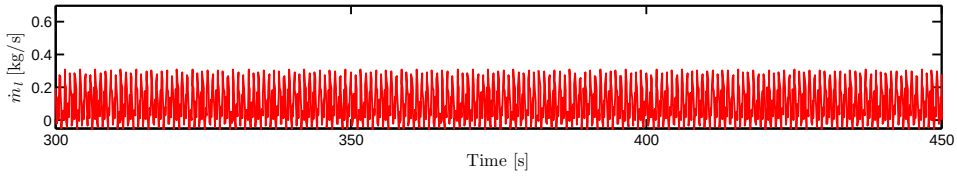

Figure 108: SLUGGIT - series III, $\dot{m}_g = 8.500 \cdot 10^{-5} [kg/s]$

9.6 SLUGGIT - series IV

Based on the observations made in Section 9.5 the simulations presented in this section have been conducted to investigate the effect of a further reduced maximum bubble section length. This implies an increased number of computational sections and hence an increase in computational demand. The automatic time step control based on the CFL criterion has therefore been a useful option for keeping the execution time on a reasonable level in this simulation series.

As described in Section 6.2, the original slug splitting procedure given in Section 6.1 was observed to artificially initiate a reduction in time step through the CFL criterion. This reduction, in combination with the higher number of computational sections handled in Section 9.5, was found to give unacceptably long execution times. This initiated the need for the alternative slug and bubble insertion procedure presented in Section 6.2, which has been used for the simulations presented in this section. The geometrical details of the simulation setup are equal to the values given in Table 4 and 5, except for the absence of fixed computational cells. The input parameters used during these simulations are:

- ACC_INJECTION_RATE $= 3 \cdot \dot{m}_g$
- BUBBLE_INIT_LENGTH $= 0.07$
- BUBBLE_FINAL_LENGTH $= 6$
- MIN_BUB_COEFF $= 4$
- MAX_BUB_COEFF $= 10$

9.6.1 Gas injection rate $= 2.000 \cdot 10^{-5} [kg/s]$

Comparison with simulation results from the same gas injection rate presented in the previous sections indicates good correspondence with respect to the period of the cyclic behaviour, which is observed to be close to 50 [s]. Inspection of the instantaneous pressure plot reveals that the oscillations in pressure are still present. This gas injection rate represents unstable production with Mode 1 characteristcs.

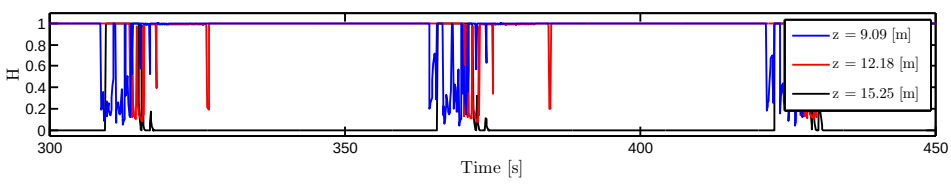

Figure 109: SLUGGIT - series IV, $\dot{m}_g = 2.000 \cdot 10^{-5} [kg/s]$

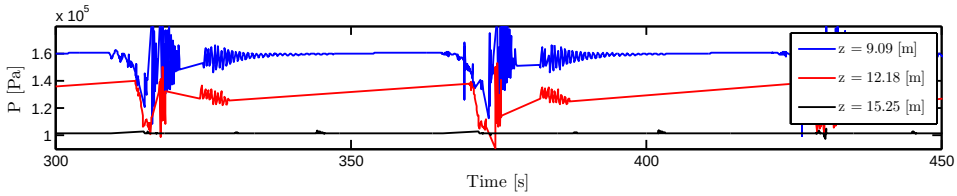

Figure 110: SLUGGIT - series IV, $\dot{m}_g = 2.000 \cdot 10^{-5} [kg/s]$

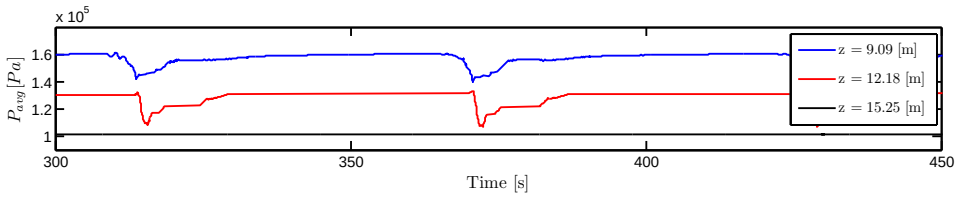

Figure 111: SLUGGIT - series IV, $\dot{m}_g = 2.000 \cdot 10^{-5} [kg/s]$

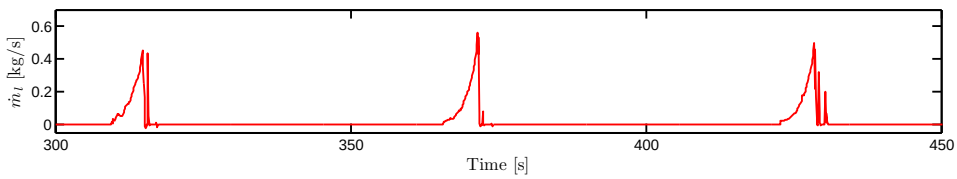

Figure 112: SLUGGIT - series IV, $\dot{m}_g = 2.000 \cdot 10^{-5} [kg/s]$

9.6.2 Gas injection rate $= 3.350 \cdot 10^{-5} [kg/s]$

This simulation represents Mode 2 production with slugs being generated continuously, but at a varying rate. Comparison with Figure 91 reveals a significantly higher number of slugs in this case. Comparison between Figure 95 and 117 indicates that the reduced bubble length in combination with an increased number of bubbles contributes to remove the high liquid production peaks seen in Figure 95. The increased number of bubbles also contributes to reduce the pressure variations during each cycle at all locations along the riser.

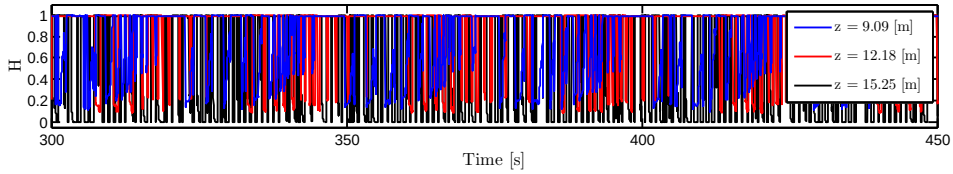

Figure 113: SLUGGIT - series IV, $\dot{m}_g = 3.350 \cdot 10^{-5} [kg/s]$

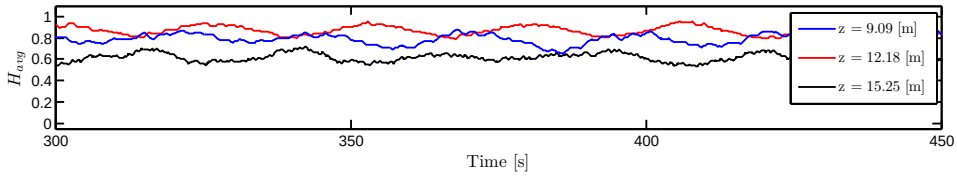

Figure 114: SLUGGIT - series IV, $\dot{m}_g = 3.350 \cdot 10^{-5} [kg/s]$

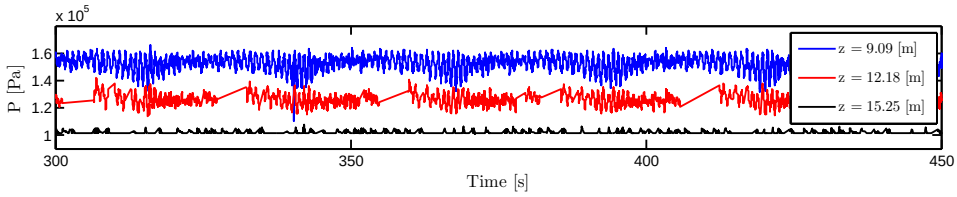

Figure 115: SLUGGIT - series IV, $\dot{m}_g = 3.350 \cdot 10^{-5} [kg/s]$

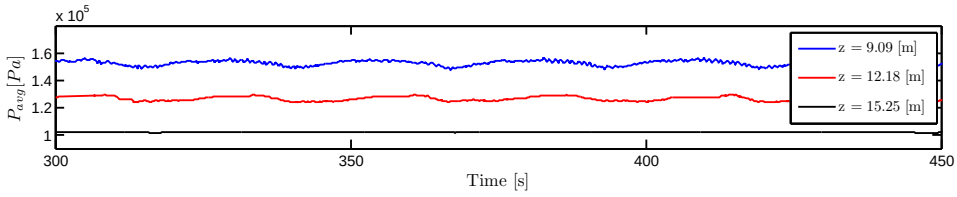

Figure 116: SLUGGIT - series IV, $\dot{m}_g = 3.350 \cdot 10^{-5} [kg/s]$

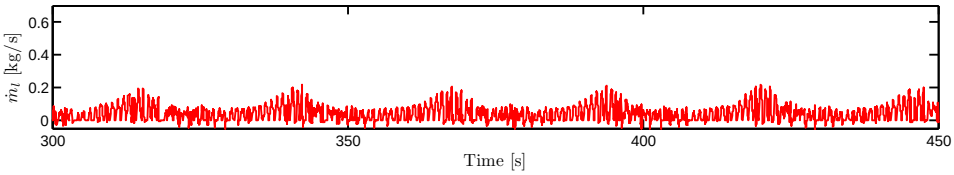

Figure 117: SLUGGIT - series IV, $\dot{m}_g = 3.350 \cdot 10^{-5} [kg/s]$

9.6.3 Gas injection rate $= 3.650 \cdot 10^{-5} [kg/s]$

Similarly to what was observed in Section 9.6.2, this simulation represents unstable production showing Mode 2 characteristics. Comparison between Figure 91 and 96 and then between Figure 113 and 118 reveals that the equalities between Figure 113 and 118 are even larger than what is observed in the first-mentioned couple of figures. This indicates that the transition from unstable to stable production is even smoother in SLUGGIT - series IV compared to what is observed in SLUGGIT - series III.

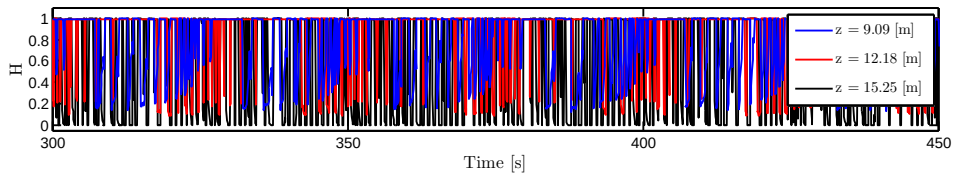

Figure 118: SLUGGIT - series IV, $\dot{m}_g = 3.650 \cdot 10^{-5} [kg/s]$

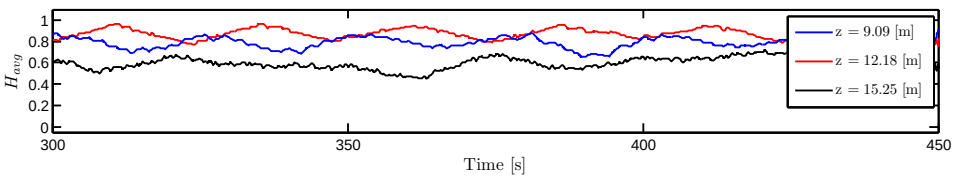

Figure 119: SLUGGIT - series IV, $\dot{m}_g = 3.650 \cdot 10^{-5} [kg/s]$

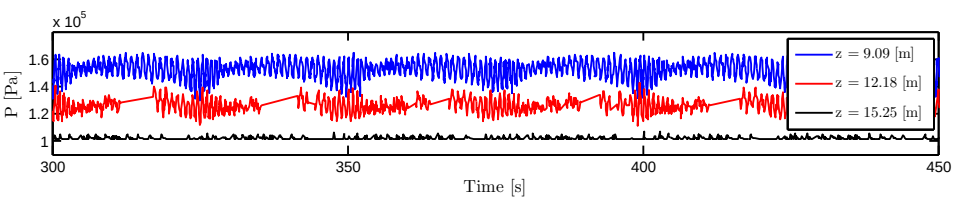

Figure 120: SLUGGIT - series IV, $\dot{m}_g = 3.650 \cdot 10^{-5} [kg/s]$

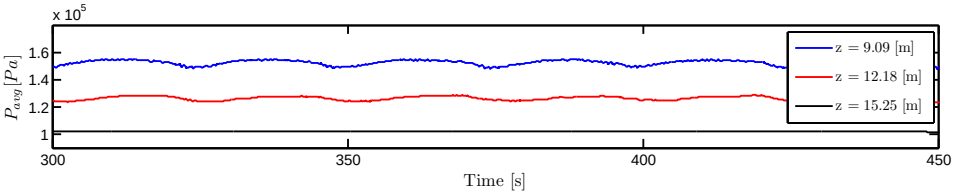

Figure 121: SLUGGIT - series IV, $\dot{m}_g = 3.650 \cdot 10^{-5} [kg/s]$

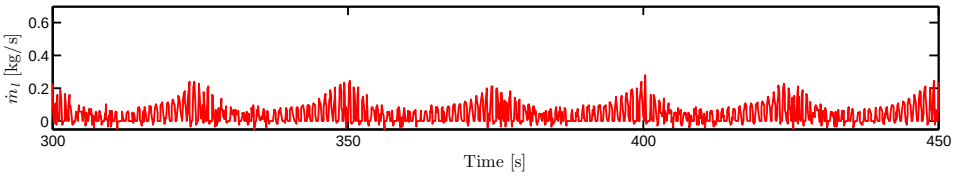

Figure 122: SLUGGIT - series IV, $\dot{m}_g = 3.650 \cdot 10^{-5} [kg/s]$

9.6.4 Gas injection rate $= 5.000 \cdot 10^{-5} [kg/s]$

Some traces of unstable production may still be observed at this gas injection rate. The instabilities observed in this simulation may represent Mode 2 production. Another possibility is that the unstable behaviour is due to gas / liquid column oscillations within the riser as illustrated in Figure 150, and that the generation of slugs at the inlet has stabilized on a constant rate implying stable Mode 3 production.

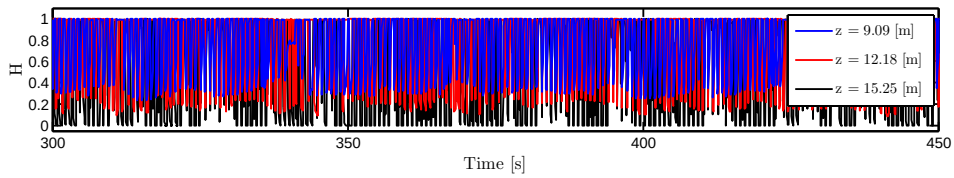

Figure 123: SLUGGIT - series IV, $\dot{m}_g = 5.000 \cdot 10^{-5} [kg/s]$

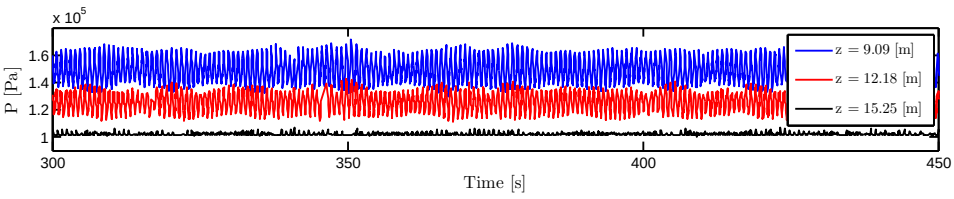

Figure 124: SLUGGIT - series IV, $\dot{m}_g = 5.000 \cdot 10^{-5} [kg/s]$

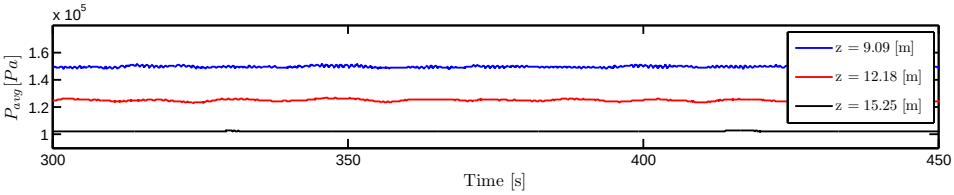

Figure 125: SLUGGIT - series IV, $\dot{m}_g = 5.000 \cdot 10^{-5}[kg/s]$

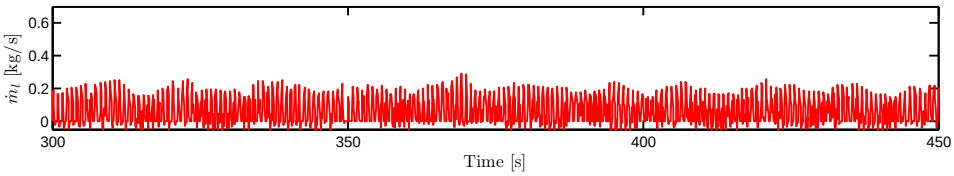

Figure 126: SLUGGIT - series IV, $\dot{m}_g = 5.000 \cdot 10^{-5}[kg/s]$

9.6.5 Gas injection rate $= 8.500 \cdot 10^{-5}[kg/s]$

The increased gas injection rate is observed to further increase the slug generation frequency. The pressure variations seen in Figure 130 are likely to originate from gas / liquid column oscillations as illustrated in Figure 150. This simulation represents Mode 3 production.

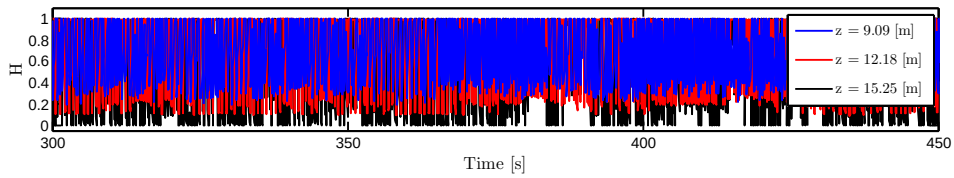

Figure 127: SLUGGIT - series IV, $\dot{m}_g = 8.500 \cdot 10^{-5}[kg/s]$

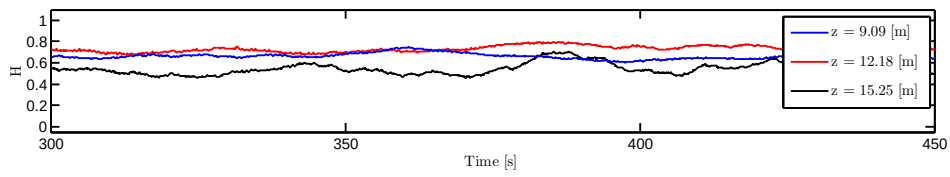

Figure 128: SLUGGIT - series IV, $\dot{m}_g = 8.500 \cdot 10^{-5}[kg/s]$

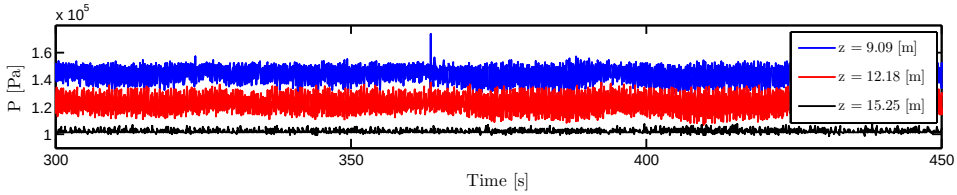

Figure 129: SLUGGIT - series IV, $\dot{m}_g = 8.500 \cdot 10^{-5} [kg/s]$

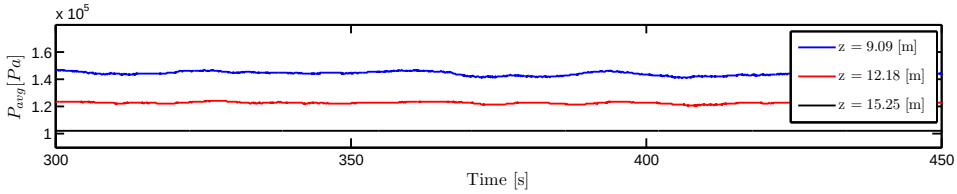

Figure 130: SLUGGIT - series IV, $\dot{m}_g = 8.500 \cdot 10^{-5} [kg/s]$

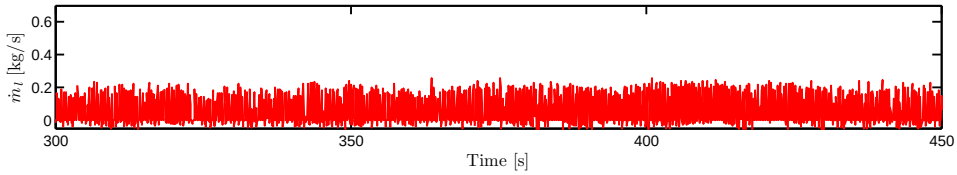

Figure 131: SLUGGIT - series IV, $\dot{m}_g = 8.500 \cdot 10^{-5} [kg/s]$

9.7 An alternative approach

The simulations presented in Section 9.1 to 9.6 were all conducted with a simulation configuration involving five pipes as shown in Figure 16. The riser inlet pressure was provided by the liquid column present within the two first pipes. The results revealed a high degree of interaction between the second and third pipe, with a liquid front being observed to travel within them. This section presents an alternative simulation based on a geometry consisting of three pipes. This alternative geometry with pressure and holdup boundary conditions is shown in Figure 132.

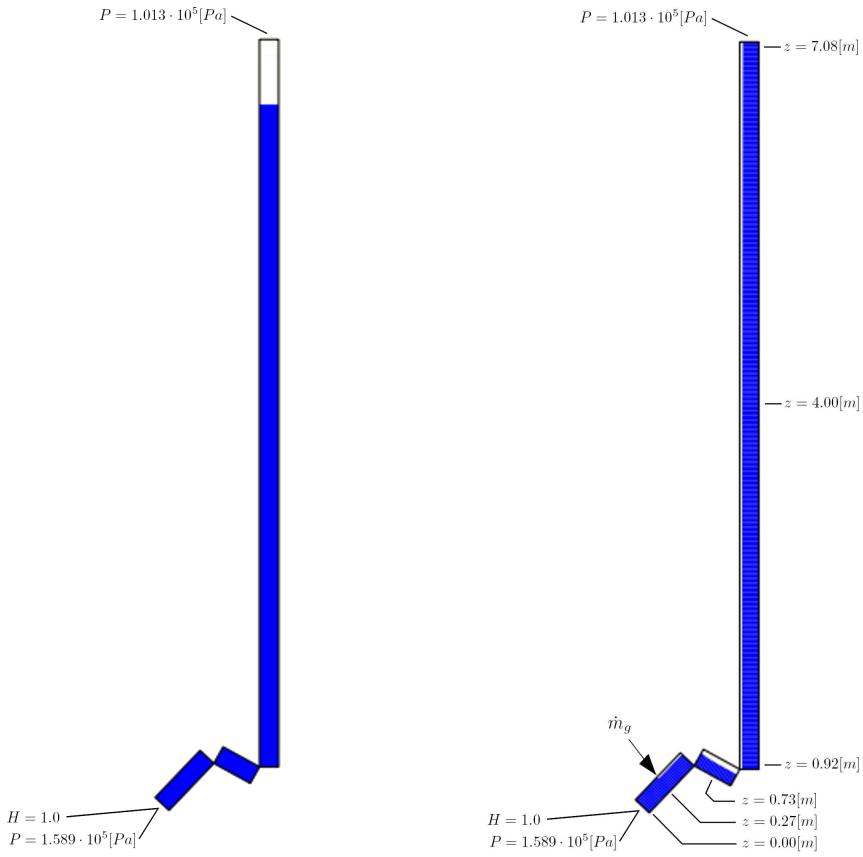

(a) Visualization of the situation from which the SLUGGIT initial conditions are obtained.

(b) The pressure and holdup boundary conditions used during both OLGA and SLUGGIT simulations are annotated at the inlet and at the outlet

Figure 132

Pipe	Length [m]	Cells	Cell length [m]	Diameter [m]	Roughness [m]	Inclination θ [°]
1	0.55	27	0.0204	0.016	2E-6	+46.7
2	0.35	17	0.0206	0.016	2E-6	-29.0
3	6.20	300	0.0207	0.016	2E-6	+90.0

Table 6: OLGA alternative simulation setup

The motivation for testing of this alternative setup is to investigate if unstable production can be obtained if the pressure at the inlet of the first pipe is not allowed to vary during the cycle. The pressure defined at the inlet with a value of $1.589 \cdot 10^5 [Pa]$ corresponds to the hydrostatic pressure calculated from the liquid surface defined by the top of the weir when no gas is injected. This corresponds to the situation shown in Figure 16b, where only hydrostatic effects define the pressure in the system.

A series of simulations was first run with OLGA. It was observed that unstable flow was only obtainable at a narrow gas injection rate range compared to what was observed in Section 9.1. The gas mass injection rate $\dot{m}_g = 3.580 \cdot 10^{-5} [kg/s]$ was found to give unstable production with oscillations not dying out. The injection rate $\dot{m}_g = 3.570 \cdot 10^{-5} [kg/s]$ resulted in simulations which quickly developed into oscillations violent enough to bring portions of the injected gas in contact with the pipeline inlet. This caused the gas to flow in the wrong direction. The injectionrate $\dot{m}_g = 3.590 \cdot 10^{-5} [kg/s]$ resulted in simulations quickly developing into a steady state with no observable oscillations in holdup. It should be noticed that the vertical axis scaling has been changed in Figure 133 to make visualization of the holdup variations possible, as the oscillation amplitudes during these simulations are small compared to what is seen in Section 9.1.

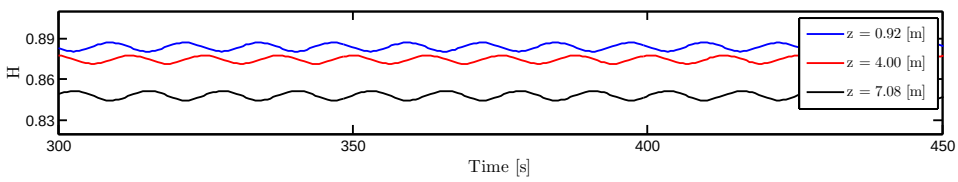

Figure 133: OLGA alternative approach, $\dot{m}_g = 3.580 \cdot 10^{-5} [kg/s]$

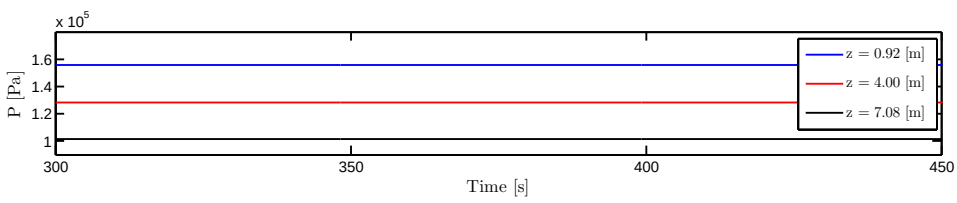

Figure 134: OLGA alternative approach, $\dot{m}_g = 3.580 \cdot 10^{-5} [kg/s]$

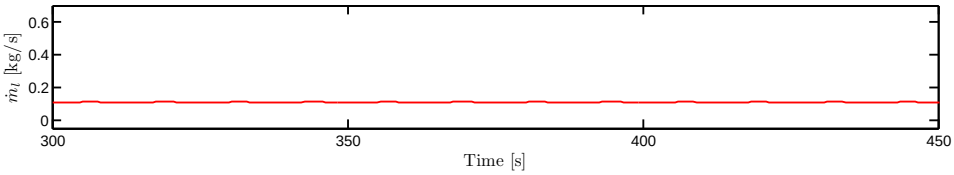

Figure 135: OLGA alternative approach, $\dot{m}_g = 3.580 \cdot 10^{-5} [kg/s]$

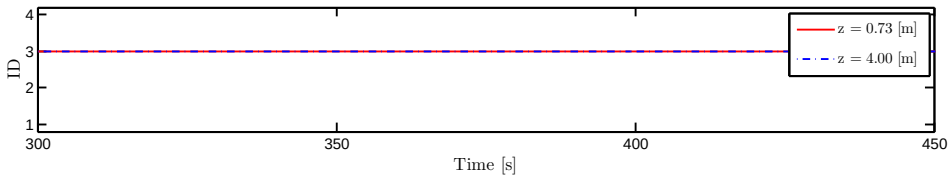

Figure 136: OLGA alternative approach, $\dot{m}_g = 3.580 \cdot 10^{-5} [kg/s]$

Attempts were made to conduct the OLGA simulations described above on a coarse grid with the cell lengths used in Section 9.2 and with the slug tracking option enabled. A SLUGVOID value of 0.05 was used together with the gas injection rate $\dot{m}_g = 3.580 \cdot 10^{-5} [kg/s]$. This value of $\dot{m}_g$ was chosen based on the observations made during the simulations in the preceeding paragraph. Tuning of the BUBBLEVOID parameter was performed in an attempt to obtain generation of slugs at the riser inlet. It was not possible to obtain slug generation in combination with any value of the BUBBLEVOID parameter.

Figure 137: SLUGGIT alternative simulation attempt

Attempts were also made to perform SLUGGIT simulations with the alternative pipe configuration. Problems were met during inclusion of the source term. As experienced during the SLUGGIT simulations presented in Secion 9.3 to 9.6, a pressure kick results from the bubble insertion described in Section 6. This kick in pressure was handled by an automatic reduction of the time step by the built-in CFL criterion. However, with this alternative pipe configuration the source is located closer to the inlet and the fixed pressure of $1.589 \cdot 10^5 [Pa]$. The introduction of a kick in pressure this close to a fixed pressure boundary condition seems to increase the need for a time step reduction. Time steps as low as $1.0 \cdot 10^{-9} [s]$ have been allowed, but the SLUGGIT simulator has not been capable of running with the source placed at its correct coordinate. The source shown in Figure 137 was located on a coordinate 2.0 [m] downstream the riser inlet, and was observed to be the closest possible location to the inlet enabling SLUGGIT to run.

10 Comparison and discussion

10.1 Experiments vs simulations

A comparison between the minimum and maximum pressure values obtained from the gas injection point is given in Figure 145 and Figure 146. The exact coordinate of the gas injection point used during the experiments has not been found. Photographs indicate that both the injection point and the riser inlet are located at approximately equal horizontal levels. This can be observed in Figure 144. During OLGA simulations the gas source was connected to a cell in the middle of the third pipe from the inlet. The minimum and maximum pressure values from this cell have been used for plotting in Figure 145.

The minimum and maximum pressure values used for plotting of the SLUGGIT instability regions given in Figure 146 have been obtained by the procedure shown in Figure 18b. The region chosen for extraction of pressure values was defined by $z_L = 8.16[m]$ and $z_R = 9.08[m]$. These coordinates are annotated in Figure 17 and span the two short pipes representing the bend configuration. The instantaneous pressure values extracted from this region may look like the red line in Figure 138. For determination of the minimum and maximum pressure values, a moving average represented by the blue line was calculated. The relatively long pressure value extraction region has been chosen to ensure a presence of bubbles as high as possible which is a necessary condition for calculation of moving averages and subsequent plotting of smooth moving average plots.

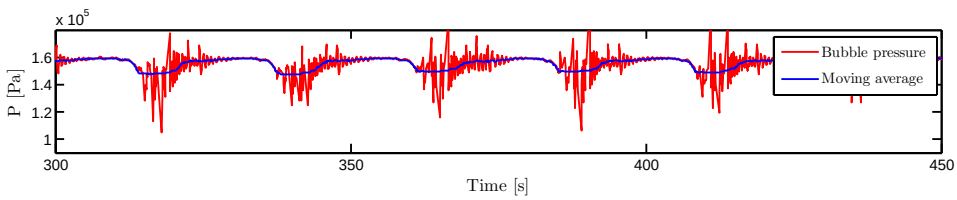

Figure 138: Bubble pressures extracted from the region $8.16[m] < z < 9.08[m]$ at $\dot{m}_g = 3.350 \cdot 10^{-5}[kg/s]$. Simulation from SLUGGIT - series III

Comparison of Figure 145 and 146 reveals that the pressure values from the SLUGGIT simulations at gas injection rates higher than $\dot{m}_g = 5.000 \cdot 10^{-5}[kg/s]$ in general are lower than than those observed in the OLGA plot. This trend may possibly have been caused by an overrepresentation of pressure values from the region to the right of the gas injection point at $z = 8.44[m]$ where the hydrostatic pressure values are known to be lower than the values upstream the injection point. The SLUGGIT values are approximately 0.1 [bar] lower than the experimental values and 0.05 [bar] lower than the OLGA values in the higher gas injection rate region. The difference in pressure between the SLUGGIT results and the experiments corresponds to approximately 1 [m] liquid column. Some of this deviation might be explained by the uncertainty associated with the experimental description and the gas injection point location. Nevertheless the uncertainty in

vertical source location is not likely to be any larger than ± 0.2 [m], implying that this uncertainty in source location cannot explain the SLUGGIT pressure deviation alone. In addition, one should then expect to se the same trend within the OLGA pressure values as both SLUGGIT and OLGA use the same simulation geometry. This is however not observed.

As described by [20] the bubble sizes in the case of bubbly flow in the riser influence the lift efficiency i.e. how well the gas is utilized for providing lift. A high lift efficiency is equivalent to long gas recidence time. Similarly the rise velocity in Taylor bubble flow influences the gas recidence time. The bubble velocity correlation given by Equation 14 is used for closure in both OLGA and SLUGGIT, with the C_0 values used by SLUGGIT given in Equation 15. The C_0 values used in the current OLGA version have not been found. At the higher flow rates the OLGA pressure values given in Figure 145 are closer to the experimental values than the corresponding SLUGGIT values given in Figure 146. Some OLGA simulations representing Mode 3 production have been extracted from Table 8 and included for further examination inside Table 7.

$\dot{m}_g$ [kg/s]	$\dot{m}_l$ [kg/s]	H	U_{sg} [m/s]	U_{sl} [m/s]	U_m [m/s]	Re_l	Re_m
$3.500 \cdot 10^{-5}$	0.0891	0.860	0.134	0.444	0.578	7080	3271
$3.650 \cdot 10^{-5}$	0.0915	0.858	0.140	0.456	0.596	7270	3340
$4.000 \cdot 10^{-5}$	0.0968	0.852	0.153	0.483	0.636	7692	3468
$4.970 \cdot 10^{-5}$	0.1093	0.836	0.190	0.545	0.735	8685	3744
$5.000 \cdot 10^{-5}$	0.1097	0.834	0.191	0.547	0.738	8717	3729
$8.500 \cdot 10^{-5}$	0.1414	0.786	0.325	0.705	1.030	11235	4346

Table 7: OLGA - series I simulations with Mode 3 production characteristics extracted from Table 8

The values presented in Table 7 have been calculated by the relations given in Equation 33 to 38. The gas density in the middle of the riser, calculated from the averaged hydrostatic pressure, has been used in Equation 33. The values computed in Table 7 may, in combination with the C_0 correlation by Frechou (1986) given in Equation 39, be used to estimate the C_0 values present during the OLGA simulations without slug tracking and the experiments. Comparison between Re_m values from Table 7 with Figure 139 indicates that the OLGA results, which are close to the experimental, represent laminar flow with a C_0 value close to 2.0. This may possibly explain the too low SLUGGIT pressure values in the higher gas injection rates in Figure 146. A too low C_0 value reduces the bubble nose velocity which again increases the gas recidence time and the average void fraction in the riser.

$$U_{sg} = \frac{\dot{m}_g}{\rho_g A} \tag{33}$$

$$U_{sl} = \frac{\dot{m}_l}{\rho_l A} \tag{34}$$

$$U_m = U_{sl} + U_{sg} \tag{35}$$

$$\upsilon_m = \upsilon_l H + \upsilon_g (1 - H) \tag{36}$$

$$\mathrm{Re}_l = \frac{U_{sl} D}{\nu_l} \tag{37}$$

$$\mathrm{Re}_m = \frac{U_m D}{\nu_m} \tag{38}$$

$$C_0 = \frac{2.27}{1 + \left(\frac{\mathrm{Re}_m}{\mathrm{Re}_l}\right)^2} + \frac{1.2}{1 + \left(\frac{\mathrm{Re}_l}{\mathrm{Re}_m}\right)^2} \tag{39}$$

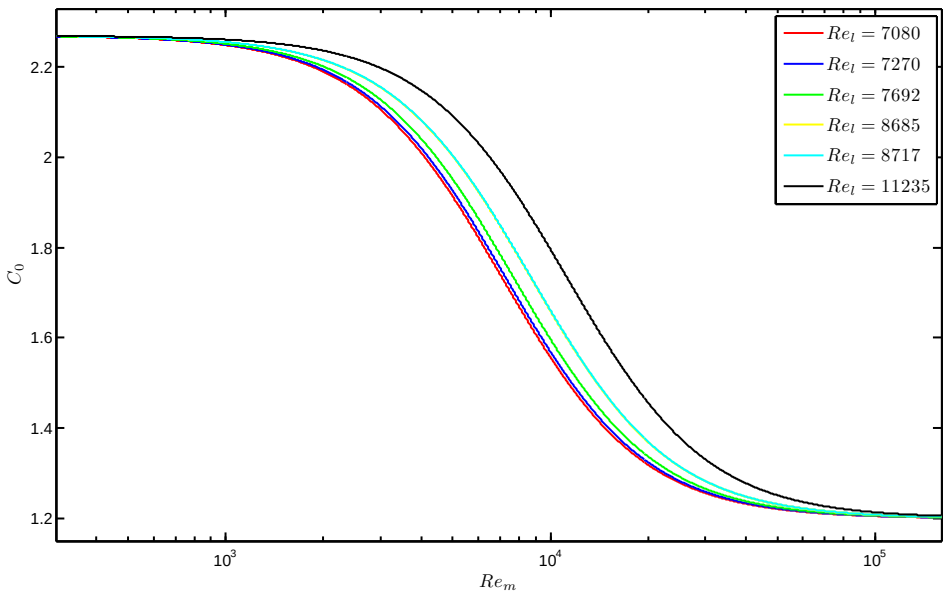

Figure 139: C_0 variation from laminar to turbulent slug flow given by Equation 39

To investigate the effect of a C_0 value of 2.0, three new SLUGGIT simulations have been run with this value. All other input parameters are the same as used in SLUGGIT - series IV. The corresponding minimum and maximum pressures are included in Figure 146 an denoted by a yellow line and the label "SLUGGIT laminar". The change in C_0 value is observed to have increased the pressure values by approximately 0.03 [bar]. This increase is however to small to bring the SLUGGIT pressures to the same level as the corresponding OLGA values.

The effect of surface tension is not included in SLUGGIT. This represents

another influencing factor on the simulation results, as the velocities are low and the pipe diameter is small, implying that surface tension is not negligible. Even though no surface tension model is implemented in SLUGGIT, this can be compensated by the drift velocity U_0, which can be determined experimentally. The U_0 values used by SLUGGIT are given in Equation 16. A U_0 correlation developed for small diameter systems by [52] is given in Equation 40. As can be seen, this small diameter correlation gives bubble nose velocity values lower than Equation 16, implying that the inclusion of small diameter and surface tension effects by this equation in SLUGGIT would have contributed to further increase the deviation from the experimental minimum and maximum pressure values.

$$U_0 = (0.28 \sin\theta + 0.23 \cos\theta)\sqrt{gD} \tag{40}$$

Another factor possibly influencing the experimental results is the wake effect, which describes the increase in bubble nose velocity when short slugs are present. A factor W_{eff} may be used to adjust the regular bubble velocity correlation given in Equation 14 to compensate for this wake effect. This is shown in Equation 41. Several correlations exist for the factor W_{eff}. An early correlation developed by [53] is given in Equation 42. The inclusion of the wake effect in the SLUGGIT simulations would have contributed to increase the bubble nose velocity, decrease the gas recidence time, increase the hydrostatic pressure contribution and hence bring the sluggit minimum and maximum pressures closer to the experimental values.

$$U_{b,corr} = W_{eff} U_b \tag{41}$$

$$W_{eff} = 1 + 8e^{-1.06\frac{L_s}{D}} \tag{42}$$

Another possible explanation to the discrepancy of the SLUGGIT pressure values may be that all gas is transported by Taylor bubbles, as no void fraction is allowed in the slugs. According to the results by [20] one might expect that the SLUGGIT pressure values would have been influenced if void fraction in slugs and hence local bubbly flow had been implemented.

Comparison of the experimental pressure values with OLGA and SLUGGIT results within the flow rates giving unstable production reveals that the minimum OLGA and SLUGGIT pressure values in general are lower than the experimental values. One exception is the SLUGGIT - series IV values which correspond quite well with the experimental values. The deviating trend may be addressed to the pipe configuration used for the simulations which is an approximate version of the experimental geometry. During the experiments, a liquid front was observed to travel inside the inlet bend following the period of the system instability. The movement of this liquid front during the different cycle stages is described in Figure 144. The liquid front was not reported to retract to locations upstream the injection point. This is however observed during the simulations. This is illustrated in Figure 141 where the dotted lines indicate the maximum liquid front retraction during experiments and simulation. This may indicate that a larger amount of gas

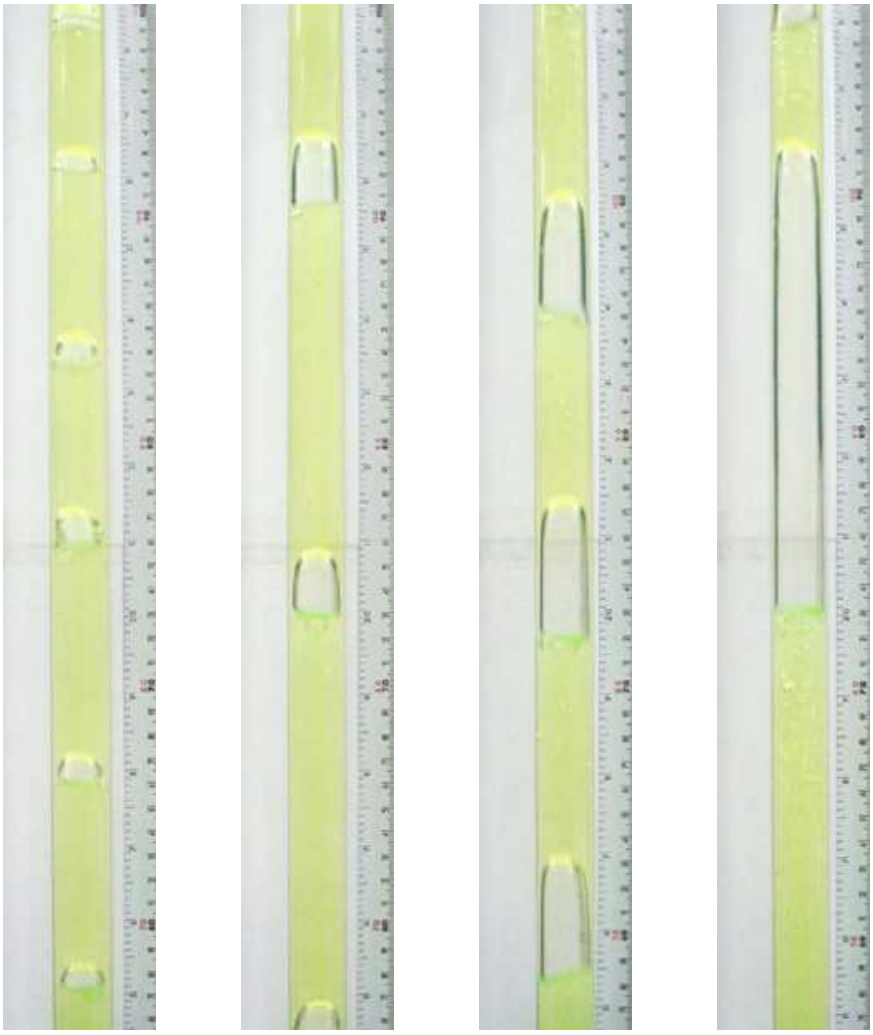

(a) (b) (c) (d)

Figure 140: Taylor bubbles from [44]

is accumulated prior to startup of each cycle during the simulations at the lower gas injection rates, and that the total gas content in the riser is higher during the liquid producing part of each cycle. This could result in a reduction in hydrostatic pressure contribution and hence lower minimum pressures.

The relatively close correspondence between SLUGGIT - series IV and experiments with regard to minimum pressure values at the gas injection point during unstable production might be explained by the ability of this simulation setup to generate small bubbles at the riser inlet, and that this may contribute to a more stable presence of gas bubbles in the riser. This implies that the gas is transported

through the riser during larger parts of the cycle, which may contribute to remove the riser gas content peak values, possibly giving the low minimum pressure values observed in the other SLUGGIT simulation series.

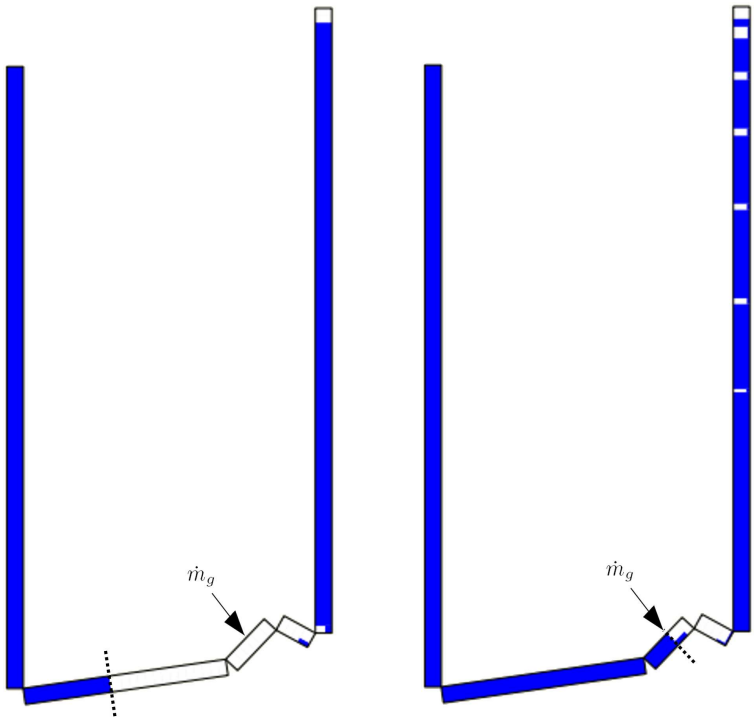

(a) Simulations (b) Experiments

Figure 141: Maximum liquid front retraction during simulations and experiments

No bubbly flow was reported during the experiments, although one should expect small bubbles to travel up the riser at the lowest gas injection rates, similarly to what is shown in Figure 6a. The smallest bubbles reported and documented by photo, were the Taylor bubbles shown in Figure 140a. SLUGGIT does not allow any void fraction in slugs. This implies that no bubbles are allowed to rise through the liquid column at the lowest flow rates. The OLGA simulations allow bubbly flow, but as the empirical correlations used in general are obtained from larger scale systems (SINTEF, Tiller), one might question the validity of these used for simulation of small scale systems.

All simulations had to be run for long times to capture one complete production cycle at the lowest gas injection rates, as the time required to fill the bend with gas then becomes long. All simulations have therefore been executed at gas injection rates higher than $\dot{m}_g = 1.0 \cdot 10^{-6}[kg/s]$.

Only one experimental time series has been found in the previous experimental work by [44]. This time series is given in Figure 142 and shows the void fraction

values along the riser at the gas injection rate $\dot{m}_g = 4.000 \cdot 10^{-5}[kg/s]$. A period of the cyclic production behaviour close to 20 [s] is observed. Similar periods were observed in some of the simulations showing Mode 2 production characteristics. This can be observed in Section 9.1.3 and 9.6.3.

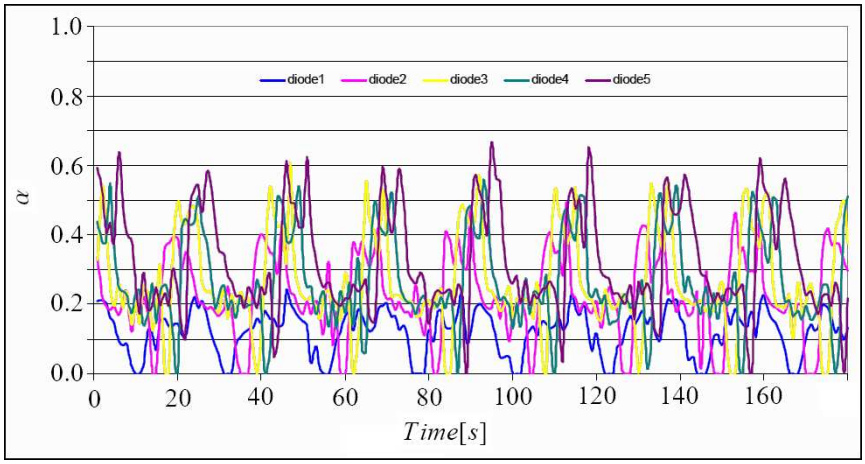

Figure 142: Experimental void fractions at $\dot{m}_g = 4.000 \cdot 10^{-5}[kg/s]$ from [44]

It should however be noticed that the period of the cyclic behaviour during the simulations was observed to vary with gas injection rate. This may be illustrated by Figure 143; If the gas injection rate is low, the system comes to rest once during each cycle. This implies that oscillations in riser liquid level resulting from the liquid unloading in the previous cycle have died, and do not contribute to bring the gas front of the newly accumulated gas volume in contact with the riser inlet. If however the gas injection rate is higher, liquid level oscillations from the prevoius cycle do not get the time they need to die before enough gas has accumulated for the next cycle to start. These oscillations do hence in some situations contribute to bring the gas front in contact with the riser inlet and then advance the cycle startup.

As described in Figure 144, the injected gas was observed to be completely transported out from the bend once during every cycle during the experiments, leaving liquid only. This was also observed during some of the SLUGGIT and OLGA simulations with Mode 2 characteristics. At cycle start the bend was reported to contain gas only, from the injection point to the bend low point. This can be seen in Figure 144a. This behaviour was not possible to obtain during the OLGA simulations without slug tracking, where some liquid was alwas present in the region between the injection point and the bend high point. This can be observed in the simulations classified as Mode 2 production. Experiments showing Mode 1 production characteristics were not reported by [44].

Average holdup values along the riser are given in Table 9. The low values at the riser outlet in the SLUGGIT simulations do probably reflect the fact that automatic removal of slugs at the outlet is implemented in SLUGGIT. Except for

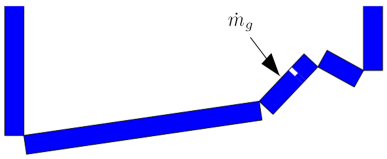

(a) Gas starts to accumulate in the bend

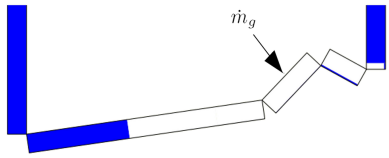

(b) The gas mass needed for the gas front to reach the riser inlet has been injected. At this stage, oscillations in liquid level close to the riser outlet have died out and do not contribute to bring the gas front in contact with the riser inlet

Figure 143: Gas accumulation in bend during Mode 1 production

the values at the riser outlet, holdup values from all the simulations show similar trends with decreasing values in the region from $z = 10.64[m]$ to $z = 13.72[m]$. This does probably reflect the gas expansion due to the reduction in hydrostatic pressure which was also observed in the experiments. The experimental holdup values are in general lower than the simulation values. This may be due to the optical holdup registration method applied. The accuracy of this method was reported to be strongly dependent on the content of colouring agent added to the water in combination with careful calibration.

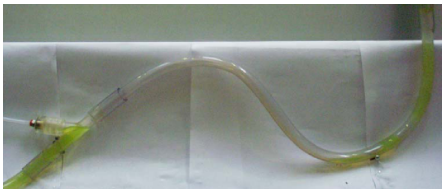

(a) At cycle start there is no liquid production at the riser outlet. Air starts to accumulate in the riser inlet bend. Small bubbles pass the bend low point and start to rise in the liquid column, causing the inlet pressure to decrease from its maximum value following a linear trend due to the reduction in hydrostatic pressure.

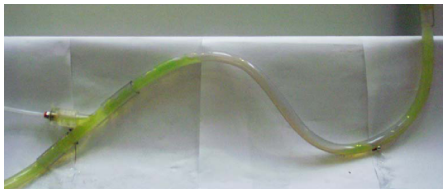

(b) There is still no liquid production at the riser outlet. Air bubbles continuously passing the low point at an increasing rate enable a liquid front to start moving into the bend. The void fraction at diode 1 increases, and the inlet pressure continues dropping.

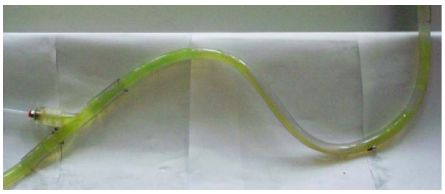

(c) Liquid production starts. The liquid front has reached the bend high point and liquid flows stratified towards the riser inlet. The inlet pressure continues dropping, and the void fraction at diode 1 stabilizes.

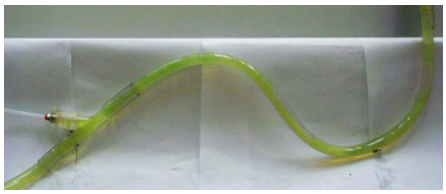

(d) Water flows from the riser outlet and no accumulated air is left in the bend. The inlet pressure reaches its minimum value. The water is observed to accelerate trough the riser. Large slugs were observed.

(e) Water is still produced, but at a decreasing rate, as the fluid content in the riser has reached a level too high for the high liquid production to continue. The increase in inlet pressure follows a linear trend.

(f) The liquid production stops, and all injected lift gas accumulates in the bend. The liquid front retracts towards the gas injection point. As all injected gas accumulates in the bend, the overall riser void fraction decreases. The inlet pressure continues growing.

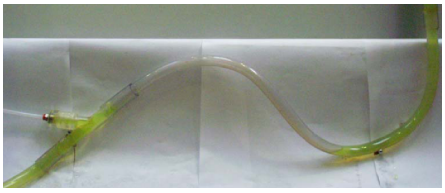

(g) There is no liquid production, and the volume of accumulated gas in the bend approaches its highest value, thus indicating the start of a new density wave cycle.

Figure 144: Riser cycle at $\dot{m}_g = 4.000 \cdot 10^{-5} [kg/s]$ from [44]

$\dot{m}_g$ [kg/s]	**OLGA series I**	**OLGA series II**	**SLUGGIT series I**	**SLUGGIT series II**	**SLUGGIT series III**	**SLUGGIT series IV**	**OLGA series I steady state pre-processor**	**OLGA series II steady state pre-processor**
$2.000 \cdot 10^{-5}$	0.0210	0.0698	0.0181	0.0161	0.0175	0.0160	0.1000	0.1000
$2.621 \cdot 10^{-5}$	0.0393	0.0539	0.0230	0.0205	0.0244	0.0233	0.1000	0.1000
$2.642 \cdot 10^{-5}$	0.0631	0.0642	0.0238	0.0216	0.0246	0.0214	0.1000	0.1000
$3.350 \cdot 10^{-5}$	0.0850	0.0853	0.0325	0.0321	0.0381	0.0356	0.1000	0.1000
$3.500 \cdot 10^{-5}$	0.0891	0.0666	0.0350	0.0278	0.0402	0.0373	0.1000	0.1000
$3.650 \cdot 10^{-5}$	0.0915	0.0904	0.0385	0.0323	0.0406	0.0399	0.1000	0.1000
$4.000 \cdot 10^{-5}$	0.0968	0.0959	0.0421	0.0409	0.0450	0.0471	0.1000	0.1000
$4.970 \cdot 10^{-5}$	0.1093	0.1087	0.0529	0.0508	0.0531	0.0619	0.1089	0.1086
$5.000 \cdot 10^{-5}$	0.1097	0.1091	0.0460	0.0476	0.0540	0.0618	0.1093	0.1090
$8.500 \cdot 10^{-5}$	0.1414	0.1412	0.0568	0.1012	0.1038	0.0613	0.1410	0.1408

Table 8: Average liquid production $\dot{m}_l$ [kg/s]

	z = 9.09 [m]	**z = 10.64 [m]**	**z = 12.18 [m]**	**z = 13.72 [m]**	**z = 15.25 [m]**
Experiments	0.88	0.77	0.73	0.73	0.68
OLGA - series I	0.85	0.86	0.85	0.84	0.82
OLGA - series II	0.88	0.87	0.85	0.83	0.80
SLUGGIT - series I	0.85	0.88	0.88	0.86	0.57
SLUGGIT - series II	0.83	0.87	0.83	0.84	0.67
SLUGGIT - series III	0.79	0.85	0.85	0.83	0.71
SLUGGIT - series IV	0.79	0.86	0.85	0.83	0.58

Table 9: Average holdup values at $\dot{m}_g = 4.000 \cdot 10^{-5} [kg/s]$

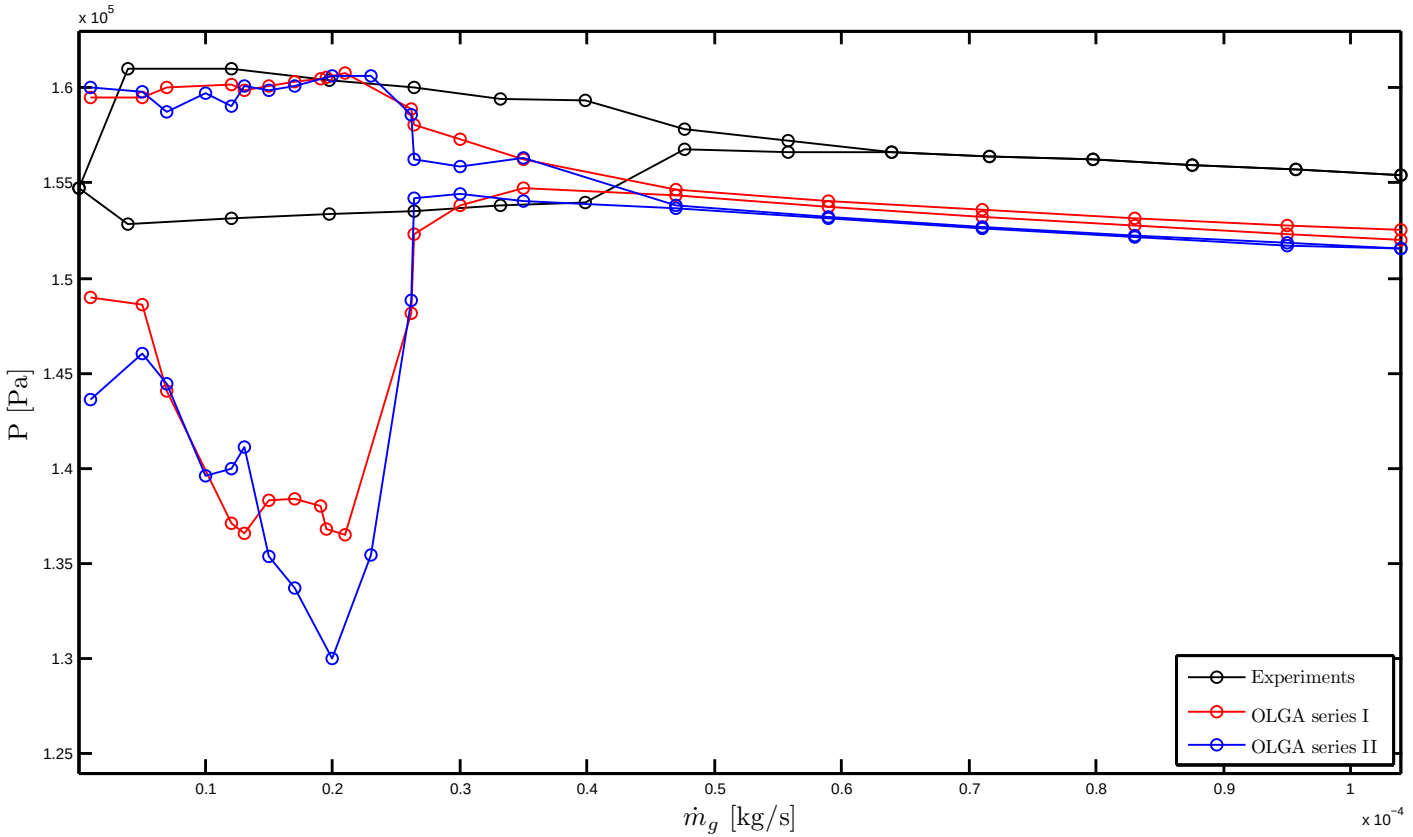

Figure 145: Instability regions from OLGA simulations and experiments. Pressure values from gas injection point

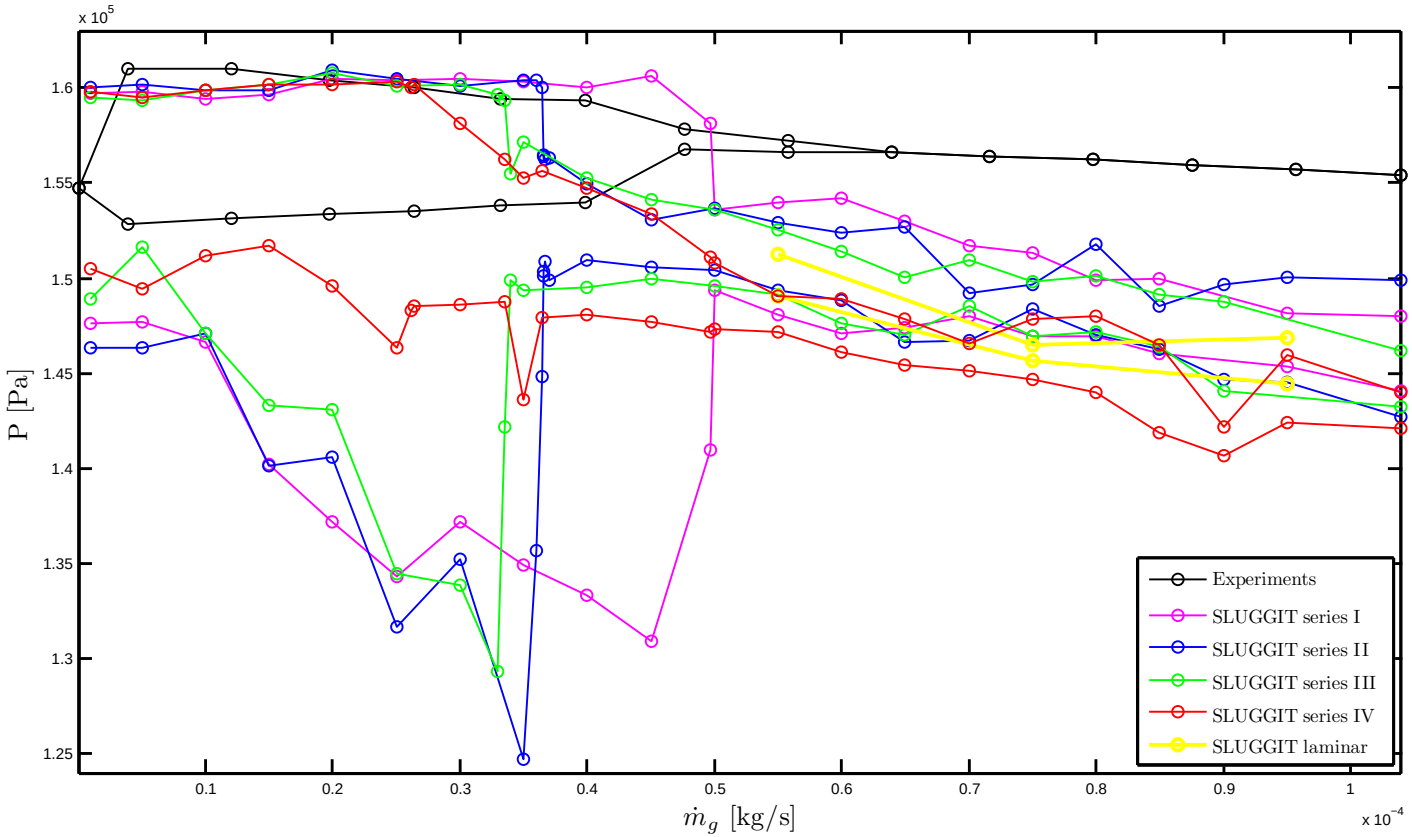

Figure 146: Instability regions from SLUGGIT simulations and experiments. Pressure values from gas injection point

10.2 Simulation series comparison

Examination of Figure 146 reveals that the production becomes stable at a lower gas injection rate in SLUGGIT - series II compared to SLUGGIT - series I. This is probably indicating that gas being injected at $\dot{m}_{inject}$ equal to $\dot{m}_g$ is not fully utilized for lift and that injected bubbles are allowed to move a short distance into the vertical riser before their remaining accumulated mass is fully injected.

The pressure variations follow a falling trend with increasing gas injection rates. This is caused by an increased amount of gas in the riser and a reduction in hydrostatic pressure.

The holdup and pressure time series presented in Section 9.3 to 9.6, representing the moving averages of the instantaneous holdup and pressure time series, do all show profiles with distinct "steps". The number of cells over which to apply the moving average, has been tuned for each simulation to obtain curves as smooth as possible. In an ideal situation a fixed number of data points over which to apply moving average should be used during processing of all the experiments in order to allow comparison. However, in the SLUGGIT case, the number of bubbles present in the system varies with the gas injection rate. This implies that the number of data points over which to apply moving average, increases with gas injection rate if smooth plots are to be obtained over the whole injection rate range. Care has been taken in order to avoid calculating the moving average over a too high number of data points as this will cause physical minima / extrema to be reduced from their correct values. It would have been possible to obtain even smoother curves if shorter bubbles had been generated at the inlet. This would though have required increased computational times due to the increased number of computational sections.

A comparison of the average liquid flow rates obtained from the simulations is given in Table 8. Comparison between the flow rates from the SLUGGIT simulations with the OLGA simulations reveals that the SLUGGIT liquid flow rates in general are lower than the OLGA values. Comparison between liquid flow rates from OLGA simulations with and without slug tracking, indicates a higher liquid production in the slug tracking simulations at the lowest gas injection rates. The liquid flow rate solution supplied by the OLGA steady state pre-processor is observed to possess a value of 0.1 [kg/s] at gas injection rates lower than $\dot{m}_g = 4.000 \cdot 10^{-5}[kg/s]$.

Generation of slugs was not possible to obtain over the whole range of gas injection rates of interest. As described in Section 9.2, the BUBBLEVOID parameter was tuned by the two different criteria in an attempt to obtain simulation results as close to the results from simulations without slug tracking as possible. This succeeded by means of enabling generation of slugs at the lowest flow rates. At flow rates higher than $\dot{m}_g = 4.700 \cdot 10^{-5}[kg/s]$, slug generation at the inlet was not obtained, leaving steady state solutions close to the steady state solutions obtained from the simulations without slug tracking.

Contrary to what was experienced during OLGA simulations without slug tracking as well as during SLUGGIT simulations, it was not possible to obtain simulations showing unstable liquid production with a relatively constant period during the OLGA simulations with slug tracking. In addition, the sharp liquid

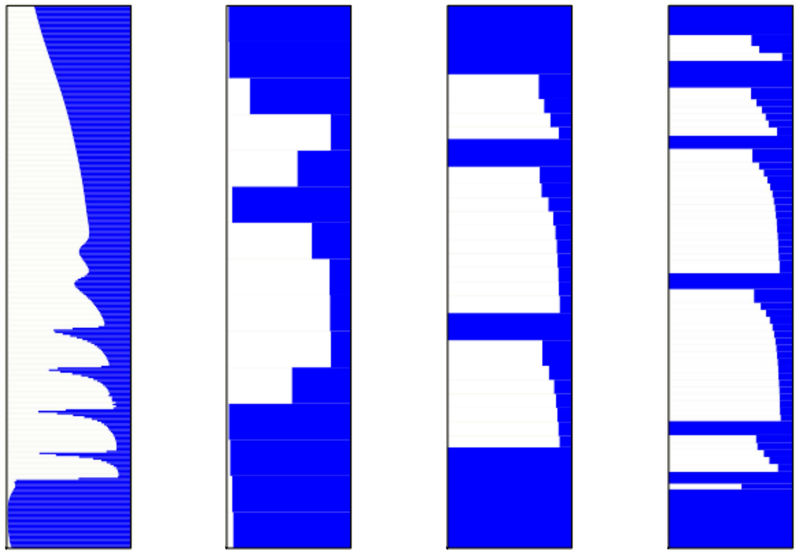

(a) OLGA - series I (b) OLGA - series II (c) SLUGGIT - series III (d) SLUGGIT - series IV

Figure 147: Riser flow details at $\dot{m}_g = 2.000 \cdot 10^{-5}[kg/s]$

fronts with holdup equal to 1.0 resulting from slugs spanning the whole cross sectional area observed during SLUGGIT simulations, were not obtained with OLGA either with or without the slug tracking module. This tendency can be observed upon comparison of Figure 147a to 147d.

Both the OLGA and the SLUGGIT simulations have been run with automatic time step control activated. These control procedures are in both the simulators based on the CFL (Courant-Friedrich-Levy) criterion, which is given by Equation 27. This criterion ensures that the time step is kept low enough during simulation. If a mass transient is to be followed correctly, an important requirement is that no mass is transported across a whole section in one time step.

When SLUGGIT was run with the first splitting procedure given in Section 6.1 together with automatic time step control, the time step was reduced to a small value in the order of $10^{-8}[s]$, the time step after the bubble had been created. This was caused by the manual border translation procedure which gives the slug an artificially high velocity. During the simulations run with the splitting procedure introduced in Section 6.2, the time step always was higher than $10^{-5}[s]$. A minimum time step in the order of $10^{-5}[s]$ had to be allowed in order to ensure generation of slugs at the riser inlet. Test simulations were conducted with a minimum time step of $10^{-4}[s]$, resulting in no slug generation at the inlet, and hence abscence of the sought smaller bubbles. Except by the instant of bubble insertion, the time step was in the order of $10^{-3}[s]$ during most of the simulation time.

The OLGA simulations were all run with a minimum time step of $10^{-6}[s]$. Most

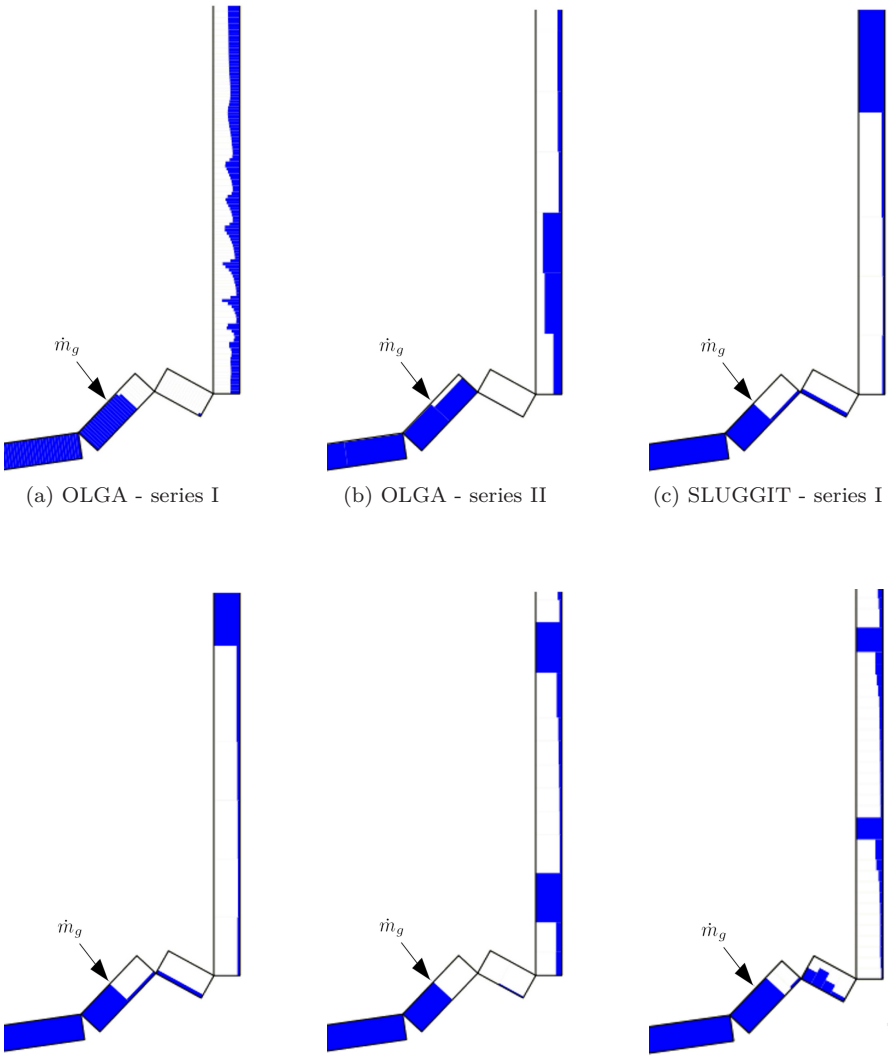

(a) OLGA - series I (b) OLGA - series II (c) SLUGGIT - series I

(d) SLUGGIT - series II (e) SLUGGIT - series III (f) SLUGGIT - series IV

Figure 148: Flow details at riser inlet, $\dot{m}_g = 2.000 \cdot 10^{-5}[kg/s]$

of the simulation time, they were running with a time step in the order of $10^{-3}[s]$.

Comparison between OLGA run without slug tracking and SLUGGIT, with respect to CPU time, indicates that OLGA on average run twice as fast as SLUGGIT when the automatic time step control option was enabled. The OLGA simulations performed without slug tracking were observed to run approximately fifteen times faster than the OLGA simulations without slug tracking. One reason for the difference between OLGA without slug tracking and SLUGGIT may be that OLGA offers parallell computing and hence was run on four processors. SLUGGIT

does not offer parallell computing and was hence not able utilize the potential of the four processors.

The SLUGGIT execution time was observed to increase as the number of computational sections (bubbles and slugs) was increased. SLUGGIT checks all its current sections in accordance with its merging, splitting and transition criteria every time step. An increased number of sections hence results. This increases the computational demands both due to the increased number of section management operations as well as to the increased sizes of the coefficient matrices to be solved.

Figure 147 shows the different resolutions used during the simulations. Figure 147a shows the fine grid used in the OLGA simulations without slug tracking. Local maxima in holdup values not reaching a value of 1.0 are observed, possibly being caused by numerical diffusion. The same tendency with local maxima is observed within Figure 147c and 147d. In these two figures maximum values equal to 1.0 are observed, illustrating the capability of the SLUGGIT simulator to preserve sharp liquid fronts even if the section lengths used are significantly longer than the grid sizes used in OLGA without slug tracking.

The SLUGGIT simulations presented in Section 9.3 to 9.5 do all show a relatively distinct shift from unstable to stable production. The simulations in Section 9.6 do not follow a similar shift. Instead, a smoother transition from unstable to stable production is observed with increasing flow rate. This is probably due to the shorter bubble lengths and the increased rate at which smaller slugs and bubbles are generated at the inlet, giving the riser a more continuous presence of bubbles.

A strong cell length dependency of the slug initiation process is observed upon comparison of the results presented in Section 9.3 to 9.6. This tendency may also be observed in the movies included in the .zip file. Different slug initiation methods based on initiation in section borders have been tested in earlier SLUGGIT versions. These methods remove the cell length dependency, but do though require a specific slug initiation model. One model used for slug initiation in pipeline low points was based on liquid accumulation outside the pipe at the location of the low point. When the accumulated liquid mass reached a predefined limit corresponding to an initial slug length, the mass was re-injected to form a slug.

The OLGA simulations without slug tracking have been conducted with a relatively fine grid, with a cell length close to one pipe diameter. This may be referred to as a slug capturing approach. An important characteristic of the slug capturing technique is the application of a fine grid. This enables the capturing of sharp liquid fronts. Contrary to the slug tracking approach used in SLUGGIT, a slug capturing approach relies on a fine grid with a cell length smaller than the minimum slug length. Higher order numerical schemes are often utilized to prevent the liquid fronts from being smeared out by numerical diffusion. These simulations are often capable of predicting flow regime transition without the application of any stability/transitional criteria. As a slug capturing simulation approach might involve cell lengths in the order of magnitude one pipe diameter, one might argue that three-dimensional effects play a role, and that these effects should be included in the modelling. Several contributions to slug capturing modelling have been given. One contributor is [54], where slug capturing simulations are performed

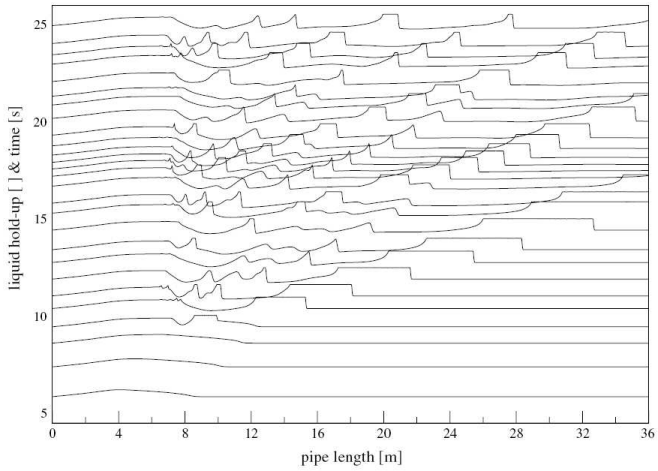

Figure 149: Holdup profiles from [54] showing sharp liquid fronts in near horizontal flow

by a two-fluid model. One drawback by using a slug capturing approach is the computational cost associated with small cell length computations.

As commented on in previous sections, the production Mode 1 was never reported from the experimental work. The reported unstable production illustrated by the stages described in Figure 144, corresponds to the unstable production Mode 2. OLGA simulations without slug tracking at gas injection rates between $\dot{m}_g = 2.642 \cdot 10^{-5}[kg/s]$ and $\dot{m}_g = 3.500 \cdot 10^{-5}[kg/s]$ are observed to reproduce this Mode 2 production quite well.

Attempts were made to obtain unstable Mode 2 production within the OLGA simulations with slug tracking, but this did not succeed. These simulations shifted directly from unstable Mode 1 production into stable Mode 3 production.

The different SLUGGIT simulation series show various transition characteristics from unstable to stable production. The generation of short bubbles at a varying rate at the riser inlet is observed to be vital for simulation of Mode 2 production.

This indicates that OLGA without slug tracking and the SLUGGIT - series 4 simulations have succeeded in reproducing the unstable production observed during the experiments. The transitions from unstable production to stable production are observed to occur in the same region for simulations and experiments. The differences in gas injection rates required for stable production to result may possibly be explained by the approximate simulation geometry used.

Unstable production was only obtained with the alternative three-pipe configuration used in Section 9.7 at a narrow gas injection rate range. A large degree of interaction between the flow in the second and third pipe was observed in the simulations made with the five-pipe configuration. The injection point pressure varied during the cycle. Thus, setting the inlet pressure fixed at the inlet of the pipe in which the gas is injected, introduces a constraint on injection point pressure which was not present during the experiments.

10.3 SLUGGIT pressure oscillations

Oscillations in pressure are observed during the SLUGGIT simulations. The reason for these oscillations are probable to originate from the bubble insertion procedure described in Section 6. Two different slug splitting procedures have been implemented and tested. These two procedures do represent the same kick with consequent oscillations in pressure.

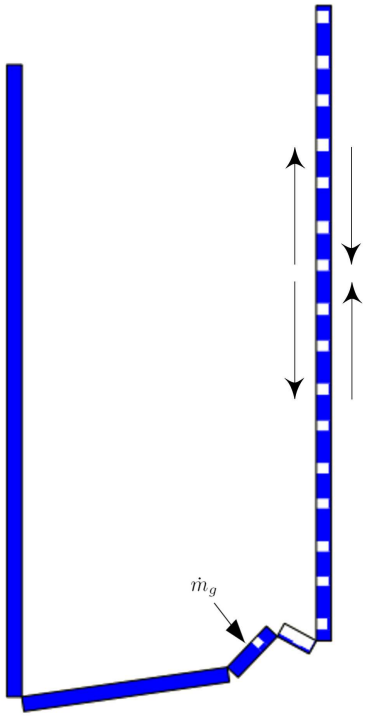

Figure 150: Gas / liquid column oscillations observed during stable Mode 3 production

The length $L_{initial}$ of the bubble inserted during the slug splitting procedure described in Section 6.1 and 6.2 is probable to influence the resulting pressure oscillations. Several values have been tested, and the resulting pressure values close to the gas injection point have been investigated. Both the splitting procedures introduce a sudden change in pressure when the new bubble is inserted. A small value of $L_{initial}$ is observed to reduce the pressure oscillations. However, if the value of $L_{initial}$ becomes too small, the borders of the inserted bubble on some occasions come into contact with each other, resulting in negative lengths and stop in program execution. In addition, round-off error may result if very small $L_{initial}$ are applied. This may potentially form a base for pressure oscillations to start regain magnitude if the value of $L_{initial}$ is set to low.

Based on Equation 2, one might reason that an inserted bubble with a small

volume V results in a large perturbation in ΔP in pressure if a perturbation ΔV in volume is imposed on the bubble. A change in bubble volume may be positive (expansion) or negative (compression) and may be imposed on the bubble as a result of pressure oscillations in the system. One might then argue that a small bubble volume resulting from the insertion of a bubble with a small value of $L_{initial}$ contributes to maintain pressure oscillations, and that longer bubbles contribute to dampen oscillations.

In addition to the instability regions observed at the lower flow rates in Figure 146, the minimum and maximum pressures are observed to continue oscillating at the higher flow rates, though on a smaller scale. These smaller pressure oscillations are probable to originate from the phenomenon illustrated in Figure 150, where the slug generation rate at the riser inlet is constant, but where the whole gas / liquid column is observed to oscillate. This type of oscillations was not reported during the experiments. They can be observed at the highest gas injection rates in the animations enclosed in the .zip file, and are in particular easy to recognize at $\dot{m}_g = 8.500 \cdot 10^{-5}[kg/s]$ in the folder SLUGGIT_SERIES_4.

10.4 Sources of error

OLGA supports printing of both gas and liquid flow rates from fixed computational cells. This option is not available in the current SLUGGIT version. Gas and liquid flow rates from the SLUGGIT simulations are hence obtained through calculations with Equation 43 and Equation 44 together with the printed computational values of U_g, U_l, H and P. The liquid density ρ_l is constant and the gas density ρ_g is obtained from the pressure P and the equation of state.

$$\dot{m}_l = \rho_l U_l A H \tag{43}$$

$$\dot{m}_g = \rho_g U_g A \alpha = \rho_g U_g A (1 - H) \tag{44}$$

Gas mass flow rates are computed at the outlet by this procedure together with subsequent time averaging for comparison with the known injected gas mass rate. These quantities are required to be equal for mass to be conserved. Nevertheless poor correspondence is observed upon comparison. The gass mass flow rate has been computed at several locations in the full length of the riser to check if this poor correspondence is caused by the accumulated gass mass being injected too slowly. This would have enabled the gas to leave the riser before fully injected and hence given too low computed gas flow rates at the outlet. This is however not a probable explanation, as the gas flow rates in some of the calculations are determined to be even higher computed upstream the outlet, compared to when computed at the outlet itself.

The current SLUGGIT version calculates individual pressures in neighbouring bubble sections. Other program versions exist where this option is not offered and where bubbles are treated as single long bubble section with one pressure value. The phase velocities U_g and U_l in the bubbles are calculated by different procedures in these two situations. One possible explanation for the discrepancy

between the calculated gas mass flow rate and the known injected gas mass rate may either be that there is an error within the phase velocity calulation code or that the computed values are printed incorrectly to the result file.

Another possible explanation for the discrepancy between the known and the calculated gas flow rates, may be the pressure fluctuations observed during the simulations, which are observed in all the SLUGGIT simulation series. The pressure is used for calculation of the gas density at each time step, resulting in a corresponding oscillation in gas density. These oscillations in gas density may influence the gas mass flow rate calculation. An attempt has been made to calculate the gas mass flow at the outlet with a fixed gas density. This did not improve the correspondence between the injected and the calculated gas mass flow.

As observed in Section 10.3 the SLUGGIT liquid flow rates are low compared to the OLGA values. One might suspect this deviation to be a results of the calculated phase velocities, similarly to the gas mass flow.

The effect of the result file printing resolution on the computed gas and liquid flow rates has also been tested. Results have been printed to file every 0.1 [s] for the simulations presented in this thesis. A printing resolution of 0.01 [s] has been tested. This did not give any improved correspondence between OLGA and SLUGGIT liquid flow rates or between known and computed gas flow rates within SLUGGIT.

The liquid flow rate time series presented in Section 9.3 to 9.6 have been obtained from Equation 43 and vector multiplication of its variables in Matlab with the computed variables obtained from the SLUGGIT result file. They show characteristics similar to what is observed during the OLGA simulations with distinct liquid production peaks associated with Mode 1 production. As commented, the average SLUGGIT liquid production values presented in Table 8 are suspected to be incorrect. As these values have been computed as the time averages of the instantaneous liquid flow rate values given in the plots, the plots should probably also be considered incorrect.

One might suspect that gas mass is not conserved during the bubble insertion procedure implemented in SLUGGIT, as a large discrepancy between the calculated average gas flow rates and the known gas injection rates were observed. This may however be argumented not to be a probable explanation if a comparison of Figure 20, 46, 67 and 87 is made. A period of the system instability close to 50 [s] is seen in all the figures. As these figures all represent the same gas injection rate and in addition require the same time for getting their bends filled with gas, one should expect the same gas mass to be injected into the bend during each cycle in the different simulations, as the injection rate $\dot{m}_g = 2.000 \cdot 10^{-5} [kg/s]$ represents Mode 1 production, implying that oscillations in liquid level from the previous cycle do not influence gas propagation into the riser in the next cycle. This is illustrated in Figure 143.

11 Conclusion and recommendations

A series of experiments on unstable gas lift have become subject to simulation with the objective of evaluating the capability of two different multiphase one-dimensional flow simulators of reproducing the unstable production observed in the experiments. In addition, a literature survey on unstable gas lift has been performed.

Several contributions to the investigation of unstable gas lift were found during the literature survey. Most of the contributions focus on the well known casing heading instability while some aim at investigating the density wave instability mechanism, a form of instability which has started to gain interest in the oil industry in the recent years. No contributions to the investigation of the presence of this mechanism in combination with a riser inlet bend configuration similar to the setup investigated in this thesis were found. This indicates that the experiments investigated in this thesis are unike in that they focus on investigating the density wave mechanism with an unconventional experimental setup.

The simulator OLGA without slug tracking as well as the SLUGGIT simulator in its modified form have proven capable of reproducing the unstable behaviour observed in the experiments, at gas mass injection rates close to the rates giving unstable production in the experimental configuration. The deviations in transition limits from unstable to stable production observed upon comparison of experiments and simulations may possibly be addressed to the geometrical differences between the experimental geometry and the adapted geometry used during simulations. The general observations made during the work are:

- Both OLGA without slug tracking and SLUGGIT in its modified form successfully reproduce the unstable Mode 2 production characteristics observed during the experiments
- Unstable production with Mode 2 characteristics has not been obtained with the slug tracking module offered in OLGA
- A fine grid was needed for the OLGA simulations without slug tracking to maintain unstable production behaviour with Mode 2 characteristics
- The maximum bubble length had to be set short in the SLUGGIT simulations in order to enable liquid back flow in the vertical riser with subsequent formation of slugs with shorter bubbles in between at the riser outlet. These short bubbles contributed to smoothen the transition zones in the stability maps, giving unstable production with Mode 2 characteristics over a larger gas injection rate region

Some general recommendations for further work are:

- Implement void fraction in slugs. Gas can then be injected directly into the slug at a continuous base, leaving the slug splitting procedure superfluous and possibly removing the pressure oscillations observed during simulations. The introduction of void fraction in slugs in combination with a bubbly flow

drift velocity correlation could probably be used to improve the simulations at the lowest gas injection rates, where bubbly flow in the riser is an important transport mechanism

- Parallellize the SLUGGIT code to enhance simulation efficiency. Management operations associated with sections splitting and merging are possibly difficult to parallellize. However, linear algebra C++ packages exist, which could possibly be used for splitting of the conservation equation coefficient matrices facilitating parallell computing

- Introduce an option for printing of slug pressures at different locations along the slug. The current SLUGGIT version supports printing of the interpolated slug pressure in the middle of each slug. This may however introduce undesired values upon plotting of values from low pressure systems where hydrostatic pressure changes are important

- Perform a series of new gas lift experiments where the pipe geometry becomes thoroughly documented. This may be obtained by use of straight pipes only, joined together with bends with well defined geometry. This will facilitate comparability between experiments and simulations. This will also enable addition of loss coefficients in new simulations. In addition, instrumentation capable of detecting the full ranges of variables of interest should be used

- Include the simplified single bubble pressure calculation procedure version used in previous SLUGGIT versions, and then investigate the effect of this change on calculated gas and liquid flow rates

- Implement an alternative slug initiation procedure where slugs are initiated at section borders by a slug initiation model. This will remove the slug initiation section length dependency.

- Implement a SLUGGIT option enabling batch study execution

References

[1] Subsea production system illustration.
URL `http://www.apachevangogh.com.au/images/maps/FPSO-schematic.gif`

[2] A. Torre, Z. Schmidt, R. Blais, D. Doty, J. Brill, Casing heading in flowing oil wells, SPE Production Engineering 2 (4) (1987) 297–304. doi:10.2118/13801-PA.

[3] O. Aamo, G. Eikrem, H. Siahaan, B. Foss, Observer design for multiphase flow in vertical pipes with gas-lift-theory and experiments, Journal of Process Control 15 (3) (2005) 247 – 257. doi:10.1016/j.jprocont.2004.07.002.

[4] F. Jansen, O. Shoham, Y. Taitel, The elimination of severe slugging - experiments and modeling, International Journal of Multiphase Flow 22 (6) (1996) 1055 – 1072. doi:10.1016/0301-9322(96)00027-4.

[5] L. Sinègre, N. Petit, P. Ménégatti, Distributed delay model for density wave dynamics in gas lifted wells, in: Decision and Control and European Control Conference, 2005, pp. 7390–7397.

[6] L. Sinègre, N. Petit, P. Ménégatti, Predicting instabilities in gas-lifted wells simulation, in: American Control Conference Minneapolis, Minesota, USA, 2006.

[7] E. Jahanshahi, K. Salahshoor, R. Kharrat, Modified distributed delay model for void wave dynamics in gas-lifted wells, Journal of Petroleum Science and Engineering 69 (3-4) (2009) 203 – 213.

[8] E. Jahanshahi, K. Salahshoor, R. Kharrat, H. Rahnema, Modeling and simulation of instabilities in gas-lifted oil wells, in: SPE North Africa Technical Conference & Exhibition, Marrakech, Morocco, 2008. doi:10.2118/112108-MS.

[9] B. Hu, M. Golan, Gas-lift instability resulted production loss and its remedy by feedback control: Dynamical simulation results, in: SPE International Improved Oil Recovery Conference in Asia Pacific, Kuala Lumpur, Malaysia, 2003. doi:10.2118/84917-MS.

[10] M. Evers, V. Beusekom, R. Henkes, Appearance and mitigation of density waves in continuously gas-lifted oil wells, in: 14th International Conference on Multiphase Production Technology, Cannes, France, BHR, 2009.

[11] N. Apazidis, Influence of bubble expansion and relative velocity on the performance and stability of an airlift pump, International Journal of Multiphase Flow 11 (4) (1985) 459 – 479. doi:DOI: 10.1016/0301-9322(85)90070-9.

[12] B. Hu, Characterizing gas-lift instabilities, Ph.D. thesis, NTNU (2004).

[13] S. Z. Kassab, H. A. Kandil, H. A. Warda, W. H. Ahmed, Air-lift pumps characteristics under two-phase flow conditions, International Journal of Heat and Fluid Flow 30 (1) (2009) 88 – 98. doi:10.1016/j.ijheatfluidflow.2008.09.002.

[14] F. D. Cachard, J. M. Delhaye, Stability of small diameter airlift pumps, International Journal of Multiphase Flow 24 (1) (1998) 17 – 34. doi:DOI: 10.1016/S0301-9322(97)00041-4.

[15] H. Monji, F. Joussellin, S. Morioka, Flow pattern transition in riser due to instability of voidage wave, Journal of the Physical Society of Japan 57 (6) (1988) 1957–1962. doi:10.1143/JPSJ.57.1957.

[16] H. Monji, Transition mechanism from bubble flow to slug flow in a riser, Fluid Dynamics Research 11 (1-2) (1993) 61–74. doi:10.1016/0169-5983(93)90005-U.

[17] J. Park, D. Drew, R. Lahey, The analysis of void waves in two-phase flow, Nuclear Engineering and Design 141 (1993) 203–224.

[18] T. Haley, D. Drew, R. Lahey, A characteristic analysis of void waves using two-fluid models, Nuclear Engineering and Design 139 (1993) 45–47.

[19] R. Lahey, Void wave propagation phenomena in two-phase flow (kern award lecture), AIChE Journal 37 (1991) 123–135. doi:10.1002/aic.690370111.

[20] J. Park, D. Drew, R. L. Jr, The measurement of void waves in bubbly two-phase flows, Nuclear Engineering and Design 149 (1994) 37–52.

[21] S. Guet, G. Ooms, Fluid mechanical aspects of the gas-lift technique, Annual Review of Fluid Mechanics 38 (1) (2006) 225–249. doi:10.1146/annurev.fluid.38.061505.093942.

[22] H. Asheim, Criteria for gas-lift stability, Journal of Petroleum Technology 40 (11) (1988) 1452–1456. doi:10.2118/16468-PA.

[23] E. Blick, P. Enga, P. Lin, Stability analysis of flowing oil wells and gas lift wells, SPE Production Engineering 3 (4) (1988) 508–514. doi:10.2118/15022-PA.

[24] F. Alhanati, Z. Schmidt, D. Doty, D. Lagerlef, Continuous gas-lift instability: Diagnosis, criteria and solutions, in: SPE Annual Technical Conference and Exhibition, Houston, Texas, 1993. doi:10.2118/26554-MS.

[25] E. Poblano, R. Camacho, Y. Fairuzov, Stability analysis of continuous-flow gas lift wells, SPE Production & Facilities 20 (1) (2005) 70–79. doi:10.2118/77732-PA.

[26] A. Bertuzzi, J. Welchon, F. Poettmann, Description and analysis of an efficient continuous-flow gas-lift installation, AIME 198 (1953) 271–278. doi:953271-G.

[27] Y. Fairuzov, I. Guerrero-Sarabia, C. Calva-Morales, R. Carmona-Diaz, T. Cervantes-Baza, N. Miguel-Hernandez, A. Rojas-Figueroa, Stability maps for continuous gas-lift wells: A new approach to solving an old problem, in: SPE Annual Technical Conference and Exhibition, Houston, Texas, 2004. doi:10.2118/90644-MS.

[28] A. Gruping, C. Luca, F. Vermuelen, Continuous-flow gas-lift: Heading action analyzed for stabilization, Oil & Gas Journal, 47-51 (July 1984).

[29] A. Gruping, C. Luca, F. Vermuelen, Continuous-flow gas-lift: These methods can eliminate or control annulus heading, Oil & Gas Journal, 186-192 (July 1984).

[30] Z. Xu, M. Golan, Criteria for operation stability of gas-lift wells, Society of Petroleum Engineers (1989) 1–18doi:19362-MS.

[31] W. Gilbert, Flowing and gas-lift well performance, Drilling and Production Practice (1954). doi:54-126.

[32] J. Fitremann, P. Vedrines, Nonsteady gas-liquid flow in pipes and gas lifted wells, in: Second International Conference on Multiphase Flow, London, 1985, 245-262.

[33] Y. Tang, Z. Schmidt, R. Blais, D. Doty, Transient dynamic characteristics of the gas-lift unloading process, SPE Journal 4 (3) (1999) 268–278. doi:10.2118/57659-PA.

[34] E. Blick, A. Nelson, Root locus stability analysis of a flowing oilwell feedback controller, in: SPE Production Operations Symposium, Oklahoma City, Oklahoma, 1989,. doi:10.2118/18874-MS.

[35] E. Storkaas, S. Skogestad, Controllability analysis of two-phase pipeline-riser systems at riser slugging conditions, Control Engineering Practice 15 (5) (2007) 567 – 581. doi:10.1016/j.conengprac.2006.10.007.

[36] B. Jansen, M. Dalsmo, L. Nøkleberg, K. Havre, V. Kristiansen, P. Lemetayer, Automatic control of unstable gas lifted wells, in: SPE Annual Technical Conference and Exhibition, Houston, Texas, 1999. doi:10.2118/56832-MS.

[37] T. Gould, M. Tek, Steady and unsteady state two-phase flow through vertical flow strings, in: SPE Symposium on Numerical Simulation, Dallas, Texas, 1970. doi:10.2118/2804-MS.

[38] R. Vázquez-Román, P. Palafox-Hernández, A new approach for continuous gas lift simulation and optimization, in: SPE Annual Technical Conference and Exhibition, Dallas, Texas, 2005. doi:10.2118/95949-MS.

[39] Y. Taitel, S. Vierkandt, O. Shoham, J. Brill, Severe slugging in a riser system: experiments and modeling, International Journal of Multiphase Flow 16 (1) (1990) 57 – 68. doi:10.1016/0301-9322(90)90037-J.

[40] C. Sarica, O.Shoham, A simplified transient model for pipeline-riser systems, Chemical Engineering Science 46 (9) (1991) 2167–2179.

[41] A. Bøe, Severe slugging characteristics, selected topics in two-phase flow, NTH, Trondheim, Norway (1981).

[42] S. Sagatun, Riser slugging: A mathematical model and the practical consequences, SPE Production & Facilities 19 (3) (2004) 168–175. doi:10.2118/87355-PA.

[43] C. Sarica, J. Tengesdal, A new technique to eliminate severe slugging in pipeline/riser systems, in: SPE Annual Technical Conference and Exhibition, Dallas, Texas, 2000. doi:10.2118/63185-MS.

[44] A. Kristiansen, R. Gjerde, Small scale laboratory experiments on unstable gas lift in wells, Master's thesis, NTNU (2005).

[45] O. Nydal, S. Banerjee, Dynamic slug tracking simulations for gas-liquid flow in pipelines, Chem. Eng. Comm. 141-142 (1996) 13–39.

[46] J. Kjølås, Plug propagation in multiphase pipelines: Modeling and small scale experiments, Ph.D. thesis, NTNU (2007).

[47] F. Renault, A lagrangian slug capturing scheme for gas-liquid flows in pipes, Ph.D. thesis, NTNU (2007).

[48] A. D. Leebeeck, A roll wave and slug tracking scheme for gas-liquid pipe flow, Ph.D. thesis, NTNU (2010).

[49] H. Bendiksen, An experimental investigation of the motion of long bubbles in inclined tubes, International Journal of Multiphase Flow (1984).

[50] K. Bendiksen, D. Malnes, R. Moe, S. Nuland, The dynamic two-fluid model olga: Theory and application, Society of Petroleum Engineers(SPE)HS2001-7.

[51] Olga 2000 user's manual, Scandpower petroleum technology (V4.0).

[52] E. Zukoski, Influence of viscosity, surface tension, and inclination angle on motion of long bubbles in closed tubes, Journal of Fluid Mechanics 25 (1966) 821–837.

[53] R. Moissis, P. Griffith, Entrance effects in a two-phase slug flow, Journal of Heat Transfer 84 (1962) 366–370.

[54] R. Issa, M. Kempf, Simulation of slug flow in horizontal and nearly horizontal pipes with the two-fluid model, International Journal of Multiphase Flow 29 (2003) 69–95. doi:10.1016/S0301-9322(02)00127-1.

Nomenclature

Symbols

μ	Dynamic viscosity
ρ	Density
σ	Surface tension
τ	Shear stress
θ	Pipe inclination
υ	Kinematic viscosity
ε	Roughness
A	Pipe cross sectional area
D	Pipe internal diameter

f	Darcy friction factor
g	Gravity
H	Holdup
L	Length
M	Molar mass
m	Mass
n	Mole
P	Pressure
Re	Reynolds number
S	Perimeter
T	Temperature
t	Time
U	Velocity
V	Volume
z	Pipe axial coordinate
α	Void fraction
Δt	Time step

Subscripts

avg	Moving average
b	Bubble
d	Droplet
$front$	Slug front
g	Gas
h	Hydraulic
i	Interphase
j	Computational cell
k	Phase

l	Liquid
m	Mixture
p	Pipeline
R	Reservoir
sep	Separator
sg	Superficial gas
sl	Superficial liquid
s	Slug
$tail$	Slug tail

Superscripts

$\cdot$	Time rate of change of a quantity
$n+1$	Next time step
n	Current time step
s	Source

Special notation

$\bar{R}$	Ideal gas constant
$\dot{m}_{inject}$	Injection rate into inserted bubble
ψ_g	Interfacial mass transfer rate
C_0	Bubble velocity coefficient
H_0	Height of weir relative to gas injection point
H_{bubble}	Holdup stratified section
h_l	Liquid height stratified zone
H_s	Height of riser outlet relative to gas injection point
ID	Flow regime indicator
IFM	Interphase Friction Multiplier
L_{final}	Final length of inserted bubble

$L_{initial}$	Initial length of inserted bubble
m_{acc}	Accumulated mass for injection into inserted bubble
R_s	Gas mass fraction at equilibrium conditions
U_0	Drift velocity
$U_{b,corr}$	Bubble velocity corrected for wake effect
$U_{l,bubble}$	Liquid phase velocity stratified section
W_{eff}	Wake effect correction factor
$z_{L,sec}$	Section left border coordinate
z_L	Left data extraction limit
$z_{R,sec}$	Section right border coordinate
z_R	Right data extraction limit

A Visualization of OLGA - series I

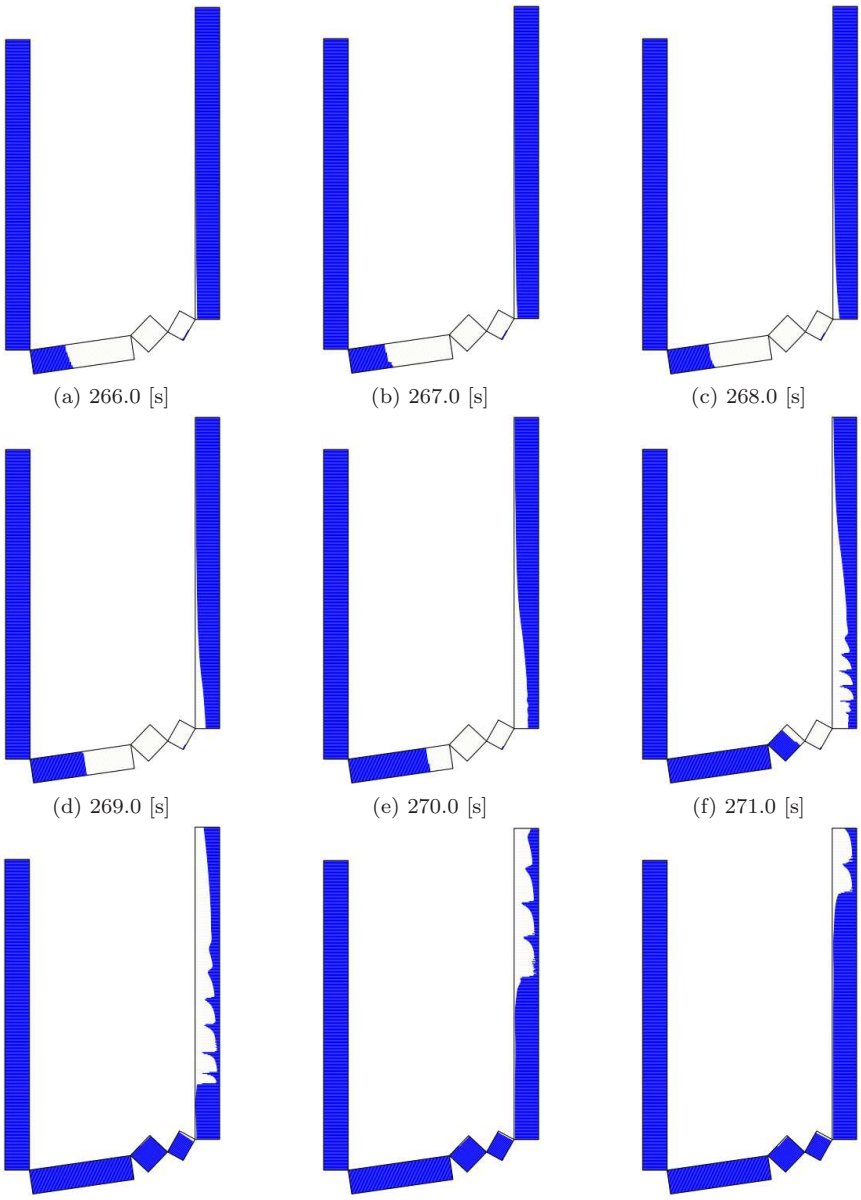

(a) 266.0 [s] (b) 267.0 [s] (c) 268.0 [s]

(d) 269.0 [s] (e) 270.0 [s] (f) 271.0 [s]

(g) 272.0 [s] (h) 273.0 [s] (i) 274.0 [s]

Figure 151: OLGA - series I, $\dot{m}_g = 2.000 \cdot 10^{-5} [kg/s]$

(a) 275.0 [s]

(b) 276.0 [s]

(c) 277.0 [s]

(d) 278.0 [s]

(e) 279.0 [s]

(f) 280.0 [s]

(g) 292.0 [s]

(h) 304.0 [s]

(i) 316.0 [s]

Figure 152: OLGA - series I, $\dot{m}_g = 2.000 \cdot 10^{-5} [kg/s]$

(a) 323.0 [s]

(b) 225.0 [s]

(c) 227.0 [s]

(d) 229.0 [s]

(e) 231.0 [s]

(f) 233.0 [s]

(g) 235.0 [s]

(h) 337.0 [s]

(i) 339.0 [s]

Figure 153: OLGA - series I, $\dot{m}_g = 2.642 \cdot 10^{-5} [kg/s]$

B Visualization of OLGA - series II

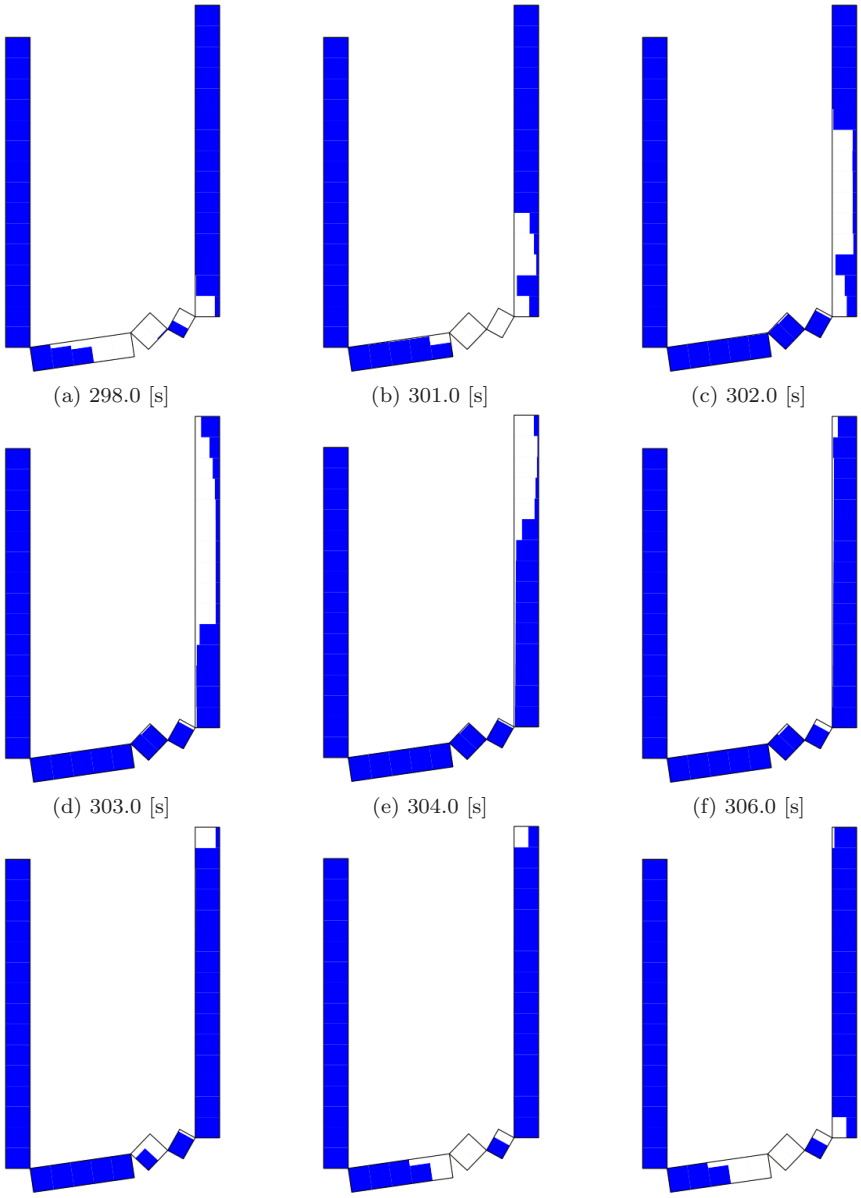

(a) 298.0 [s] (b) 301.0 [s] (c) 302.0 [s]

(d) 303.0 [s] (e) 304.0 [s] (f) 306.0 [s]

(g) 311.0 [s] (h) 326.0 [s] (i) 338.0 [s]

Figure 154: OLGA - series II, $\dot{m}_g = 2.000 \cdot 10^{-5} [kg/s]$

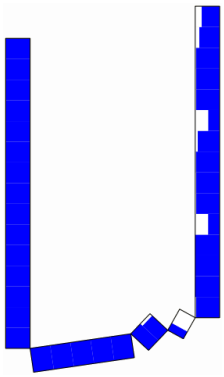

(a) 276.0 [s]

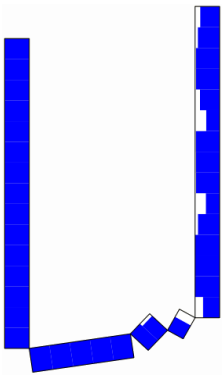

(b) 276.4 [s]

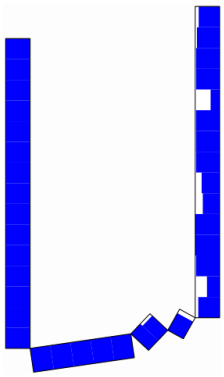

(c) 276.8 [s]

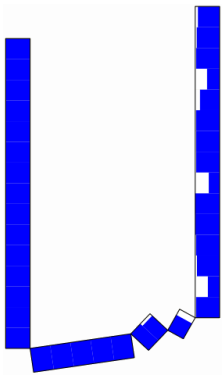

(d) 277.2 [s]

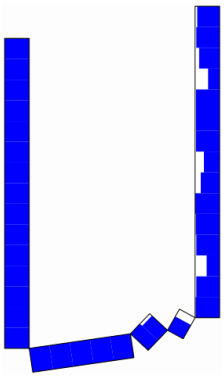

(e) 277.6 [s]

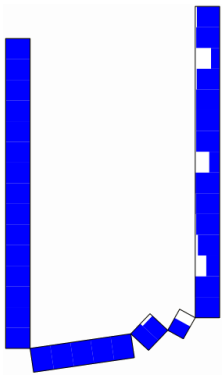

(f) 278.0 [s]

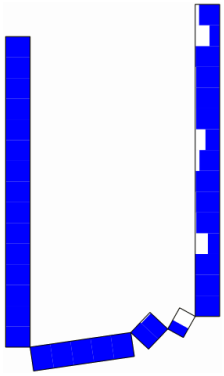

(g) 278.4 [s]

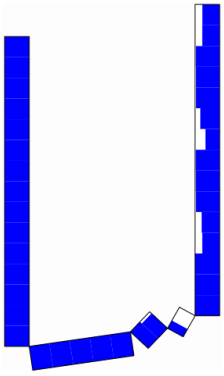

(h) 278.8 [s]

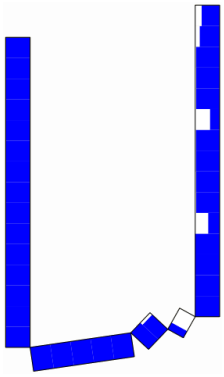

(i) 279.2 [s]

Figure 155: OLGA - series II, $\dot{m}_g = 2.642 \cdot 10^{-5} [kg/s]$

C Visualization of SLUGGIT - series I

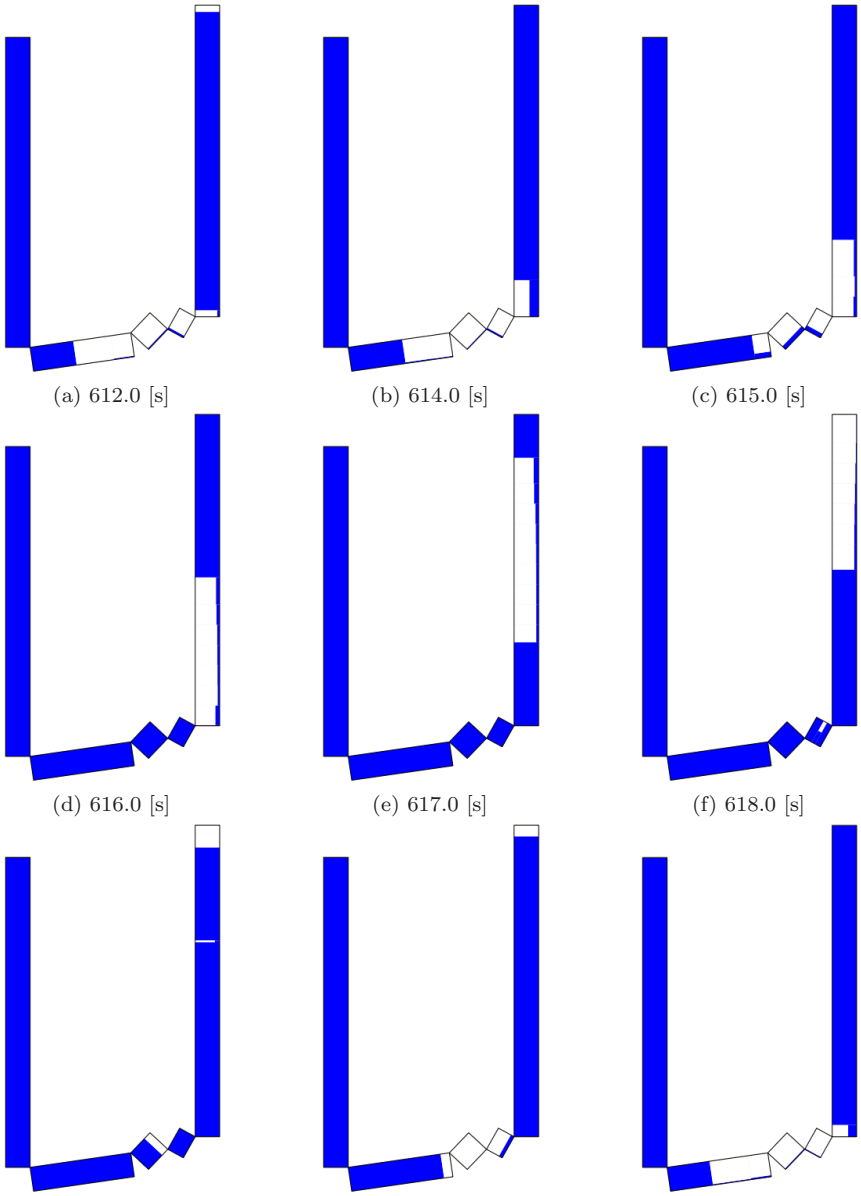

(a) 612.0 [s] (b) 614.0 [s] (c) 615.0 [s]

(d) 616.0 [s] (e) 617.0 [s] (f) 618.0 [s]

(g) 626.0 [s] (h) 646.0 [s] (i) 662.0 [s]

Figure 156: SLUGGIT - series I, $\dot{m}_g = 2.000 \cdot 10^{-5} [kg/s]$

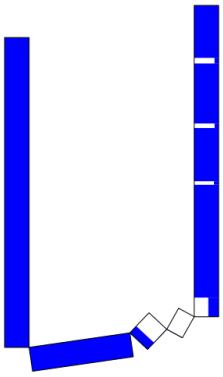

(a) 1244.2 [s]

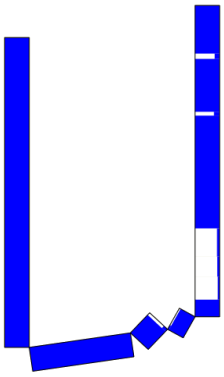

(b) 1246.4 [s]

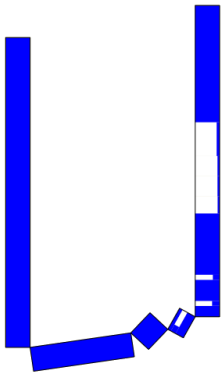

(c) 1248.6 [s]

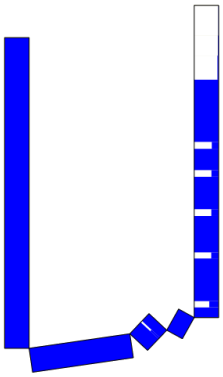

(d) 1250.8 [s]

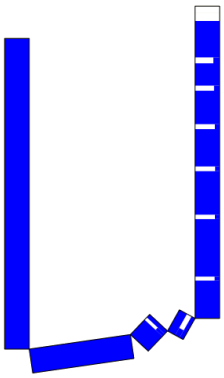

(e) 1253.0 [s]

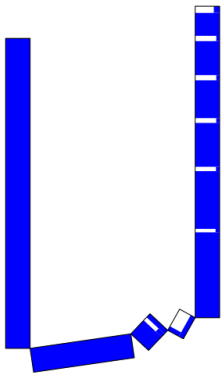

(f) 1255.2 [s]

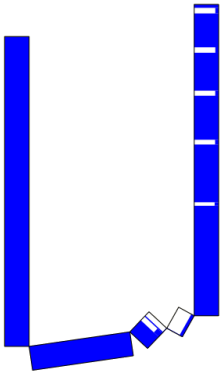

(g) 1257.4 [s]

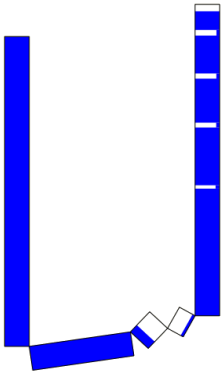

(h) 1259.6 [s]

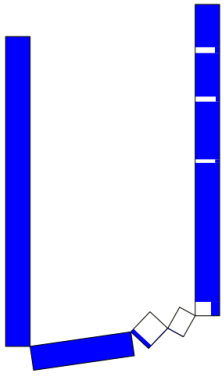

(i) 1261.8 [s]

Figure 157: SLUGGIT - series I, $\dot{m}_g = 4.970 \cdot 10^{-5} [kg/s]$

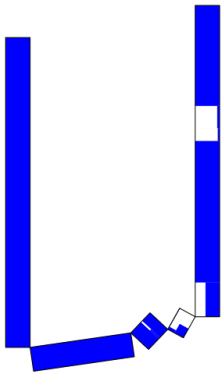

(a) 454.6 [s]

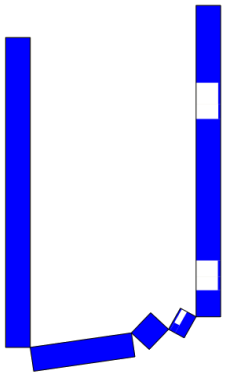

(b) 455.4 [s]

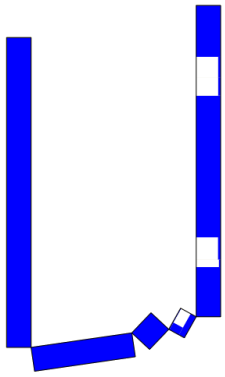

(c) 456.2 [s]

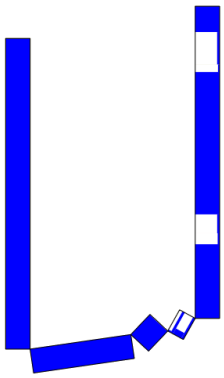

(d) 457.0 [s]

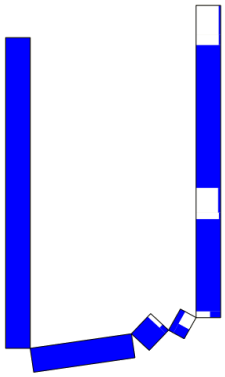

(e) 457.8 [s]

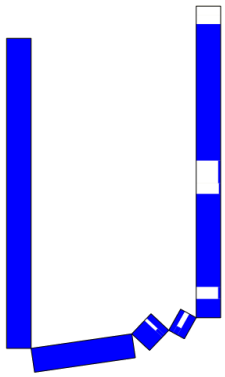

(f) 458.6 [s]

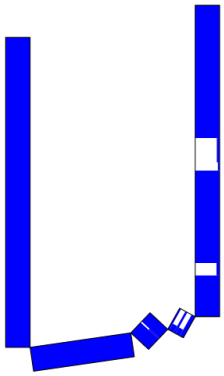

(g) 459.4 [s]

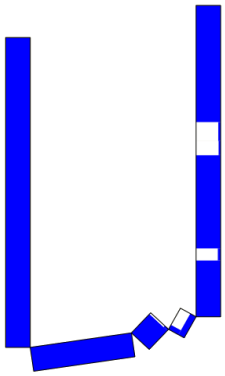

(h) 460.2 [s]

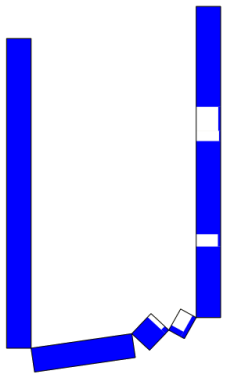

(i) 461.0 [s]

Figure 158: SLUGGIT - series I, $\dot{m}_g = 5.000 \cdot 10^{-5} [kg/s]$

D Visualization of SLUGGIT - series III

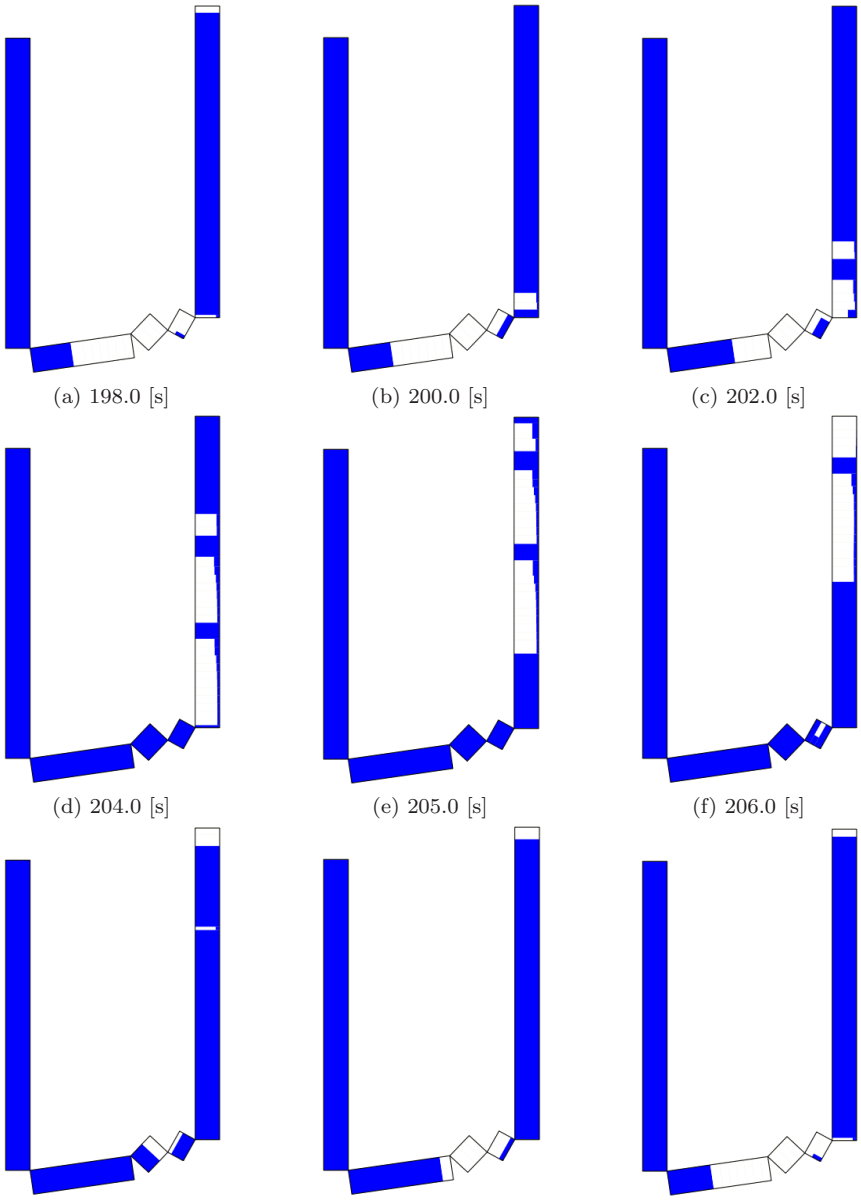

(a) 198.0 [s] (b) 200.0 [s] (c) 202.0 [s]

(d) 204.0 [s] (e) 205.0 [s] (f) 206.0 [s]

(g) 217.0 [s] (h) 230.0 [s] (i) 250.0 [s]

Figure 159: SLUGGIT - series III, $\dot{m}_g = 2.000 \cdot 10^{-5} [kg/s]$

E Visualization of SLUGGIT - series IV

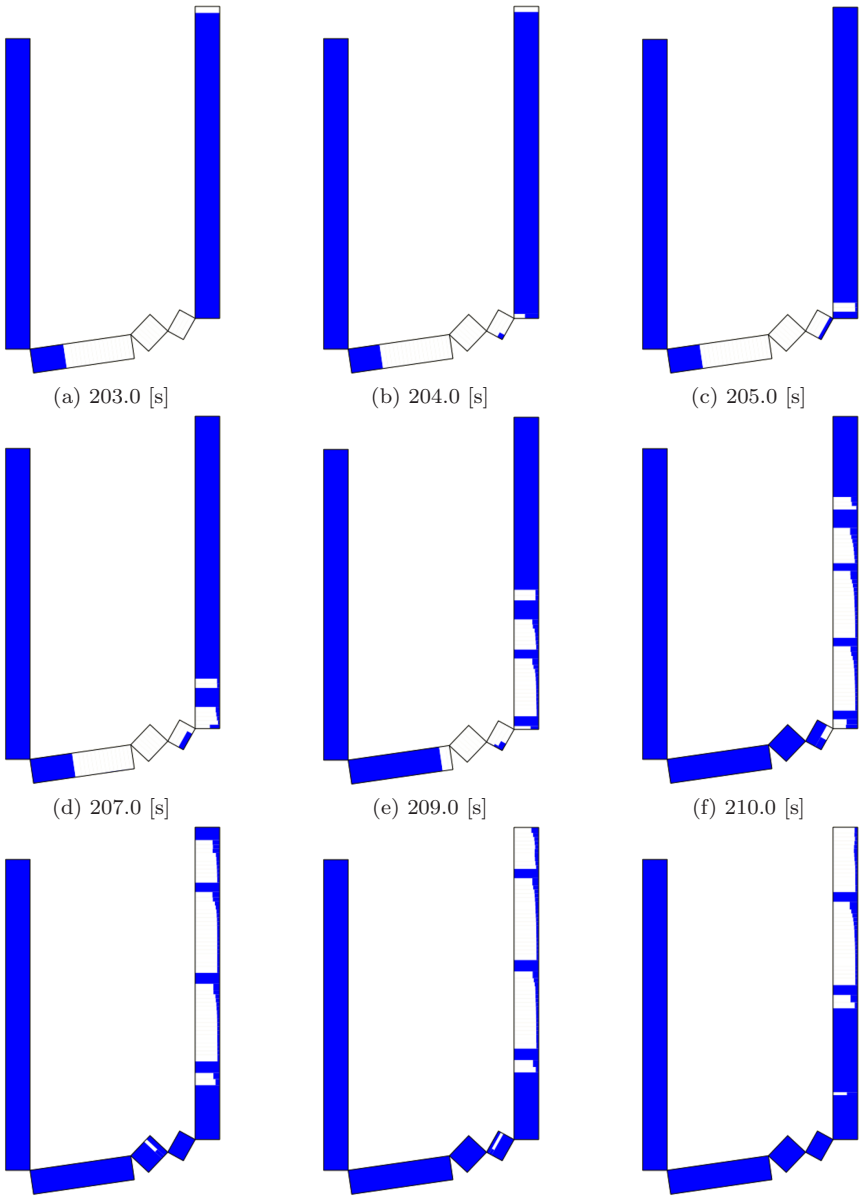

(a) 203.0 [s] (b) 204.0 [s] (c) 205.0 [s]

(d) 207.0 [s] (e) 209.0 [s] (f) 210.0 [s]

(g) 211.0 [s] (h) 211.2 [s] (i) 211.9 [s]

Figure 160: SLUGGIT - series IV, $\dot{m}_g = 2.000 \cdot 10^{-5} [kg/s]$

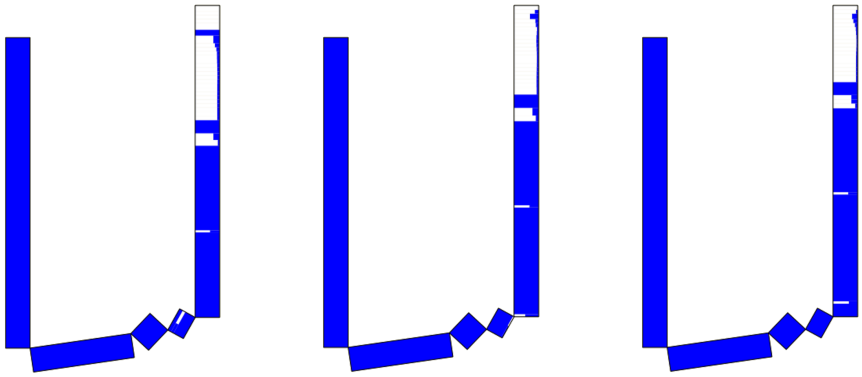

(a) 212.6 [s]

(b) 213.0 [s]

(c) 213.2 [s]

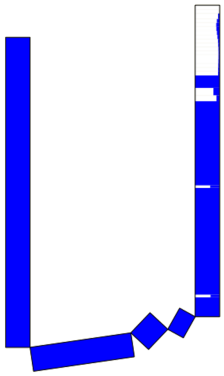

(d) 213.3 [s]

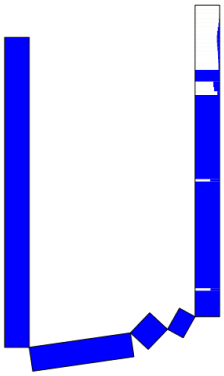

(e) 213.4 [s]

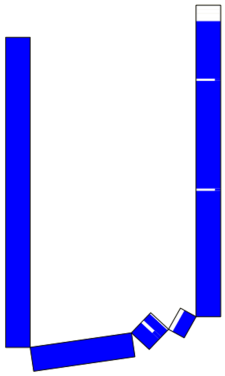

(f) 218.0 [s]

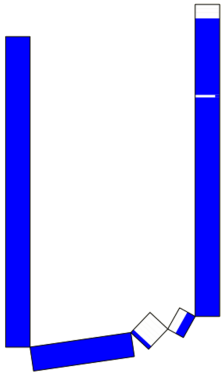

(g) 230.0 [s]

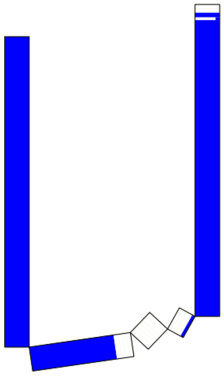

(h) 240.0 [s]

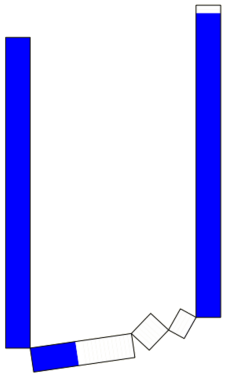

(i) 256.0 [s]

Figure 161: SLUGGIT - series IV, $\dot{m}_g = 2.000 \cdot 10^{-5} [kg/s]$

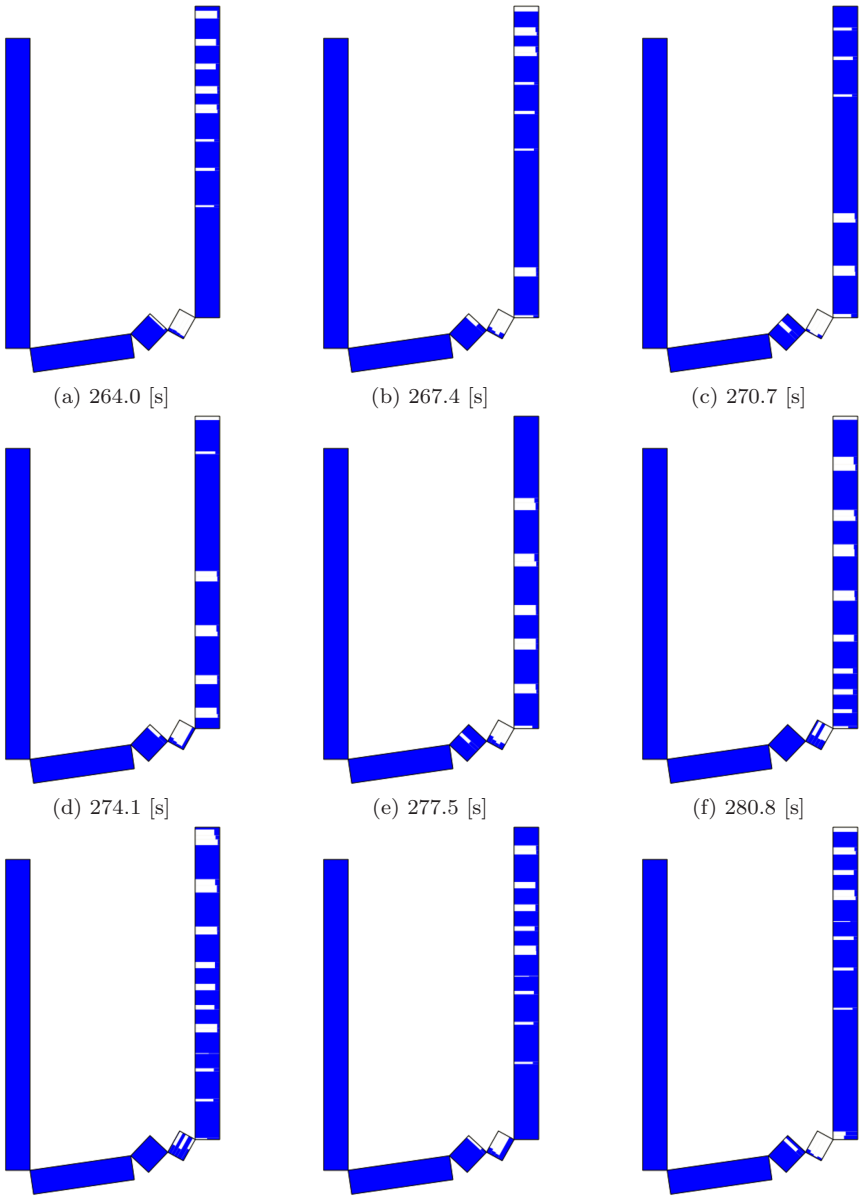

(a) 264.0 [s] (b) 267.4 [s] (c) 270.7 [s]

(d) 274.1 [s] (e) 277.5 [s] (f) 280.8 [s]

(g) 284.2 [s] (h) 287.5 [s] (i) 290.9 [s]

Figure 162: SLUGGIT - series IV, $\dot{m}_g = 3.500 \cdot 10^{-5} [kg/s]$

F OLGA input files

```
%%%%%%%%%%%%%%%%%%%%%%%%%%%%%%%%%%%%%%%%%%%%%%%%%%%%%%%%%%%%%%%%%%%%%%%%%%%%%%%%
%%%%%%%%%%%%%%%  OLGA input file - series I  %%%%%%%%%%%%%%%%%%%%%%%%%%%%%%%%%%%
%%%%%%%%%%%%%%%%%%%%%%%%%%%%%%%%%%%%%%%%%%%%%%%%%%%%%%%%%%%%%%%%%%%%%%%%%%%%%%%%

!*******************************************************************************
!        CASE
!*******************************************************************************
!
!*******************************************************************************
!        OPTIONS
!*******************************************************************************
OPTIONS DEBUG=ON, SLUGVOID=AIR, TEMPERATURE=OFF, STEADYSTATE=NOTEMP
!
!*******************************************************************************
!        FILES
!*******************************************************************************
FILES PVTFILE="./air_water.tab"
!
!*******************************************************************************
!        INTEGRATION
!*******************************************************************************
INTEGRATION DTSTART=0.001 S, ENDTIME=800 s, MAXDT=1 S, MINDT=1e-006 s, STARTTIME=0 S
!
!*******************************************************************************
!        GEOMETRY
!*******************************************************************************
GEOMETRY LABEL=GEOMETRY-1, XSTART=0 M, YSTART=0 M, ZSTART=0 M
PIPE LABEL=PIPE-1, ROUGHNESS=2E-06 M, XEND=3.77791E-16 M, YEND=-6.17 M, DIAMETER=0.016 M,"
   NSEGMENT=300, LSEGMENT=(0.0205667, 0.0205667, 0.0205667, 0.0205667, 0.0205667, 0.0205667,"
   0.0205667, 0.0205667, 0.0205667, 0.0205667, 0.0205667, 0.0205667, 0.0205667, 0.0205667,"
   0.0205667, 0.0205667, 0.0205667, 0.0205667, 0.0205667, 0.0205667, 0.0205667, 0.0205667,"
   0.0205667, 0.0205667, 0.0205667, 0.0205667, 0.0205667, 0.0205667, 0.0205667, 0.0205667,"
   0.0205667, 0.0205667, 0.0205667, 0.0205667, 0.0205667, 0.0205667, 0.0205667, 0.0205667,"
   0.0205667, 0.0205667, 0.0205667, 0.0205667, 0.0205667, 0.0205667, 0.0205667, 0.0205667,"
   0.0205667, 0.0205667, 0.0205667, 0.0205667, 0.0205667, 0.0205667, 0.0205667, 0.0205667,"
   0.0205667, 0.0205667, 0.0205667, 0.0205667, 0.0205667, 0.0205667, 0.0205667, 0.0205667,"
   0.0205667, 0.0205667, 0.0205667, 0.0205667, 0.0205667, 0.0205667, 0.0205667, 0.0205667,"
   0.0205667, 0.0205667, 0.0205667, 0.0205667, 0.0205667, 0.0205667, 0.0205667, 0.0205667,"
   0.0205667, 0.0205667, 0.0205667, 0.0205667, 0.0205667, 0.0205667, 0.0205667, 0.0205667,"
   0.0205667, 0.0205667, 0.0205667, 0.0205667, 0.0205667, 0.0205667, 0.0205667, 0.0205667,"
   0.0205667, 0.0205667, 0.0205667, 0.0205667, 0.0205667, 0.0205667, 0.0205667, 0.0205667,"
   0.0205667, 0.0205667, 0.0205667, 0.0205667, 0.0205667, 0.0205667, 0.0205667, 0.0205667,"
   0.0205667, 0.0205667, 0.0205667, 0.0205667, 0.0205667, 0.0205667, 0.0205667, 0.0205667,"
   0.0205667, 0.0205667, 0.0205667, 0.0205667, 0.0205667, 0.0205667, 0.0205667, 0.0205667,"
   0.0205667, 0.0205667, 0.0205667, 0.0205667, 0.0205667, 0.0205667, 0.0205667, 0.0205667,"
   0.0205667, 0.0205667, 0.0205667, 0.0205667, 0.0205667, 0.0205667, 0.0205667, 0.0205667,"
   0.0205667, 0.0205667, 0.0205667, 0.0205667, 0.0205667, 0.0205667, 0.0205667, 0.0205667,"
   0.0205667, 0.0205667, 0.0205667, 0.0205667, 0.0205667, 0.0205667, 0.0205667, 0.0205667,"
   0.0205667, 0.0205667, 0.0205667, 0.0205667, 0.0205667, 0.0205667, 0.0205667, 0.0205667,"
   0.0205667, 0.0205667, 0.0205667, 0.0205667, 0.0205667, 0.0205667, 0.0205667, 0.0205667,"
   0.0205667, 0.0205667, 0.0205667, 0.0205667, 0.0205667, 0.0205667, 0.0205667, 0.0205667,"
   0.0205667, 0.0205667, 0.0205667, 0.0205667, 0.0205667, 0.0205667, 0.0205667, 0.0205667,"
   0.0205667, 0.0205667, 0.0205667, 0.0205667, 0.0205667, 0.0205667, 0.0205667, 0.0205667,"
   0.0205667, 0.0205667, 0.0205667, 0.0205667, 0.0205667, 0.0205667, 0.0205667, 0.0205667,"
   0.0205667, 0.0205667, 0.0205667, 0.0205667, 0.0205667, 0.0205667, 0.0205667, 0.0205667,"
   0.0205667, 0.0205667, 0.0205667, 0.0205667, 0.0205667, 0.0205667, 0.0205667, 0.0205667,"
   0.0205667, 0.0205667, 0.0205667, 0.0205667, 0.0205667, 0.0205667, 0.0205667, 0.0205667,"
   0.0205667, 0.0205667, 0.0205667, 0.0205667, 0.0205667, 0.0205667, 0.0205667, 0.0205667,"
   0.0205667, 0.0205667, 0.0205667, 0.0205667, 0.0205667, 0.0205667, 0.0205667, 0.0205667,"
   0.0205667, 0.0205667, 0.0205667, 0.0205667, 0.0205667, 0.0205667, 0.0205667, 0.0205667,"
   0.0205667, 0.0205667, 0.0205667, 0.0205667, 0.0205667, 0.0205667, 0.0205667, 0.0205667,"
   0.0205667, 0.0205667, 0.0205667, 0.0205667, 0.0205667, 0.0205667, 0.0205667, 0.0205667,"
   0.0205667, 0.0205667, 0.0205667, 0.0205667, 0.0205667, 0.0205667, 0.0205667, 0.0205667,"
   0.0205667, 0.0205667, 0.0205667, 0.0205667, 0.0205667, 0.0205667, 0.0205667, 0.0205667,"
   0.0205667, 0.0205667, 0.0205667, 0.0205667, 0.0205667, 0.0205667, 0.0205667, 0.0205667,"
   0.0205667, 0.0205667, 0.0205667, 0.0205667, 0.0205667, 0.0205667, 0.0205667, 0.0205667,"
   0.0205667, 0.0205667, 0.0205667, 0.0205667, 0.0205667, 0.0205667, 0.0205667, 0.0205667,"
   0.0205667, 0.0205667, 0.0205667, 0.0205667, 0.0205667, 0.0205667, 0.0205667, 0.0205667,"
   0.0205667, 0.0205667, 0.0205667, 0.0205667, 0.0205667, 0.0205667) M
```

```
PIPE LABEL=PIPE-2, ROUGHNESS=2E-06 M, XEND=1.97886 M, YEND=-5.88 M, DIAMETER=0.016 M,"
   NSEGMENT=100, LSEGMENT=(0.02, 0.02, 0.02, 0.02, 0.02, 0.02, 0.02, 0.02, 0.02, 0.02,"
   0.02, 0.02, 0.02, 0.02, 0.02, 0.02, 0.02, 0.02, 0.02, 0.02, 0.02, 0.02, 0.02, 0.02,"
   0.02, 0.02, 0.02, 0.02, 0.02, 0.02, 0.02, 0.02, 0.02, 0.02, 0.02, 0.02, 0.02, 0.02,"
   0.02, 0.02, 0.02, 0.02, 0.02, 0.02, 0.02, 0.02, 0.02, 0.02, 0.02, 0.02, 0.02, 0.02,"
   0.02, 0.02, 0.02, 0.02, 0.02, 0.02, 0.02, 0.02, 0.02, 0.02, 0.02, 0.02, 0.02, 0.02,"
   0.02, 0.02, 0.02, 0.02, 0.02, 0.02, 0.02, 0.02, 0.02, 0.02, 0.02, 0.02, 0.02, 0.02,"
   0.02, 0.02, 0.02, 0.02, 0.02, 0.02, 0.02, 0.02, 0.02, 0.02, 0.02, 0.02, 0.02, 0.02,"
   0.02, 0.02, 0.02, 0.02, 0.02, 0.02) M
PIPE LABEL=PIPE-3, ROUGHNESS=2E-06 M, XEND=2.35636 M, YEND=-5.48 M, DIAMETER=0.016 M,"
   NSEGMENT=27, LSEGMENT=(0.0203706, 0.0203706, 0.0203706, 0.0203706, 0.0203706, 0.0203706,"
   0.0203706, 0.0203706, 0.0203706, 0.0203706, 0.0203706, 0.0203706, 0.0203706, 0.0203706,"
   0.0203706, 0.0203706, 0.0203706, 0.0203706, 0.0203706, 0.0203706, 0.0203706, 0.0203706,"
   0.0203706, 0.0203706, 0.0203706, 0.0203706, 0.0203706) M
PIPE LABEL=PIPE-4, ROUGHNESS=2E-06 M, XEND=2.6623 M, YEND=-5.65 M, DIAMETER=0.016 M,"
   NSEGMENT=17, LSEGMENT=(0.0205882, 0.0205882, 0.0205882, 0.0205882, 0.0205882, 0.0205882,"
   0.0205882, 0.0205882, 0.0205882, 0.0205882, 0.0205882, 0.0205882, 0.0205882, 0.0205882,"
   0.0205882, 0.0205882, 0.0205882) M
PIPE LABEL=PIPE-5, ROUGHNESS=2E-06 M, XEND=2.66299 M, YEND=0.55 M, DIAMETER=0.016 M,"
   NSEGMENT=300, LSEGMENT=(0.0206667, 0.0206667, 0.0206667, 0.0206667, 0.0206667, 0.0206667,"
   0.0206667, 0.0206667, 0.0206667, 0.0206667, 0.0206667, 0.0206667, 0.0206667, 0.0206667,"
   0.0206667, 0.0206667, 0.0206667, 0.0206667, 0.0206667, 0.0206667, 0.0206667, 0.0206667,"
   0.0206667, 0.0206667, 0.0206667, 0.0206667, 0.0206667, 0.0206667, 0.0206667, 0.0206667,"
   0.0206667, 0.0206667, 0.0206667, 0.0206667, 0.0206667, 0.0206667, 0.0206667, 0.0206667,"
   0.0206667, 0.0206667, 0.0206667, 0.0206667, 0.0206667, 0.0206667, 0.0206667, 0.0206667,"
   0.0206667, 0.0206667, 0.0206667, 0.0206667, 0.0206667, 0.0206667, 0.0206667, 0.0206667,"
   0.0206667, 0.0206667, 0.0206667, 0.0206667, 0.0206667, 0.0206667, 0.0206667, 0.0206667,"
   0.0206667, 0.0206667, 0.0206667, 0.0206667, 0.0206667, 0.0206667, 0.0206667, 0.0206667,"
   0.0206667, 0.0206667, 0.0206667, 0.0206667, 0.0206667, 0.0206667, 0.0206667, 0.0206667,"
   0.0206667, 0.0206667, 0.0206667, 0.0206667, 0.0206667, 0.0206667, 0.0206667, 0.0206667,"
   0.0206667, 0.0206667, 0.0206667, 0.0206667, 0.0206667, 0.0206667, 0.0206667, 0.0206667,"
   0.0206667, 0.0206667, 0.0206667, 0.0206667, 0.0206667, 0.0206667, 0.0206667, 0.0206667,"
   0.0206667, 0.0206667, 0.0206667, 0.0206667, 0.0206667, 0.0206667, 0.0206667, 0.0206667,"
   0.0206667, 0.0206667, 0.0206667, 0.0206667, 0.0206667, 0.0206667, 0.0206667, 0.0206667,"
   0.0206667, 0.0206667, 0.0206667, 0.0206667, 0.0206667, 0.0206667, 0.0206667, 0.0206667,"
   0.0206667, 0.0206667, 0.0206667, 0.0206667, 0.0206667, 0.0206667, 0.0206667, 0.0206667,"
   0.0206667, 0.0206667, 0.0206667, 0.0206667, 0.0206667, 0.0206667, 0.0206667, 0.0206667,"
   0.0206667, 0.0206667, 0.0206667, 0.0206667, 0.0206667, 0.0206667, 0.0206667, 0.0206667,"
   0.0206667, 0.0206667, 0.0206667, 0.0206667, 0.0206667, 0.0206667, 0.0206667, 0.0206667,"
   0.0206667, 0.0206667, 0.0206667, 0.0206667, 0.0206667, 0.0206667, 0.0206667, 0.0206667,"
   0.0206667, 0.0206667, 0.0206667, 0.0206667, 0.0206667, 0.0206667, 0.0206667, 0.0206667,"
   0.0206667, 0.0206667, 0.0206667, 0.0206667, 0.0206667, 0.0206667, 0.0206667, 0.0206667,"
   0.0206667, 0.0206667, 0.0206667, 0.0206667, 0.0206667, 0.0206667, 0.0206667, 0.0206667,"
   0.0206667, 0.0206667, 0.0206667, 0.0206667, 0.0206667, 0.0206667, 0.0206667, 0.0206667,"
   0.0206667, 0.0206667, 0.0206667, 0.0206667, 0.0206667, 0.0206667, 0.0206667, 0.0206667,"
   0.0206667, 0.0206667, 0.0206667, 0.0206667, 0.0206667, 0.0206667, 0.0206667, 0.0206667,"
   0.0206667, 0.0206667, 0.0206667, 0.0206667, 0.0206667, 0.0206667, 0.0206667, 0.0206667,"
   0.0206667, 0.0206667, 0.0206667, 0.0206667, 0.0206667, 0.0206667, 0.0206667, 0.0206667,"
   0.0206667, 0.0206667, 0.0206667, 0.0206667, 0.0206667, 0.0206667, 0.0206667, 0.0206667,"
   0.0206667, 0.0206667, 0.0206667, 0.0206667, 0.0206667, 0.0206667, 0.0206667, 0.0206667,"
   0.0206667, 0.0206667, 0.0206667, 0.0206667, 0.0206667, 0.0206667, 0.0206667, 0.0206667,"
   0.0206667, 0.0206667, 0.0206667, 0.0206667, 0.0206667, 0.0206667, 0.0206667, 0.0206667,"
   0.0206667, 0.0206667, 0.0206667, 0.0206667, 0.0206667, 0.0206667, 0.0206667, 0.0206667,"
   0.0206667, 0.0206667, 0.0206667, 0.0206667, 0.0206667, 0.0206667, 0.0206667, 0.0206667,"
   0.0206667, 0.0206667, 0.0206667, 0.0206667, 0.0206667, 0.0206667, 0.0206667, 0.0206667,"
   0.0206667, 0.0206667, 0.0206667, 0.0206667, 0.0206667, 0.0206667, 0.0206667, 0.0206667,"
   0.0206667, 0.0206667, 0.0206667, 0.0206667, 0.0206667, 0.0206667, 0.0206667, 0.0206667,"
   0.0206667, 0.0206667, 0.0206667, 0.0206667, 0.0206667, 0.0206667, 0.0206667, 0.0206667,"
   0.0206667, 0.0206667, 0.0206667, 0.0206667, 0.0206667, 0.0206667, 0.0206667, 0.0206667,"
   0.0206667, 0.0206667, 0.0206667, 0.0206667, 0.0206667, 0.0206667, 0.0206667, 0.0206667,"
   0.0206667, 0.0206667, 0.0206667, 0.0206667, 0.0206667, 0.0206667, 0.0206667, 0.0206667,"
   0.0206667, 0.0206667, 0.0206667, 0.0206667, 0.0206667, 0.0206667, 0.0206667, 0.0206667,"
   0.0206667, 0.0206667, 0.0206667, 0.0206667, 0.0206667, 0.0206667, 0.0206667, 0.0206667,"
   0.0206667, 0.0206667, 0.0206667, 0.0206667, 0.0206667, 0.0206667, 0.0206667, 0.0206667,"
   0.0206667, 0.0206667, 0.0206667, 0.0206667, 0.0206667, 0.0206667, 0.0206667, 0.0206667,"
   0.0206667, 0.0206667, 0.0206667, 0.0206667, 0.0206667, 0.0206667, 0.0206667, 0.0206667,"
   0.0206667, 0.0206667, 0.0206667, 0.0206667, 0.0206667, 0.0206667, 0.0206667, 0.0206667,"
   0.0206667, 0.0206667, 0.0206667, 0.0206667, 0.0206667, 0.0206667, 0.0206667, 0.0206667,"
   0.0206667, 0.0206667, 0.0206667, 0.0206667, 0.0206667, 0.0206667, 0.0206667, 0.0206667,"
   0.0206667, 0.0206667, 0.0206667, 0.0206667, 0.0206667, 0.0206667, 0.0206667, 0.0206667,"
   0.0206667, 0.0206667, 0.0206667, 0.0206667, 0.0206667, 0.0206667, 0.0206667, 0.0206667,"
   0.0206667, 0.0206667, 0.0206667, 0.0206667, 0.0206667, 0.0206667) M
!
!*****************************************************************************
!        NODE
!*****************************************************************************
NODE LABEL=inlet, TYPE=TERMINAL
NODE LABEL=outlet, TYPE=TERMINAL
!
!*****************************************************************************
!        BRANCH
!*****************************************************************************
BRANCH LABEL=test pipe, FROM=inlet, TO=outlet, GEOMETRY=GEOMETRY-1, FLUID="luft_vann"
```

```
!
!*****************************************************************************
!        BOUNDARY
!*****************************************************************************
BOUNDARY NODE=inlet, TYPE=PRESSURE, TEMPERATURE=20 C, PRESSURE=101300 Pa, GASFRACTION=0
BOUNDARY NODE=outlet, TYPE=PRESSURE, TEMPERATURE=20 C, PRESSURE=101300 Pa
!
!*****************************************************************************
!        INITIALCONDITIONS
!*****************************************************************************
INITIALCONDITIONS BRANCH=test pipe, INTEMPERATURE=20 C, OUTTEMPERATURE=20 C
!
!*****************************************************************************
!        CONTROLLER
!*****************************************************************************
!
!*****************************************************************************
!        SOURCE
!*****************************************************************************
SOURCE LABEL=lift gas source, TIME=0 s, TEMPERATURE=20 C, BRANCH=test pipe, PIPE=PIPE-3,"
   SECTION=14, MASSFLOW=1e-006 kg/s, GASFRACTION=1
!
!*****************************************************************************
!        OUTPUT
!*****************************************************************************
OUTPUT DTOUT=0.1 s
!
!*****************************************************************************
!        TREND
!*****************************************************************************
TREND DTPLOT=0.1 s
TREND BRANCH=test pipe, VARIABLE=GLT, PIPE=PIPE-5, SECTION=300
TREND BRANCH=test pipe, VARIABLE=(HOL, PT), PIPE=PIPE-5, SECTION=(1, 75, 150, 225,"
   300)
TREND BRANCH=test pipe, VARIABLE=(PT, PTMAX, PTMIN), PIPE=PIPE-3, SECTION=14
TREND BRANCH=test pipe, VARIABLE=ID, PIPE=PIPE-3, SECTION=(2, 10, 18, 26)
TREND BRANCH=test pipe, VARIABLE=ID, PIPE=PIPE-4, SECTION=(1, 9, 17)
TREND BRANCH=test pipe, VARIABLE=ID, PIPE=PIPE-5, SECTION=(1, 75, 150, 225, 300)
!
!*****************************************************************************
!        PROFILE
!*****************************************************************************
PROFILE DTPLOT=0.1 s
PROFILE BRANCH=test pipe, VARIABLE=HOL

ENDCASE



%%%%%%%%%%%%%%%%%%%%%%%%%%%%%%%%%%%%%%%%%%%%%%%%%%%%%%%%%%%%%%%%%%%%%%%%%%%%%%%%
%%%%%%%%%%%%%%%  OLGA input file - series II  %%%%%%%%%%%%%%%%%%%%%%%%%%%%%%%%%
%%%%%%%%%%%%%%%%%%%%%%%%%%%%%%%%%%%%%%%%%%%%%%%%%%%%%%%%%%%%%%%%%%%%%%%%%%%%%%%%

!*****************************************************************************
!        CASE
!*****************************************************************************
!
!*****************************************************************************
!        OPTIONS
!*****************************************************************************
OPTIONS DEBUG=ON, SLUGVOID=AIR, TEMPERATURE=OFF, STEADYSTATE=NOTEMP
!
!*****************************************************************************
!        FILES
!*****************************************************************************
FILES PVTFILE="./air_water.tab"
!
!*****************************************************************************
```

```
!        INTEGRATION
!*****************************************************************************
INTEGRATION DTSTART=1e-006 s, ENDTIME=1000 s, MAXDT=1 S, MINDT=1e-006 s, STARTTIME=0 S
!
!*****************************************************************************
!        GEOMETRY
!*****************************************************************************
GEOMETRY LABEL=GEOMETRY-1, XSTART=0 M, YSTART=0 M, ZSTART=0 M
PIPE LABEL=PIPE-1, ROUGHNESS=2E-06 M, XEND=3.77791E-16 M, YEND=-6.17 M, DIAMETER=0.016 M,"
   NSEGMENT=15, LSEGMENT=(0.411333, 0.411333, 0.411333, 0.411333, 0.411333, 0.411333,"
   0.411333, 0.411333, 0.411333, 0.411333, 0.411333, 0.411333, 0.411333, 0.411333, 0.411333) M
PIPE LABEL=PIPE-2, ROUGHNESS=2E-06 M, XEND=1.97886 M, YEND=-5.88 M, DIAMETER=0.016 M,"
   NSEGMENT=5, LSEGMENT=(0.399999, 0.399999, 0.399999, 0.399999, 0.399999) M
PIPE LABEL=PIPE-3, ROUGHNESS=2E-06 M, XEND=2.35636 M, YEND=-5.48 M, DIAMETER=0.016 M,"
   NSEGMENT=2, LSEGMENT=(0.275003, 0.275003) M
PIPE LABEL=PIPE-4, ROUGHNESS=2E-06 M, XEND=2.6623 M, YEND=-5.65 M, DIAMETER=0.016 M,"
   NSEGMENT=1, LSEGMENT=0.349999 M
PIPE LABEL=PIPE-5, ROUGHNESS=2E-06 M, XEND=2.66299 M, YEND=0.55 M, DIAMETER=0.016 M,"
   NSEGMENT=15, LSEGMENT=(0.413333, 0.413333, 0.413333, 0.413333, 0.413333, 0.413333,"
   0.413333, 0.413333, 0.413333, 0.413333, 0.413333, 0.413333, 0.413333, 0.413333, 0.413333) M
!
!*****************************************************************************
!        NODE
!*****************************************************************************
NODE LABEL=inlet, TYPE=TERMINAL
NODE LABEL=outlet, TYPE=TERMINAL
!
!*****************************************************************************
!        BRANCH
!*****************************************************************************
BRANCH LABEL=test pipe, FROM=inlet, TO=outlet, GEOMETRY=GEOMETRY-1, FLUID="luft_vann"
!
!*****************************************************************************
!        SLUGTRACKING
!*****************************************************************************
SLUGTRACKING HYDRODYNAMIC=OFF, LEVEL=ON, STARTTIME=0 s, ENDTIME=500 s, SLUGVOID=0.05,"
   BUBBLEVOID=0.4046
!
!*****************************************************************************
!        BOUNDARY
!*****************************************************************************
BOUNDARY NODE=inlet, TYPE=PRESSURE, TEMPERATURE=20 C, PRESSURE=101300 Pa, GASFRACTION=0
BOUNDARY NODE=outlet, TYPE=PRESSURE, TEMPERATURE=20 C, PRESSURE=101300 Pa, GASFRACTION=1
!
!*****************************************************************************
!        INITIALCONDITIONS
!*****************************************************************************
INITIALCONDITIONS BRANCH=test pipe, INTEMPERATURE=20 C, OUTTEMPERATURE=20 C
!
!*****************************************************************************
!        CONTROLLER
!*****************************************************************************
!
!*****************************************************************************
!        SOURCE
!*****************************************************************************
SOURCE LABEL=lift gas source, TIME=0 s, TEMPERATURE=20 C, BRANCH=test pipe, PIPE=PIPE-3,"
   SECTION=2, MASSFLOW=1e-006 kg/s, GASFRACTION=1
!
!*****************************************************************************
!        OUTPUT
!*****************************************************************************
OUTPUT DTOUT=0.1 s
!
!*****************************************************************************
!        TREND
!*****************************************************************************
TREND DTPLOT=0.1 s
```

```
TREND BRANCH=test pipe, VARIABLE=(GLT, HOL, PT), PIPE=PIPE-5, SECTION=(1, 3, 7, 11,"
   15)
TREND BRANCH=test pipe, VARIABLE=(PTMAX, PTMIN, PT), PIPE=PIPE-3, SECTION=2
!
!*****************************************************************************
!        PROFILE
!*****************************************************************************
PROFILE DTPLOT=0.1 s
PROFILE BRANCH=test pipe, VARIABLE=HOL

ENDCASE
```

G PVT table

```
%%%%%%%%%%%%%%%%%%%%%%%%%%%%%%%%%%%%%%%%%%%%%%%%%%%%%%%%%%%%%%%%%%%%%%%%%%%%%%%%
%%%%%%%%%%%%%%%%  OLGA PVT table  %%%%%%%%%%%%%%%%%%%%%%%%%%%%%%%%%%%%%%%%%%%%%%
%%%%%%%%%%%%%%%%%%%%%%%%%%%%%%%%%%%%%%%%%%%%%%%%%%%%%%%%%%%%%%%%%%%%%%%%%%%%%%%%

PVTTABLE LABEL = "luft_vann",PHASE = TWO,"
COMPONENTS = ("H2O","AIR"),"
MOLWEIGHT = (18.02,28,97) g/mol,"
STDPRESSURE = 1.0 ATM,"
STDTEMPERATURE = 293.16 K,"
GOR = -999 Sm3/Sm3,"
GLR = -999 Sm3/Sm3,"
STDGASDENSITY = 1.204 kg/m3,"
STDOILDENSITY = 998 kg/m3,"
MESHTYPE = STANDARD,"
PRESSURE =    ( 100 , 5.00E+06) Pa,"
TEMPERATURE = ( 18       , 22      ) C,"
COLUMNS =        ( PT       , TM , ROG         , ROHL , DROGDP      , DROHLDP ,
PVTTABLE POINT = ( 1.00E+02 , 18 , 1.19676E-03 , 998  , 1.19676E-05 , 0.0     ,
PVTTABLE POINT = ( 1.00E+02 , 22 , 1.18054E-03 , 998  , 1.18054E-05 , 0.0     ,
PVTTABLE POINT = ( 5.00E+06 , 18 , 5.98380E+01 , 998  , 1.19676E-05 , 0.0     ,
PVTTABLE POINT = ( 5.00E+06 , 22 , 5.90270E+01 , 998  , 1.18054E-05 , 0.0     ,



 DROGDT       , DROHLDT , RS  , VISG      , VISHL     , CPG       , CPHL      ,
-4.11031E-06   , 0.0     , 100 , 1.825E-05 , 1.002E-03 , 1.007E+03 , 4.182E+03 ,
-3.99966E-06   , 0.0     , 100 , 1.825E-05 , 1.002E-03 , 1.007E+03 , 4.182E+03 ,
-2.05516E-01   , 0.0     , 100 , 1.825E-05 , 1.002E-03 , 1.007E+03 , 4.182E+03 ,
-1.99983E-01   , 0.0     , 100 , 1.825E-05 , 1.002E-03 , 1.007E+03 , 4.182E+03 ,



HG , HHL , TCG       , TCHL      , SIGGHL    , SEG , SEHL )
0  , 0   , 2.514E-02 , 5.98E-01 , 7.29E-02 , 0   , 0    )
0  , 0   , 2.514E-02 , 5.98E-01 , 7.29E-02 , 0   , 0    )
0  , 0   , 2.514E-02 , 5.98E-01 , 7.29E-02 , 0   , 0    )
0  , 0   , 2.514E-02 , 5.98E-01 , 7.29E-02 , 0   , 0    )
```

H SLUGGIT input file

```
// This is the input file to sluggitServer (the slug tracking scheme). The slug tracking scheme
// is run with the Visual studio project called sluggitServer. It is found in the folder called
// sluggitServer. The path to this file needs to be specified in the command arguments.
// E.g. ../testcase_Patm/input.txt

// **************
// Pipe Geometry
// **************
// List the pipes in order and label them 1, 2, 3, etc in sequence.
// WALL_LABEL is used if pipe insulation is being considered. For wave simulations it was not used.

GEOMETRY:PIPE_LABEL=1,DIAMETER=0.016,ANGLE=-90.0,LENGTH=6.17,ROUGHNESS=2e-006,WALL_LABEL=WALL1
GEOMETRY:PIPE_LABEL=2,DIAMETER=0.016,ANGLE= 8.3 ,LENGTH=2.00,ROUGHNESS=2e-006,WALL_LABEL=WALL1
GEOMETRY:PIPE_LABEL=3,DIAMETER=0.016,ANGLE= 46.7,LENGTH=0.55,ROUGHNESS=2e-006,WALL_LABEL=WALL1
GEOMETRY:PIPE_LABEL=4,DIAMETER=0.016,ANGLE=-29.0,LENGTH=0.35,ROUGHNESS=2e-006,WALL_LABEL=WALL1
GEOMETRY:PIPE_LABEL=5,DIAMETER=0.016,ANGLE= 90.0,LENGTH=6.20,ROUGHNESS=2e-006,WALL_LABEL=WALL1

// ******************
// initial conditions
// ******************
// _zL = distance from pipe inlet (m)
// _id = section id, 1 for a slug or 2 for a bubble.
// _H = initial holdup in the pipe.
// _p = initial pressure in the pipe (Pa)
// _ug = initial gas phase velocity in the pipe
// _ul = initial liquid phase velocity in the pipe
// _Tg and _Tl are initial liquid and gas temperatures (K)
// At time = 0, starting at _zL and ending at the pipe outlet
// The initial conditions for _H, _p, _ug, _ul, _Tg, and _Tl are as given.

INITCOND: _zL=0,_id=1,_H=1.0,_p=1.0e5,_ug=0,_ul=0,_Tg=295,_Tl=295

// ************************
// USG and USL at the inlet
// ************************

// USG = 0.0
// USL = 0.0

// ************
// Temperatures
// ************
// For ambient conditions, inlet, outlet.
// For isothermal, TEMP_AMB = TEMP_INLET = TEMP_OUTLET = TRE.
// ISOTHERMAL = 1 means energy equations will be ignored (for wave simulations). 0 - use energy
// equations.

TEMP_AMB = 293.16
TEMP_INLET = 293.16
TEMP_OUTLET = 293.16
TRE   = 293.16
ISOTHERMAL = 1

// ******
// Holdup
// ******
// HOLDUP_INLET needs to be set so that inlet phase velocities can be calculated using HOLDUP_INLET,
// USG, and USL.

HOLDUP_INLET = 1.00
//HOLDUP_OUTLET = 0

// EXPLICIT: 0 -  implicit formulation, 1 - explicit formulation. Should be 0.

EXPLICIT = 0
```

```
// ****************
// Fluid properties
// ****************
// RHOL in kg/m3, VISL, VISG in kg/m.s, M_GAS = molecular mass of gas in kg/mole.

RHOL   = 998
VISL   = 0.001002
VISG   = 1.825e-005
M_GAS   = 0.02897

// **************
// Closed or open
// **************

OUTLET_IS_CLOSED = 0
// 0 - open outlet, needs POUTLET.
INLET_IS_OPEN = 1
// 0 - closed inlet, needs USG, USL, INLET HOLDUP to calculate inlet phase velocities.
// 1 - open inlet, needs PINLET.

// **************************
// Inlet and outlet pressures
// **************************
// Pressure units are in Pa.
// PINLET is the open inlet boundary condition.
// PINLET also needs to be specified for a closed inlet so that the gas density can be calculated.
// POUTLET is the open outlet boundary condition.
// Patm = 1e5 Pa.

POUTLET = 1.013e5
PINLET = 1.013e5

// *****
// Waves
// *****
// WAVE_INIT: 1 - insert waves. 0 - no waves will be inserted.
// DELAY_WAVE: the time between waves inserted, related to insertion frequency (sec)
// DISCHARGE_COEF: for orifice type relation in waves. Open parameter.
// Values used have been between 0.2 and 0.4.
// 0.2 gives best agreement to Patm data. 0.4 gives best agreement to 8 bar data.

WAVE_INIT = 0
DELAY_WAVE = 2
DISCHARGE_COEF = 0.4

// max holdup in a wave or a stratified section (at a low point for e.g.) before a slug is created.

HOLDUP_MAX = 0.99

// *********************
// Simulation parameters
// *********************
// SPLIT_DURING_SIM: allows slugs, bubbles to be split during the simulation. Should be 1.
SPLIT_DURING_SIM  = 1
// DT_RESTART: data is saved every DT_RESTART sec.
DT_RESTART = 50

// Grid sizes (in multiples of pipe diameter)
// minimum slug length, minimum stratified section length, maximum stratified section length.
MIN_SLUG_COEF     = 1
MIN_BUB_COEF      = 8      // 8
MAX_BUB_COEF      = 20     // 50

// Times: Start time, end time, time step.

T_START = 0
T_END  = 600.0
T_STEP  = 0.01
```

```
// Output data to file every DT_PLOT seconds.

DT_PLOT = 0.1

// Time step adjustments.
// CONST_DT: option if time step size is constant or not. Should be 0.
// 0 - time step is optimized according to CFL criterion. If 1, time step is constant.

CONST_DT = 0

// Adjust time step by this TIMESTEPFACTOR if necessary following CFL criterion.

TIMESTEPFACTOR = 0.01

//Max time step

MAX_DT = 1

//Min time step

MIN_DT = 1e-8

// option to restart from end of last simulation.
// Keep as is.

RESTART = 1
FIX_OUTPUTFILES_ON_RESTART = 1

// PLOT: 1 - create output file. 0 - Don't create output file.
// Should be 1.
// An output file called UTPLOT.out will be created.
// A file called geometry.txt will be created listing the pipe geometry.

PLOT=1

// *************
// Other options
// *************
// interface friction factor = multiplier*gas wall friction factor.
// Kept at 1.

INTERFACE_FRICTION_MULTIPLIER = 1

// Specify an output directory for the output files.
// OUTDIR = ../testcase_Patm/

// If there are bends, valves, etc in the pipe, add additional friction factor.
// Used for undulating pipeline simulations.
// Add to lambda friction factor accounting for bends, tees, valves etc.
// Determined by (Total Loss coefficient * D) / pipe length
// ADD_LAMBDA = 0.1

// Add a source of mass
// location of source, phase type, mass flow rate, temperature, phase velocity, pressure.

SOURCE:_zL=8.445,phase=gas,dmdt=3.35e-5,temp=295,u=0,press=1.0e5

// Turn friction off
// FRICTION_OFF = 1
// Default is 0. Keep friction on.

// Specifiy a maximum slug length.
// Default is 1e100 meters.
// MAX_SLUG_LENGTH  = 500

// Add pigs
// PIG
```

```
// Add wall insulation
// WALL

// Execute a command at a certain time, e.g. change the USG
// EXECUTE: Time = 20, USG=0.3

//Extension for output file. Not used anymore.

OUTFILE_EXT = _vdip.out

// NOT USED: Don't delete. Keep for future reference.
// Not used. WALL for defining pipe insulation.

WALLSECLENGTH = 1

// option to print output file for wall data (1) or not (0)

PRINT_UT_WALL = 0

// wall: U = 10 W/m2 (based on id)
// WALL:_label=WALL1, _density=1300, _CP=1500, _width=0.005, _T=295, _k = .16 // steel
// WALL:_label=WALL1, _density=500, _CP=1000, _width=0.005, _T=295, _k = 0.03 // insulation
// WALL:_label=ADIABATIC, _density=1300, _CP=1500, _width=0.005, _T=295, _k = 0 // isolated

// NOT USED:
// Properties of insulation. Not used.

SURFCONDUCTANCE_GL = 10
SURFCONDUCTANCE_AMB = 1000000
SURFCONDUCTANCE_LIQ = 1000000
SURFCONDUCTANCE_GAS = 1000000
HEATCAPACITY_LIQ = 4169
HEATCAPACITY_GAS = 1000
HEATCONDUCTANCE_LIQ = 0.603
HEATCONDUCTANCE_GAS = 0.1460

// NOT USED:
// For gas in slugs. Not used.

SLIP_RELATION = MALNES
MAX_SLUG_ENTRAINMENT = 0.05
```

I Matlab filter

```
clc
clear all

%%%%%%%%%%%%%%%%%%%%%%%%%%%%%%%%%%%%%%%%%%%%%%%%%%%%%%%%%%%%%%%%%%%%%%%%%%%%%%%%%%%%%%%%%
%%%%%%%%%%%%%%%%%%%%%%%%%%%%%%%%%%%%%%%%%%%%%%%%%%%%%%%%%%%%%%%%%%%%%%%%%%%%%%%%%%%%%%%%%
%%%%  This program converts a .ppl file from OLGA into a file utplot.out   %%%%%%%%%%%%%%
%%%%  with a format accepted by the visualization tool PLOTIT.             %%%%%%%%%%%%%%
%%%%  The user specifies: "cells" and "lengths".  The .ppl file from OLGA  %%%%%%%%%%%%%%
%%%%  should only contain holdup values. For conversion of .ppl files      %%%%%%%%%%%%%%
%%%%  containing additional variables, this program can NOT be used       %%%%%%%%%%%%%%
%%%%  without modifications .                                              %%%%%%%%%%%%%%
%%%%%%%%%%%%%%%%%%%%%%%%%%%%%%%%%%%%%%%%%%%%%%%%%%%%%%%%%%%%%%%%%%%%%%%%%%%%%%%%%%%%%%%%%
%%%%%%%%%%%%%%%%%%%%%%%%%%%%%%%%%%%%%%%%%%%%%%%%%%%%%%%%%%%%%%%%%%%%%%%%%%%%%%%%%%%%%%%%%

cells   = [15 5 2 1 15];                % The user specifies number of cells in each pipe
lengths = [6.17 2.0 0.55 0.35 6.2];     % The user specifies the length of each pipe

%%%%%%%%%%%%%%%%%%%%%%%%%%%%%%%%%%%%%%%%%%%%%%%%%%%%%%%%%%%%%%%%%%%%%%%%%%%%%%%%%%%%%%%%%
%%%%%%%%%%%%%%%%%%%%%%%%%%%%%%%%%%%%%%%%%%%%%%%%%%%%%%%%%%%%%%%%%%%%%%%%%%%%%%%%%%%%%%%%%

C = sum(cells);                                      % number of cells in pipe
introlines_OLGA_ppl = 28;                            % the number of intro lines to skip
position_elevation_lines = (ceil(C/5))*2;
skip_lines = introlines_OLGA_ppl + position_elevation_lines;

OLGAMATRISE=textread('C:"........"6.ppl','',-1,'delimiter',' ','headerlines',...
skip_lines,'emptyvalue',0);

MATRISE = OLGAMATRISE(:,1:6);
cell_length = lengths./cells;
A = size(MATRISE);
F = length(cells);             % number of pipes
rows_pr_timestep = ceil(C/6);

for i = 1:(rows_pr_timestep+1):A(1);
TIME_STEP(i) = MATRISE(i,1);
end

[r,c,v] = find(TIME_STEP);
clear TIME_STEP
TIME_STEP(1) = 0;
TIME_STEP(2:length(v)+1) = v;
B = length(TIME_STEP);          % number of time steps

D = B*C;                        % number of rows in utplot.out

ALL_LENGTHS = zeros(1,C);
cumulative_sum = cumsum(cells);
stop  = cumulative_sum;
start = cumulative_sum + 1 - cells;

for j = 1:F
   ALL_LENGTHS(start(j):stop(j)) = cell_length(j);
end

ALL_LENGTHS(1) = cell_length(1);
NYMATRISE = zeros(D,13);

for j = 1:B
    NYMATRISE((j-1)*C+1:(j-1)*C+C,1) = TIME_STEP(j);
    NYMATRISE( 1+ (j-1)*C    :C+  (j-1)*C     ,3)       = ALL_LENGTHS;
    dummy = cumsum(ALL_LENGTHS);
    NYMATRISE( 2+ (j-1)*C    :C+  (j-1)*C     ,2)       = dummy(1:C-1);
end

HOLDUP = zeros(1,D);
```

```
vector = zeros(1,C);
s=0;

for j = 2:(rows_pr_timestep+1):A(1);
    for i = 1:rows_pr_timestep
        vector((i-1)*6 +(1:6)) = MATRISE(j+i-1,1:6);
    end
    s=s+1;
    HOLDUP((s-1)*C  + (1:C)) = vector(1:C);
end

NYMATRISE(:,6) = HOLDUP(:);
NYMATRISE(:,5) = 22;
NYMATRISE(:,11) = 2;

MA = NYMATRISE;
ss = size(MA);
last = ss(1);

fid = fopen('utplot.out','w');

for i=1:last
fprintf(fid,'%.6f,  %.6f,  %.6f,  %d,  %d,  %.6f,  %.6f,  %d,  %.6f,...
%.6f,  %d,  %d,  %d,"n' ,MA(i,1:13));
end
fclose(fid);
```

J Matlab plotting file

```
clear all
clc

%navn = 'utplot_2_0_x3_ny';  % 50
%navn = 'utplot_3_35_x3_ny'; % 30
%navn = 'utplot_3_65_x3_ny'; % 70
%navn = 'utplot_5_0_x3_ny';  % 70
%navn = 'utplot_8_5_x3_ny';  % 100

filnavn = [navn,'.out'];
utnavn  = [navn,'_P_smooth'];

[T,z,L,UBor,border_id,H,p,pipenr,ul,Ug,section_id,nr,wave]= ,...
textread(filnavn,'%f %f %f %f %f %f %f %f %f %f %f %f %f ','delimiter',',','headerlines',2);

z_span = 0.4;
factor = 100;

zpipe_1 = 9.09;   % position 1 in meters from inlet
zpipe_2 = 12.18;  % position 2 in meters from inlet
zpipe_3 = 15.25;  % position 3 in meters from inlet

zpipe_1_L = zpipe_1 - z_span;
zpipe_1_R = zpipe_1 + z_span;

zpipe_2_L = zpipe_2 - z_span;
zpipe_2_R = zpipe_2 + z_span;

zpipe_3_L = zpipe_3 - z_span;
zpipe_3_R = zpipe_3 + z_span;

ind_1    = z > zpipe_1_L & (z+L)< zpipe_1_R & section_id == 2 ;
indeks_1 = find(ind_1);

ind_2    = z > zpipe_2_L & (z+L)< zpipe_2_R & section_id == 2;
indeks_2 = find(ind_2);

ind_3    = z > zpipe_3_L & (z+L)< zpipe_3_R & section_id == 2;
indeks_3 = find(ind_3);

%%%%%%%%%%%%%%%%%%%%%%%%%%%%%%%%%%%%%%%%%%%%%%%%%%%%%%%%%%%%%%%%%%%%%%%%%%%%
close
% scrsz = get(0,'ScreenSize');
%figure('OuterPosition',[1 1 scrsz(3) scrsz(4)])
figure('OuterPosition',[3 300 1020 290])
set(gca, 'position', [0.052 0.23 0.934 0.63]);
box on
%%%%%%%%%%%%%%%%%%%%%%%%%%%%%%%%%%%%%%%%%%%%%%%%%%%%%%%%%%%%%%%%%%%%%%%%%%%%


hold on

glatt_p_1 = smooth(p(indeks_1),factor);     %90
glatt_p_2 = smooth(p(indeks_2),factor);     %90
glatt_p_3 = smooth(p(indeks_3),factor);     %90

p1 = plot(T(indeks_1),glatt_p_1,'-b','LineWidth',1.5);
p2 = plot(T(indeks_2),glatt_p_2,'-r','LineWidth',1.5);
p3 = plot(T(indeks_3),glatt_p_3,'-k','LineWidth',1.5);

xlim([300 450])
ylim([0.9*10^5 1.8*10^5])

h=legend([p1 p2 p3],'z = 9.09 [m]',...
                    'z = 12.18 [m]',...
                    'z = 15.25 [m]');
```

```
set(h,'location','NorthEast','FontSize',12);

xlabel('Time [s]','FontSize',14);
ylabel('$$P_{avg} [Pa]$$','FontSize',14);

set(gca,'YTick',1*10^5:0.2*10^5:1.6*10^5)
set(gca,'FontSize',12,'LineWidth',1.5)
set(gcf, 'PaperPositionMode', 'auto')
set(get(gca,'xlabel'),'interpreter','latex');
set(get(gca,'ylabel'),'interpreter','latex');
set(legend(),'interpreter','latex');

plottnavn = ['C:"Documents and Settings"Tor"My Documents",...
2010"prosjekt 2010"Masteroppgave_LaTex"',utnavn,'.eps'];

print('-r0','-depsc',plottnavn)
```